THE QUANTIFICATION OF NEURAL AND BEHAVIORAL CHROMATIC SENSITIVITIES

Michael A. Barnett

A DISSERTATION

in

Psychology

Presented to the Faculties of the University of Pennsylvania

in

Partial Fulfillment of the Requirements for the

Degree of Doctor of Philosophy

2022

Supervisor of Dissertation

David H. Brainard

Professor of Psychology

Co-Supervisor of Dissertation

Geoffrey K. Aguirre

Professor of Neurology

Graduate Group Chairperson

Russell A. Epstein

Professor of Psychology

Dissertation Committee

Johannes Burge, Associate Professor of Psychology

Michael J. Arcaro, Assistant Professor of Psychology

THE QUANTIFICATION OF NEURAL AND BEHAVIORAL CHROMATIC SENSITIVITIES

Dedication

To my parents.

ACKNOWLEDGMENT

I would like to thank my advisors David Brainard and Geoff Aguirre for their guidance throughout graduate school. In particular, I would like to highlight their careful approach to science. I would also like to thank my committee, Johannes Burge and Michael Arcaro, for their advice as well as for their collaboration. I am grateful for the work of Benjamin Chin who developed and worked on the color tracking project with me. Without Ben, this work would not have been possible.

I am grateful for the long-term support of my previous advisors. I want to thank Emily Grossman for introducing me to the world of brain research and her guidance over these years. I want to thank Kalanit Grill-Spector for her continued mentorship which has helped me develop as a scientist.

The work presented here was made possible through the help of the Agiurre/Brainard lab members. I want to thank them for their expertise and many discussions about science and careers. I want to thank Lingqi Zhang, Ana Radonjic, Nicolas Cottaris, Ozzy Taskin, Joris Vincent, Jack Ryan, Briana Haggerty, Harry McAdams, and Semin Oh.

I want thanks my friends and acting thesis supervising committee for their support. They have edited documents, sat through practice talks, and were able to transiently pause existential crises such that I was able to complete my

doctorate. I am grateful to Jesse Gomez, Noam Roth, and Katie Tregillus for their continued help along the way. I would not have completed this document without them.

I want to thank my friends in the CNI where I have worked for the last 6 years. I have appreciated ~94% of our conversations ranging from technical questions to bizarre hypotheticals. In particular, I want to acknowledge Jiang Mao, Gaia Tavoni, Arvind Iyer, Kyra Schapiro, Cheng Qiu, Takahiro Doi, Catrina Hacker, Seha Kim, Mary Schreck, Ariana Familiar, Nathan Tardiff, Dave White, Kara McGaughey, Barnes Januzzi, Simon Bohn.

I want to thank my Penn cohort friends Rivka Cohen, Anne Park, and Dilara Berkay whose support and late-night work sessions throughout graduate school helped me navigate the more challenging times. I would like to thank Kayla Barekat for all her friendship and help since undergrad.

I want to thank my friends from Stanford for their guidance. I want to thank Kevin Weiner, Michael Perry, Moqian Tian, Lior Bugatus, Swaroop Guntupalli, Vaidehi Natu, and Nathan Witthoft.

Most importantly, I would like to thank my family. I am grateful to the lifetime of support provided by them. None of this would have been possible without their constant encouragement.

ABSTRACT

THE QUANTIFICATION OF NEURAL AND BEHAVIORAL CHROMATIC SENSITIVITIES

Michael A. Barnett

David H. Brainard

Geoffrey K. Aguirre

The first stage of human color vision is the encoding of light by the long (L), medium (M), and short (S) wavelength sensitive cone photoreceptors. These signals are subsequently recombined into three post-receptoral pathways, two chromatic opponent and one luminance. The two chromatic pathways take the difference of cone activity (L-M and S-(L+M)) and the third luminance pathway sums the cone activity (L+M). Beyond the level of these post-receptoral mechanisms, the computations performed and their location in the brain are not well characterized. Across two studies, we examined the sensitivity of the underlying chromatic mechanisms using both functional magnetic resonance imaging and psychophysics. In both types of experiments, we employ the use of 'silent substitution' which allows for the selective modulation of activity of cone photoreceptors, and their combinations. In the first experiment, we collected BOLD fMRI responses in human V1 to spatially uniform, temporal chromatic modulations that systematically vary in chromatic direction and contrast. From

this, we found that within the LM cone contrast plane, V1 is most sensitive to L-M contrast modulations and least sensitive to L+M contrast modulations. Within V1, we observe little to no change in chromatic sensitivity as a function of eccentricity. In the subsequent experiment, we measured the temporal impulse response functions associated with tracking chromatic Gabor patches and measured how the lag functions change as a function of chromatic direction and contrast, confined to the LS cone contrast plane. We measured detection thresholds for stimuli matched in their spatial, temporal, and chromatic properties. We found that for both tracking and detection, within the LS cone contrast plane, the underlying mechanisms are most sensitive to L-isolating contrast modulations and least sensitive to S-isolating contrast modulations. Across all experiments, we developed color-contrast separable models that allow us to model the relative sensitivities of the chromatic mechanisms in a way that is independent from the effect of contrast. We use these models to further quantify the sensitivities of the underlying chromatic mechanisms. This work advances our understanding of human color perception and places important constraints on building more generalized models of color processing.

TABLE OF CONTENTS

LIST OF TABLES

LIST OF ILLUSTRATIONS

CHAPTER 1

General Introduction

The role of vision in the nervous system, which includes color vision, is to create an internal representation of the physical environment as sensed by light. This representation is built up by multiple stages of processing, the first of which starts in the eye. The encoding of light by the L-, M-, and S-cone photoreceptors is the first stage of color vision. This stage of color vision processing transduces the light that enters the eye into neural signals. The second stage of color vision processing recombines the cone signals into a set of post-receptoral pathways. This is done at the level of the retinal ganglion cells and the lateral geniculate nucleus. These cells project to primary visual cortex (area V1) where a variety of cell types and computations are performed. It remains unknown how the various cortical areas and computations build up our internal representation of the physical world.

In order to better understand how this representation is built, we need a way of transforming descriptions of the physical environment as coded by light to produce patterns of observable behaviors. To capture such a complex relationship, knowledge of many physical and biological factors is required. Some factors that must be well characterized include: 1. Light interacting with the environment to reach the eye; 2. Imaging of the light by the optics of the eye and

the formation of the retinal image; 3. Encoding of light by cone photoreceptors to produce the retinal image; 4. The transformations between the cone input and the retinal output; 5. The correspondence between behavioral measures and subcortical/cortical responses. Further understanding of any of these factors will improve our understanding of the relationship between light in the environment and color perception.

The field of color science has made much progress in its understanding of the psychophysical and physiological computations that underlie color perception. One popular approach is to frame how the visual system processes color information in a mechanistic manner. In particular, the following chapters focus on the mechanisms that process the signals originating at the level of the photoreceptors. This is examined from both a neural and a behavioral standpoint. Chapter 2 examines the neural signals arising from the selective stimulation of the L- and M-cones using functional magnetic resonance imaging to measure the chromatic sensitivities in V1. We developed a model that allows for the prediction of the BOLD fMRI response of any stimulus in the LM cone contrast plane and we examine how the parameters of the model vary as a function of eccentricity. Chapter 3 examines the temporal impulse response functions associated with tracking chromatic Gabor patches and measured how processing speed changes as a function of chromatic direction and contrast, within the LS cone contrast

plane. Detection thresholds were also measured for stimuli matched in their spatial, temporal, and chromatic properties of those used in the tracking experiment. Further, a similar model to the one in Chapter 2 is used to make predictions of the measured of lags and percent correct. In both chapters, a mechanistic approach is taken to better understand human color vision. The following sections review instances of mechanistic approaches to the study of color processing.

Evidence for Trichromacy:

Trichromacy refers to the result that humans can match the color appearance of any test light with a mixture of three independent primary lights as long as no light is a combination of the other two. This finding is due to the initial stage of color vision where the cone photoreceptors (L, M, and S) transduce the light that falls on the retina into neural signals. Importantly, the three classes of cone photoreceptors are independent which mean that activity of each class does not affect the activity of the others. It is also necessary that the encoding of light by the photoreceptors follows the principle of univariance. Univariance states that once absorbed, the effect of a photon on the visual system is the same regardless of its wavelength. These three photosensitive elements of the eye were first hypothesized by Thomas Young who stated "…each sensitive

filament of the nerve may consist of three portions, one for each principal colour" (Young, 1802). Helmholtz later expanded this theory such that these three "portions" need to be long-, medium-, and short- wavelength selective supported by evidence from color matching experiments (Kaiser & Boynton, 1996).

The color matching paradigm operates by having subjects adjust the relative intensities of three primary lights to match the color appearance of a test light. Two main versions of color matching experiments have been performed. The first, by Maxwell in 1860, had subjects adjust the relative intensity of two primaries added to a fixed wavelength light to match a fixed white test light (Judd, 1945; Stockman & Brainard, 2010). Another version of the color matching experiment was used by Wright (Wright, 1928) and Guild (Guild, 1931) in which subjects controlled the relative intensities of three fixed wavelength primaries to match a fixed wavelength test light. In both methods, the wavelength of the fixed element was parametrically varied in order to obtain a set of color matching functions (CMF). Both methods show that human observers can match any test light by simply adjusting the relative intensities of three fixed wavelength lights, an explicit test of the theory of trichromacy.

The color matching experiments show that there exist three independent mechanisms (L-, M-, and S-cones) and that these mechanisms are sufficient to explain the color matching results. The primary factor that mediates the results

of the color matching experiment is absorption rates of the cones as a function of wavelength. These are defined by what is referred to as the spectral sensitivity functions. Since this stage of the visual system is well approximated by a linear system, the spectral sensitivity functions provide a full account of these first stage mechanisms.

The first estimates of the spectral sensitivity functions were made by König and Dieterici in 1886 using normal and dichromat color matches (König & Dieterici, 1886). The use of dichromatic observers allowed for the use of the loss hypothesis. The loss hypothesis assumes that the selective loss of a photoreceptor type does not alter the functionality of the remaining receptors (Judd, 1945). This endeavor, and subsequent experiments, allowed for the color matching function to be converted to cone spectral sensitives via a linear transformation. Modern instantiations of this logic have resulted in sets of functions that describe the nominal observer with high precision.

The account of the cone spectral sensitivity functions, for a large portion of their existence, have been estimated solely through psychophysical methods. Physiological validation is needed for a definitive conclusion on the shapes of these functions to be reached. These initial chromatic mechanisms are a nice example of when psychology and physiology are complementary, with psychophysical predictions and physiological confirmation. The physiological

support for the spectral sensitivity functions have come in a variety of methods include retinal densitometry and microspectrophotometry (Kaiser & Boynton, 1996). Baylor, Nunn, and Schnapf (Baylor, Nunn, & Schnapf, 1987) used suction microelectrodes attached to the outer segments of L-cones, M-cones, and S-cones from nonhuman primates and recorded their responses as a function of stimulus wavelength. From this, they were able measure the cone fundamentals of the L-, M-, and S- cones directly. These measurements were directly compared to the 2° and 10° color matching functions of Stiles and Birch with excellent agreement (Stiles, 1955; Stiles & Burch, 1959). Taken together, the evidence from trichromacy has resulted in a well validated account of the mechanisms of the first stage of color vision processing.

Evidence for Post-Receptoral Mechanisms:

Trichromacy does not provide a full account of all the aspects of human color vision. The trichromatic visual mechanisms are not enough to make predictions of known perceptual phenomena. These include, for example, the predominance of red and green hue percepts at low stimulus intensities and a shift to yellow and blue hue percepts at high intensities. One of the earliest and best-known critiques of trichromacy was put forth by Ewald Hering in 1878 who used subjective color appearance as a means of refute (Hering, 1878). This

insight was that while colors could be described as being reddish-blue or greenish-yellow, they never appeared to be reddish-green or yellowish-blue. From this observation, Herring claimed that there existed four unique hues. Moreover, it seemed that these unique hues were arranged in pairs that are diametrically opposed. Unique red and unique green represent different ends of a single axis.

These two axes are set to be orthogonal and can be thought of as creating a red/green mechanism and a blue/yellow mechanism that do not interact each other. A third mechanism exists, orthogonal to both the red-green and blue-yellow plane, which corresponds to the black-white axis. This system of independent opponent mechanisms allows for any hue to be described by a pair of red/green and blue/yellow value. An account that takes the trichromatic mechanisms as the first stage of visual processing followed by a subsequent opponent mechanisms stage was first proposed by von Kries (Judd, 1966). Evidence for opponent mechanisms as the second stage of color processing exists from both psychological and physiological experiments. The first studies to start to quantify the relative strengths of color opponency were performed by Jameson and Hurvich (1957). They sought to determine if it was possible to measure the color appearance and mechanism responses of opponent processing using a hue cancellation task.

The primary piece of psychophysical evidence identifying the post-receptoral mechanisms comes from using adaptation. Krauskopf, Williams, and Heeley (1982) used selective habituation of the post-receptoral mechanisms while measuring changes in color discrimination. The authors found that when the adapting field lines up with the red-green and blue-yellow mechanisms they observed selective habituation. This means that habituating to one mechanism does not affect thresholds of the orthogonal mechanism. Furthermore, adapting to backgrounds halfway between the red/green and blue/yellow axes results did not result in selective habituation along the adapting direction. This study finds strong evidence for the existence of two chromatic mechanisms that line up with the blue/yellow and red/green directions.

Psychophysics does not provide information as to the location of these mechanisms in the visual pathways. To address these questions, we must examine the physiological studies. The first example of using electrophysiology to study cone opponent mechanisms was by Svaetichin and MacNichols (1958) when they recorded from the retina of fish. The most well know physiological study of post-receptoral mechanisms was that of Derrington, Krauskopf, and Lennie (1984). This work used electrophysiological recordings in macaque LGN and found cells that clustered into three categories. The mechanism found by this study are L-M (red-green opponent), S-(L+M) (blue-yellow opponent), and L+M

(luminance). The mechanisms found fit well with the results of the cardinal directions of Krauskopf, Williams, and Heeley which provide a mechanistic account of the second stage of color.

Beyond the Post-Receptoral Mechanisms:

Even with the inclusion of the opponent mechanism, unexplained results still exist in various color experiments. This observation naturally leads to the idea of including more mechanisms to account for this unexplained variance. Difficulties arise when trying answer the questions of how many mechanisms exist, what computation do they perform, and where in the brain they are located? Attempting to answer these questions has resulted in many psychophysical and neural studies which have produced a variety of results.

Attempting to figure out the computations of the chromatic mechanisms has resulted in a series of experiments in which these computations are described by an isoresponse contours (or surfaces). An isoresponse contour is defined by a set of stimuli that all evoke the same response. The isoresponse contour as a model of visual mechanisms considers both the combination rule of the cones as well as their relative sensitivities. The combination rule defines the shape of the contour, for example a model that linearly combines the cone responses can produce parallel lines while a model that squares and sums

(quadratic) the cone responses can produce an ellipse. The relative sensitivity of the cones controls the orientation of the contours. The isoresponse contour is task specific but the most common task used in evaluating visual mechanisms is the detection task which define isodetection contours. Poirson et al (1990) set out a procedure for fitting such contours and surfaces and show that elliptical shape is reasonable when compared to the other common shapes used (rectangles and parallelograms). Knoblauch et al. (1996) in an extensive experiment were unable to reject the use of ellipsoidal isodiscrimination surfaces as a model of color vision mechanisms. The use of isoresponse contours is extensive in the following chapters, with the goal of examining how they change as a function of either retinal field location or behavioral task to inform about color vision mechanisms.

As to the number of mechanisms, Krauskopf et al. (1986) used the original data for the cardinal mechanisms experiment alongside new data to find evidence for a recombination of signals from the cardinal mechanisms. They refer to this recombination as “higher-order” color mechanisms which are proposed to be tuned to color directions that are intermediate between cardinal directions. Another approach that is used to study these mechanisms is using noise masking studies to measure chromatic discrimination thresholds. Such studies find the existence of multiple broadly tuned mechanisms exist (Hansen &

Gegenfurtner, 2013). These finding conflict with other studies that find the existence of a limited number of mechanisms (Eskew, 2009).

The question of localizing the function of higher-order color mechanisms to their cortical locations requires methods other than psychophysics. To answer this question, neural measurements must be used. We know that higher-order color mechanisms do not exist in a single cortical stage (Zeki & Marini, 1998). Unfortunately, just as with estimates of the number of mechanisms, localizing function to specific neural sites are in equal disagreement. Many groups have performed studies in the cortex using electrophysiology and functional magnetic resonance imaging (fMRI) to examine cortical localization of color processing and their response properties (Derrington, Krauskopf, & Lennie, 1984; Cottaris & De Valois, 1998; Livingstone & Hubel, 1984; Horwitz & Hass, 2012; Engel, Zhang, & Wandell, 1997; Lafer-Sousa, Conway, & Kanwisher, 2016). From this work, the field has learned about a subset of the computations performed at specific cortical locations.

One question important to these issues examines how and where signals from the cones are combined in the cortex and what are their relative sensitivities. One study that addressed this was Engel, Zhang, and Wandell (1997) which used fMRI to examine the sensitivity of primary visual cortex (V1) to stimulus modulations made in cone contrast space. From this, they observed that

the V1 BOLD fMRI signal was maximally sensitive to L-M stimulus modulations and least sensitive to modulation made in the S-(L+M) direction. These finding are consistent with the cardinal mechanisms being represented in area V1.

In a more recent paper, Horwitz and Hass (2012) used a closed-loop real time staircase procedure in which they recorded from neurons in macaque V1 to fit isoresponse surfaces to individual neurons. Isoresponse surfaces describe the relative sensitivities of individual neurons to any direction in cone contrast space. They found three types of isoresponse surfaces from the neurons they recorded from. Half of the cells they recorded from had their responses explained by a planar isoresponse surface. This means that they were tuned to a preferred direction and unresponsive to a chromatic plane. The other isoresponse surfaces were quadric surfaces which means they had a nonlinear relationship with the cone inputs. One type of surface was cup shaped showing narrow tuning for a particular direction and, like the planar surfaces, was unresponsive to a chromatic plane. The last type of isoresponse surface was ellipsoidal, which showed sensitivity to all color directions. These results may highlight why the psychophysical literature is so complicated to interpret. The cells in V1 show response profiles that are a mix of linear and nonlinear units. This requires more thought as to how the combinations of these mechanisms may help to explain psychophysical results.

CHAPTER 2

A Quadratic Model Captures the Human V1 Response to Variations in Chromatic Direction and Contrast

Michael A. Barnett[1], Geoffrey K. Aguirre[2], David H. Brainard[1]

[1]Department of Psychology, University of Pennsylvania

[2]Department of Neurology, University of Pennsylvania

This chapter has been previously published in eLife: Barnett, M. A., Aguirre, G. K., & Brainard, D. (2021). A quadratic model captures the human V1 response to variations in chromatic direction and contrast. eLife, 10, e65590.

Abstract:

An important goal for vision science is to develop quantitative models of the representation of visual signals at post-receptoral sites. To this end, we develop the quadratic color model (QCM) and examine its ability to account for the BOLD fMRI response in human V1 to spatially-uniform, temporal chromatic modulations that systematically vary in chromatic direction and contrast. We find that the QCM explains the same, cross-validated variance as a conventional general linear model, with far fewer free parameters. The QCM generalizes to allow prediction of V1 responses to a large range of modulations. We replicate

the results for each subject and find good agreement across both replications and subjects. We find that within the LM cone contrast plane, V1 is most sensitive to L-M contrast modulations and least sensitive to L+M contrast modulations. Within V1, we observe little to no change in chromatic sensitivity as a function of eccentricity.

Introduction:

The initial stage of human color vision is well characterized. The encoding of light by the three classes of cone photoreceptors (L, M and S) is described quantitatively by a set of spectral sensitivity functions, one for each class. Knowledge of the spectral sensitivities allows for the calculation of cone excitations from the spectral radiance of the light entering the eye (Brainard & Stockman, 2010). This quantitative characterization supports the analysis of the information available to subsequent processing stages (Geisler, 1989; Cottaris, Jiang, Ding, Wandell, & Brainard, 2019), supports the precise specification of visual stimuli (Brainard, 1996; Brainard, Pelli, & Robson, 2002), and enables color reproduction technologies (Wandell & Silverstein, 2003; Hunt, 2004). An important goal for vision science is to develop similarly quantitative models for the representation of visual signals at post-receptoral sites.

The second stage of color vision combines the signals from the cones to create three post-receptoral mechanisms. Psychophysical evidence supports the

existence of two cone-opponent mechanisms, which represent differences between cone signals (S-(L+M) and L-M), and a luminance mechanism, which represents an additive combination (L+M) (Krauskopf, Williams, & Heeley, 1982; Stockman & Brainard, 2010). Physiological evidence shows that this recombination begins in the retina with correlates observed in the responses of retinal ganglion cells and subsequently in the neurons of the lateral geniculate nucleus (DeValois, Abramov, & Jacobs, 1966; Derrington, Krauskopf, & Lennie, 1984; Lennie & Movshon, 2005). While the outlines of this second stage seem well established, the precise links between retinal physiology and visual perception remain qualitative and subject to debate (Stockman & Brainard, 2010; Shevell & Martin, 2017).

Studies focused on developing quantitative parametric models of the chromatic response properties of neurons in primary visual cortex of primates (area V1) have not yet converged on a widely-accepted model (Johnson, Hawken, & Shapley, 2004; Solomon & Lennie, 2005; Tailby, Solomon, Dhruv, & Lennie, 2008; Horwitz & Hass, 2012; Weller & Horwitz, 2018). In part, this is due to the considerable heterogeneity of chromatic response properties found across individual cortical neurons (Gegenfurtner, 2001; Lennie & Movshon, 2005; Solomon & Lennie, 2007; Shapley & Hawken, 2011; Horwitz, 2020). In addition, variation in stimulus properties across studies limits the ability to compare and integrate results.

The chromatic response of V1 has also been studied using blood oxygen level dependent (BOLD) functional magnetic resonance imaging (fMRI) (Wandell, Dumoulin, & Brewer, 2006). This includes studies that characterize the relative responsiveness of V1 (and other visual areas) to various chromatic and achromatic stimuli (Engel, Zhang, & Wandell, 1997; Hadjikhani, Liu, Dale, Cavanagh, & Tootell, 1998; Beauchamp, Haxby, Jennings, & DeYoe, 1999; Bartels & Zeki, 2000; Mullen, Dumoulin, McMahon, de Zubicaray, & Hess, 2007; Goddard, Mannion, McDonald, Solomon, & Clifford, 2011; Lafer-Sousa, Conway, & Kanwisher, 2016) and how this depends on the spatial and temporal properties of the stimulus (Liu & Wandell, 2005; D'Souza, Auer, Frahm, Strasburger, & Lee, 2016; Mullen, Thompson, & Hess, 2010).

Few studies, however, have pursued a quantitative model of the V1 BOLD response to arbitrary chromatic stimulus modulations. Development of such a model is important, since it would enable generalizations of what is known from laboratory measurements to natural viewing environments, where stimuli rarely isolate single mechanisms. Further, the parameters of such a model provide a succinct summary of processing that could be used to understand the flow of chromatic information through cortex. Notably, Engel, Zhang, and Wandell (1997) conducted a pioneering study that varied the chromatic content and temporal frequency of stimuli and observed that the V1 BOLD fMRI signal was maximally sensitive to L-M stimulus modulations.

In the present study, we focus on the signals that reach V1 from stimulus modulations confined to the L- and M-cone contrast plane (LM contrast plane). Specifically, we measured responses with fMRI to flickering modulations designed to systematically vary combinations of L- and M-cone contrast. Using these data, we developed a model—the quadratic color model (QCM)—that predicts the V1 BOLD fMRI response for any arbitrary stimulus in the LM contrast plane, using a small set of parameters. We validate the QCM through comparison to a less constrained general linear model (GLM). Importantly, the parameters of the QCM are biologically meaningful, and describe the sensitivity of V1 to chromatic modulations. Further, we generate cortical surface maps of model parameters across early visual cortex, allowing us to examine how chromatic sensitivity changes across V1 as a function of visual field eccentricity.

Quadratic Color Model (QCM):

This section provides an overview of the Quadratic Color Model (QCM); a full mathematical description is provided in the Model Appendix. Given a description of the stimulus, the QCM provides a prediction of the BOLD fMRI response within V1. Our stimuli were full field temporal chromatic modulations that can be specified by their contrast (vector length of the stimulus in the LM contrast plane) and chromatic direction (angle of the stimulus measured counterclockwise with

respect to the positive abscissa). From this stimulus specification, the model employs three stages that convert the input to the BOLD fMRI response (Figure 2-1). First, a quadratic isoresponse contour is defined that allows for the transformation of contrast and direction into what we term the “equivalent contrast”. Second, a single non-linear function transforms the equivalent contrast to a prediction of the population neuronal response underlying the BOLD response. Finally, the neuronal response is converted to a predicted BOLD response by convolution with a hemodynamic response function.

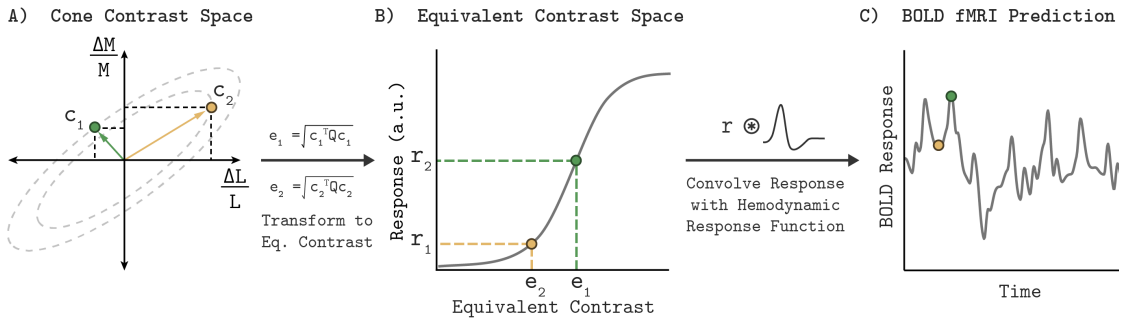

Figure 2-1: Quadratic Color Model.

A) The LM contrast plane representing two example stimuli (c_1 and c_2) as the green and yellow vectors. The vector length and direction specify the contrast and chromatic direction of the positive arm of the symmetric modulation (see Visual Stimuli in Methods). Using the parameters of an elliptical isoresponse contour (panel A, dashed gray ellipses), fit per subject, we can construct a 2x2 matrix Q that allows us to compute the equivalent contrast of any stimulus in the LM contrast plane (panel B; e1 and e2; See Model Appendix). B) Transformation of equivalent contrast to neuronal response. The equivalent contrasts of the two example stimuli from panel A are plotted against their associated neuronal response. A single Naka-Rushton function describes the relationship between equivalent contrast and the underlying neuronal response. C) To predict the BOLD fMRI response, we convolve the neuronal response output of the Naka-Rushton function with a subject specific hemodynamic response function. Note that the BOLD fMRI response prediction for the green point is greater than the prediction for the yellow point, even though the yellow point has greater cone contrast. This is because of where the stimuli lie relative to the isoresponse contours. The difference in chromatic direction results in the green point producing a greater equivalent contrast, resulting in the larger BOLD response.

Isoresponse Contours and Equivalent Contrast:

The first stage of the QCM computes the equivalent contrast of a stimulus from its cone contrast using a subject-specific elliptical isoresponse contour. Equivalent contrast is the effective contrast of a stimulus in V1 once it has been adjusted to account for differences in the neuronal sensitivity to stimulation across different chromatic directions. An isoresponse contour is defined as a set of stimuli that evoke the same neuronal response. In the QCM, the loci of such stimuli form an elliptical isoresponse contour in the LM cone contrast plane. All points on this elliptical isoresponse contour have the same equivalent contrast (Figure 2-1A, dashed gray ellipses). As the amplitude of the neuronal response increases, the ellipse that defines the set of stimuli producing that response also grows in overall scale. Importantly, the QCM assumes that the aspect ratio and orientation of elliptical isoresponse contours do not change as a function of the response level; only the overall scale of the ellipse changes. The use of elliptical isoresponse contours is motivated by prior psychophysical (Poirson, Wandell, Varner, & Brainard, 1990; Knoblauch & Maloney, 1996), electrophysiological (Horwitz & Hass, 2012), and fMRI experiments (Engel, Zhang, & Wandell, 1997) which have successfully used ellipses to model chromatic isoresponse contours.

The elliptical isoresponse contours are described by a symmetric quadratic function that defines the major and minor axes of the ellipse. We use this quadratic function to compute the equivalent contrast for each stimulus. The vector lengths of all stimuli that lie on a single isoresponse contour provide the cone contrasts required to elicit an equal neuronal response. The minor axis of the elliptical isoresponse contour corresponds to the chromatic direction that requires the least amount of cone contrast to produce this equal neuronal response, and is therefore the most sensitive chromatic direction. The major axis corresponds to the direction of least sensitivity. At this stage, the model is only concerned with the shape of the elliptical contour, thus we adopt the convention of normalizing the ellipse used to define equivalent contrast so that its major axis has unit length. This allows the length of the minor axis to directly represent the relative sensitivity, which is taken as a ratio of the minor axis (maximal sensitivity) to major axis (minimal sensitivity), referred to as the minor axis ratio. The angle of the major axis in the LM contrast plane (ellipse angle) orients these maximally and minimally sensitive directions.

Response Non-Linearity:

Since all the stimuli that lie on a single isoresponse contour produce the same response, we can represent these points by their common equivalent

contrast. The neuronal responses to stimuli across different color directions are a function of this single variable, and therefore we can transform equivalent contrast into predicted neuronal response via a single static non-linear function (Figure 2-1B). Here we employ the four-parameter Naka-Rushton function (see Model Appendix).

Transformation to BOLD fMRI Signal:

To predict the BOLD fMRI signal, we obtain the time-varying neuronal response prediction from the Naka-Rushton function for a stimulus sequence presented in the fMRI experiment. This neuronal response is convolved with a subject-specific hemodynamic response function to produce a prediction of the BOLD fMRI signal (Figure 2-1C).

QCM Summary:

In summary, the QCM takes as input the temporal sequence of stimulus modulations, defined by their chromatic direction and contrast in the LM cone contrast plane, and outputs a prediction of the BOLD fMRI time course. The QCM has 6 free parameters: two that define the shape of the normalized elliptical

isoresponse contour and four that define the Naka-Rushton equivalent contrast response function.

Results:

To evaluate the QCM, three subjects underwent fMRI scanning while viewing stimuli consisting of spatially uniform (0 cycles per degree) chromatic temporal modulations, presented using a block design. Each 12 second block consisted of a 12 Hz bipolar temporal modulation in one of 8 chromatic directions and at one of 5 log-spaced contrast levels. We split the chromatic directions into two sessions and subjects viewed each of the 20 combinations of chromatic direction (4 directions) and contrast (5 levels) once per run in a pseudorandomized order (see Materials and Methods, Figure 2-10 & 2-11). For each subject, a measurement set consisted of 20 functional runs conducted across the two scanning sessions. We collected two complete measurement sets (referred to as Measurement Set 1 and 2) for each subject, and fit the model to each set separately to test for the replicability of our findings. We first modeled the data using a conventional GLM that accounts for the response to each of the 40 stimulus modulations independently. The fit of this relatively unconstrained model was used as a benchmark to evaluate the performance of QCM. Results were similar for all three subjects. In the main text, we illustrate our findings with

the data from one subject (Subject 2); results from the other two subjects may be found in the supplementary materials.

Characterizing Cortical Responses with a Conventional GLM:

To examine the basic chromatic response properties of V1, we grouped the GLM beta weights by their corresponding chromatic direction and plotted them as a function of contrast, indicated as the filled circles in each of the eight panels of Figure 2-2 (data from Subject 2). For each chromatic direction, the V1 BOLD response generally increased with contrast, as expected. This result is consistent across the two independent measurement sets for Subject 2, as can be seen by comparing the green and purple points in Figure 2-2. Further, the increasing response with stimulus contrast was also observed in both measurement sets for the other two subjects (Figure 2 – figure supplement 1-2).

The rate at which V1 BOLD responses increase with contrast varied with chromatic direction. This can be seen in Figure 2-2 by noting that the maximum stimulus contrast differed considerably across chromatic directions, while the maximum response remained similar. For example, a modulation in the 45° direction required ~60% stimulus contrast to elicit a response of 0.6 while stimuli modulated in the -45° direction required only ~12% stimulus contrast to produce a similar response.

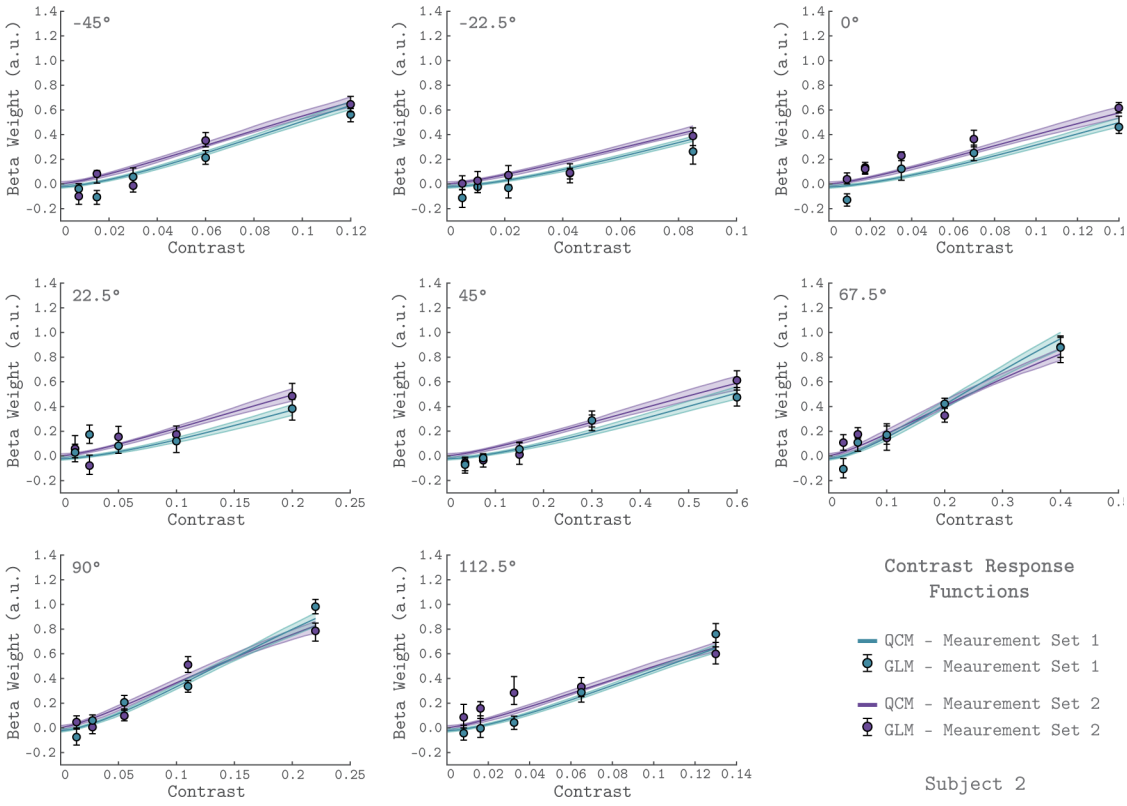

Figure 2-2: V1 Contrast Response Functions.

V1 contrast response functions for the eight measured chromatic directions from Subject 2. Each panel plots the contrast response function of V1, aggregated over 0° to 20° eccentricity, for a single chromatic direction. The x-axis is contrast, the y-axis is the BOLD response (taken as the GLM beta weight for each stimulus). The chromatic direction of each stimulus is indicated in the upper left of each panel. The curves represent the QCM prediction of the contrast response function. Error bars indicate 68% confidence intervals obtained by bootstrap resampling. Measurement Sets 1 and 2 are shown in green and purple. The x-axis range differs across panels as the maximum contrast used varies with chromatic direction. All data shown have had the baseline estimated from the background condition subtracted such that we obtain a 0 beta weight at 0 contrast.

The GLM places no constraints on the values of GLM beta weights, and we observed that these values did not always increase monotonically with contrast. Given the a priori expectation that the BOLD response itself increases monotonically with contrast, this raises the possibility that the GLM overfits the

data, using its flexibility to account for the noise as well as the signal in the response. To examine this, we fit a series of more constrained models that enforce the requirement that the fit response within chromatic direction increases monotonically with contrast. These models employed a Naka-Rushton function to describe the contrast response function in each chromatic direction. Across the models, we constrained varying numbers of the parameters to be constant across chromatic direction. The most general of these models fits a separate Naka-Rushton function to each color direction, allowing all but the offset parameter to be independent across chromatic directions. We also explored locking the amplitude parameter (in addition to the offset), the exponent parameter (in addition to the offset), and the amplitude, exponent, and offset parameters (allowing only the semi-saturation parameter to vary with chromatic direction). To evaluate how well these models fit the data, we ran a cross-validation procedure, described below, to compare the Naka-Rushton model fits with those of the GLM. The cross-validated R^2 for all of the Naka-Rushton models was slightly better than for the GLM, indicating that enforcing smooth monotonicity reduces a slight overfitting. These cross-validation results can be seen in Figure 4 – figure supplement 1. For simplicity, and due to the small differences in fit, we retain the GLM as the point of comparison for the performance of the QCM.

Quality of GLM Time Course Fit:

We examined how well the GLM fit the measured BOLD response from area V1. Figure 2-3 shows the fit of the GLM for six example runs from Subject 2. In each panel, the measured BOLD percent signal change is shown as the thin grey line, while the fit obtained from the GLM is shown as the orange line. The orange shaded region represents the 68% confidence interval of the fit found using bootstrap resampling. The GLM fit captured meaningful stimulus-driven variation in the BOLD response, with some variation in fit quality across runs. The median R^2 value across runs was 0.41 for Measurement Set 1 and 0.32 for Measurement Set 2. Fits for the other two subjects are provided as Figure 3 – figure supplement 1-2. Due to the randomized stimulus order within each run, it was not straightforward to determine the degree to which the unmodeled variance was due to stimulus-driven structure not modeled by the GLM (e.g., carry-over effects) as opposed to measurement noise. Overall, the quality of the GLM fits supported using the GLM as a benchmark model, as well as using the GLM beta weights as a measure of the V1 response.

Characterizing Cortical Responses with the Quadratic Color Model:

The QCM is a parametric special case of the GLM that predicts the BOLD time course using a small number of parameters and allows for response predictions to modulations in any chromatic direction and contrast in the LM plane. Figure 2-2 shows the QCM V1 contrast response functions for Subject 2 (the solid lines). The green and purple lines represent fits to Measurement Set 1 and 2, respectively. The shaded region around both lines represent the 68% confidence intervals for the fits obtained using bootstrap resampling. The QCM contrast response functions agree well with the beta weights obtained from the GLM. The QCM contrast response functions increase monotonically with contrast in all chromatic directions, potentially smoothing measurement variability in the GLM beta weights. There was excellent agreement between the fits to both measurement sets for Subject 2. Similar agreement between the QCM and the GLM and between measurement sets was found for the other two subjects (Figure 2 – figure supplement 1-2).

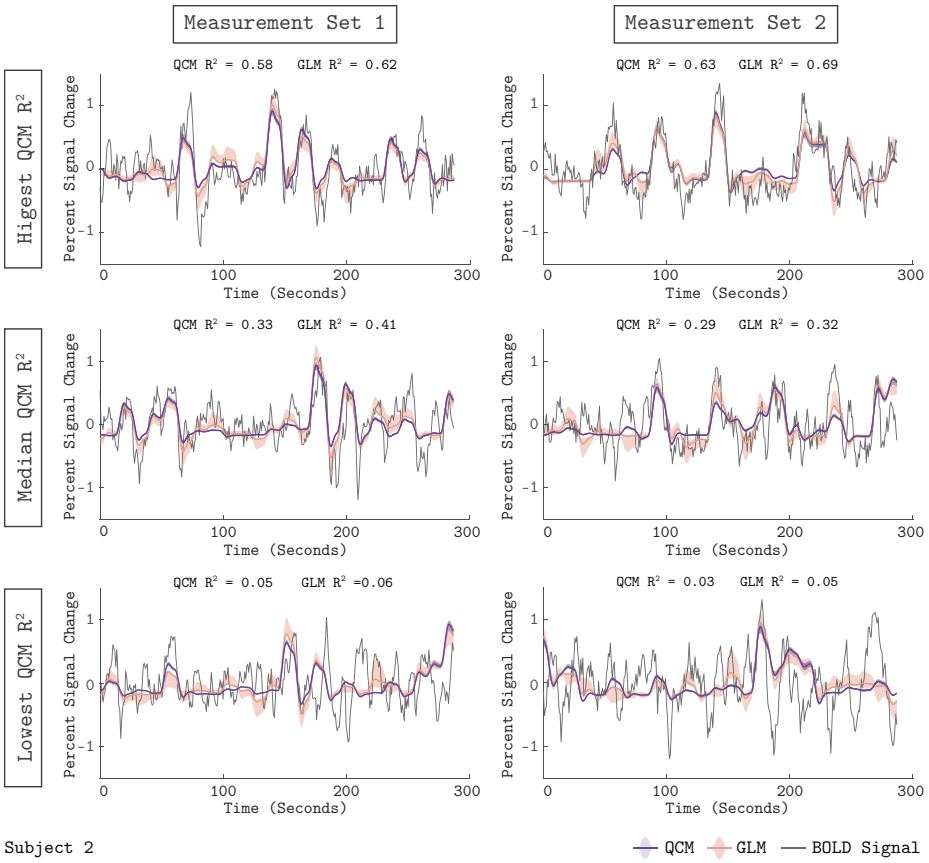

Figure 2-3: Model Fits to the V1 BOLD Time Course.

The measured BOLD time course (thin gray line) is shown along with the model fits from the QCM (thick purple line) and GLM (thin orange line) for 6 runs from Subject 2. Individual runs consisted of only half the total number of chromatic directions. The left column shows data and fits from Measurement Set 1 and the right column for Measurement Set 2. The three runs presented for each measurement set were chosen to correspond to the highest, median, and lowest QCM R^2 values within the respective measurement set; the ranking of the GLM R^2 values across runs was similar. The R^2 values for the QCM and the GLM are displayed at the top of each panel. The shaded error regions represent the 68% confidence intervals for the GLM obtained using bootstrapping.

We assessed the quality of the QCM fit to the V1 BOLD time course. The purple line in Figure 2-3 shows the QCM fit to the BOLD time course with the shaded region representing the 68% confidence interval obtained using bootstrapping. The QCM fit of the time course was of similar quality to the GLM

fit. Importantly, the QCM fit was based on only 6 free parameters, compared to the 41 free parameters of the GLM. Similar quality of fits for QCM can be seen for the other two subjects in Figure 3 – figure supplement 1-2.

Comparison of GLM and QCM:

We used a leave-runs-out cross-validation procedure to compare the GLM and the QCM (See Methods section for details). This cross-validation compares the ability of the models to predict data not used to fit the parameters, accounting for the possibility that more flexible models (such as the GLM) may overfit the data. Figure 2-4 shows the results of the cross-validation comparison for all subjects. Both models track meaningful variation in the signal, although less so for the data from Subject 3 in Measurement Set 2. Importantly, we see that the

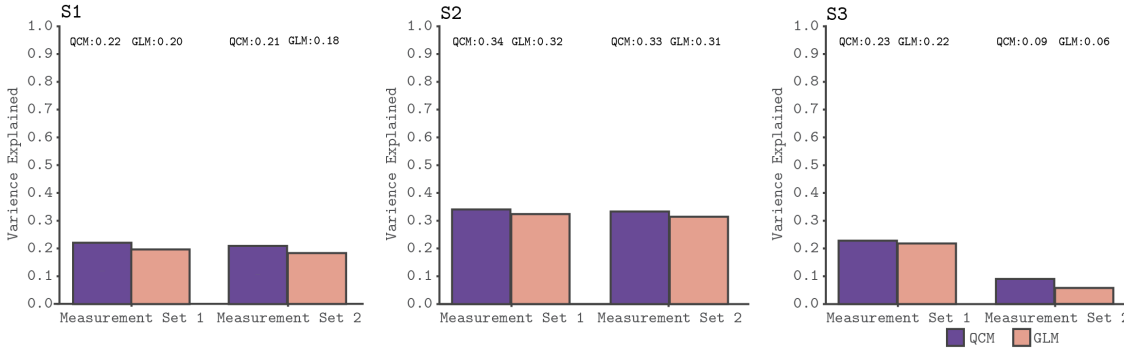

Figure 2-4*:* Cross-Validated Model Comparison

Cross-validated model comparison for the QCM and the GLM, from the V1 ROI and for all three subjects. In each panel, the mean leave-one-out cross-validated R^2 for the QCM (purple bars) and the GLM (orange bars). These values are displayed at the top of each panel. Within each panel, the left group is for Measurement Set 1 and the the right group is for Measurement Set 2.

QCM cross-validated R^2 is essentially indistinguishable from the GLM cross-validated R^2, although in all cases slightly higher.

To further assess differences between the GLM and the QCM, we analyzed the model residuals as a function of the stimulus condition, to check for systemic patterns in the residuals as well as any differences between the two models in this regard. We first examined each direction/contrast pair separately by plotting the residuals of the GLM and QCM over the 14 TRs after the start of each stimulus block. We did not observe any systematic variation in the residuals as a function of contrast level within a single chromatic direction. Therefore, we examined the mean residual value, taken from 4 to 14 TRs after stimulus onset, for all trials in a chromatic direction (collapsed over contrast). We plot these mean residuals for both the GLM and the QCM, as a function of chromatic direction, for each subject and session in Figure 3 – figure supplement 3. From this, we observe no consistent pattern of residuals within or across models. Note that the residual values for the GLM and QCM mostly overlap, despite the GLM having separate parameters for each stimulus direction.

QCM Generalization:

We also employed a leave-session-out cross-validation procedure to assess the generalizability of the QCM (See Materials and Methods for details). Given that Sessions 1 and 2 do not share any common chromatic directions, we were able to evaluate how effectively the QCM generalizes to chromatic directions not used to derive the model parameters. The green contrast response functions shown in Figure 2-5 result from fitting the QCM to either Session 1 or Session 2, and predicting the responses from the held-out session. The generalization from Session 1 to Session 2 (right-hand subplots) is excellent for this subject. The generalization from Session 2 to Session 1 is also good, albeit with a large confidence interval for the 45° direction. For other subjects and measurement sets, the QCM generalizes reasonably well (Figure 5 – figure supplement 1-3). Overall, generalizations from Session 1 to Session 2 perform better than those from Session 2 to Session 1. This finding may reflect the particular set of chromatic directions presented in each session: only Session 1 includes a chromatic direction close to the major axis of the ellipse, which better constrains the QCM fit. Therefore, the QCM is capable of generalizing well to unmeasured chromatic directions, with the requirement that the stimuli include chromatic directions and contrasts that adequately constrain the model parameters.

QCM Characterization of V1 BOLD Response:

Conceptually, the parameters of the QCM characterize two key model components. The first component defines the contrast-independent shape of

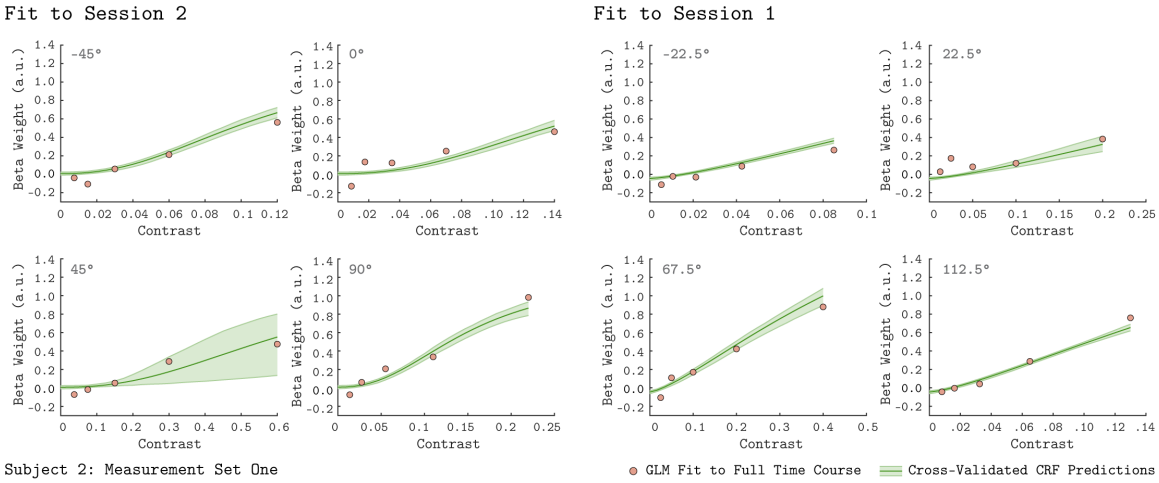

Figure 2-5: Leave-Sessions-Out Cross Validation.

The contrast response functions in each panel (green lines) are the result of a leave-sessions-out cross-validation to test the generalizability of the QCM. The QCM was fit to data from four out of the eight tested chromatic directions, either from Session 1 or Session 2. The fits were used to predict the CRFs for the held out four directions. The orange points in each panel are the GLM fits to the full data set. The data shown here are for Subject 2, Measurement Set 1. The shaded green error regions represent the 68% confidence intervals for the QCM prediction obtained using bootstrapping. See Figure 5 - figure supplement 1-3 for cross-validation plots from other subjects and measurement sets.

elliptical isoresponse contour. This describes the relative sensitivity of V1 to modulations in all chromatic directions within the LM contrast plane. The second component defines the response nonlinearity, which is independent of chromatic direction. It operates on equivalent contrast to produce the underlying neural response.

Elliptical Isoresponse Contours:

The isoresponse contour is described by two parameters: the direction of least sensitivity (ellipse angle; counterclockwise to the positive abscissa) and the ratio of vector lengths between the most and least sensitive directions (minor axis ratio; see Quadratic Color Model Section and Model Appendix). Within the QCM, the angle and minor axis ratio provide a complete description of chromatic sensitivity that is contrast independent.

Figure 2-6 shows the QCM isoresponse contours for all 3 subjects and both measurement sets. We found that for all subjects and measurement sets, the angle of the isoresponse contours was oriented at approximately 45°. An ellipse angle of 45° indicates that V1 was least sensitive to stimuli modulated in the L+M

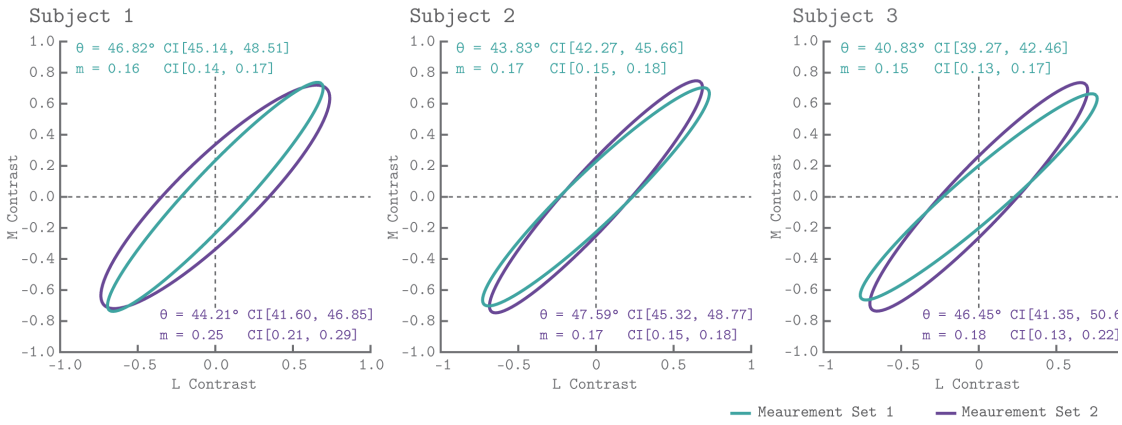

Figure 2-6: V1 Isoresponse Contours.

The normalized elliptical isoresponse contours from the QCM are plotted, for each subject, in the LM contrast plane. The green ellipses show the QCM fits to Measurement Set 1 and the purple ellipses show fits to measurement 2. The angles and minor axis ratios along with their corresponding 68% confidence intervals obtained using bootstrapping are provided in the upper left (Measurement Set 1) and lower right (Measurement Set 2) of each panel.

direction, and most sensitive to stimuli modulated in the L-M direction. Across all subjects and measurement sets, the minor axis ratio parameters ranged between 0.15 and 0.25. Thus, for the spatial and temporal properties of our modulations, V1 was roughly 5 times more sensitive to modulations in the L-M direction than the L+M direction. We found good agreement between the isoresponse contours from the independent measurement sets as well as across subjects.

Equivalent Contrast Nonlinearity:

Figure 2-7 shows the V1 equivalent contrast nonlinearity of the QCM for Subject 2 for both measurement sets. This non-linearity describes how the underlying neuronal response increases with increasing equivalent contrast. We used the isoresponse contour of the QCM to convert the chromatic direction and cone contrast of each stimulus to its equivalent contrast. This allowed us to replot each beta weight derived from the GLM (Figure 2-2) on an equivalent contrast axis (Figure 2-7; closed circles). For all subjects, the single nonlinearity accurately captured the dependence of the GLM beta weight on equivalent contrast, with no apparent bias across chromatic directions. The agreement between the GLM beta weight points and QCM fits demonstrated that separating the effects of chromatic direction and contrast in the QCM is reasonable. Figure 7

– figure supplement 1 provides the same plots for Subjects 1 and 3. Note that our stimuli did not drive the response into the saturated regime.

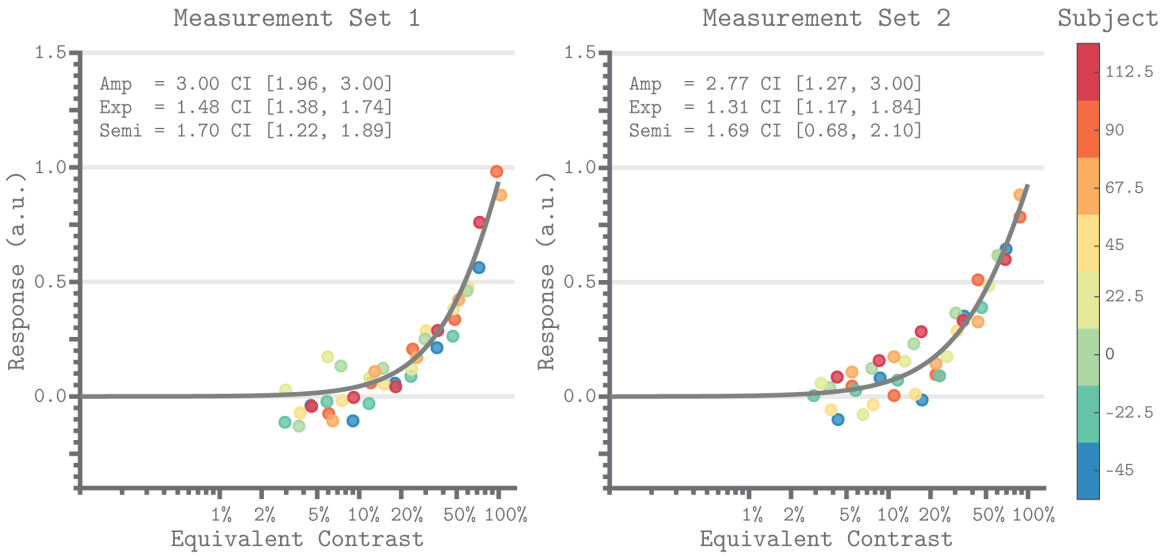

Figure 2-7: Equivalent Contrast Non-Linearities of the QCM for V1 from Subject 2.

The x-axis of each panel marks the equivalent contrast and the y-axis is the neuronal response. The gray curve in each panel is the Naka-Rushton function obtained using the QCM fit. These curves show the relationship between equivalent contrast and response. The parameters of the Naka-Rushton function are reported in upper left of each panel along with the 68% confidence intervals obtained using bootstrapping. The points in each panel are the GLM beta weights mapped via the QCM isoresponse contours of Subject 2 onto the equivalent contrast axis (see Model Appendix). The color of each point denotes the chromatic direction of the stimuli, as shown in the color bar. The left panel is for Measurement Set 1 and the right panel is for Measurement Set 2. Note that our maximum contrast stimuli do not produce a saturated response.

Isoresponse Contour Parameter Maps:

There is considerable interest in how sensitivity to modulations in the LM contrast plane varies with eccentricity. Understanding such variation is important both for describing visual performance and for drawing inferences regarding the neural circuitry that mediates color vision. Since the QCM separates chromatic

sensitivity from the dependence of the response on contrast, examining how the shape of the QCM isoresponse contour varies with eccentricity addresses this question in a contrast-independent manner. We fit the QCM to the BOLD time course of each vertex in the template map of visual areas developed by Benson et al. (2014). This allowed us to visualize how the parameters that describe the isoresponse contour varied with eccentricity within V1.

Figure 2-8 shows the QCM parameter maps for the ellipse angle, the minor axis ratio, and the variance explained displayed on the cortical surface. Here the data were averaged across all subjects and measurement sets. In all panels, the full extent of V1 is denoted by the black outline on the cortical surface, while the 20° eccentricity ROI used in the V1 analyses above is shown by the black dashed line. Apparent in the maps is that neither parameter varied systematically within V1, a feature of the data that is consistent across measurement sets and subjects. Outside of V1, the R^2 values were markedly lower, and there was higher variability in the QCM parameters.

We further examined the variance explained by the GLM, fit to every vertex on the cortical surface. Within early visual cortex (EVC, the spatial extent of the Benson template), we did not observe differences in R^2 larger than 0.03 in non-cross-validated model fits between the GLM and the QCM (GLM – QCM). We generally found that the variance explained by the GLM in vertices outside

of V1 was close to zero, with the exception of a small patch of values in the vicinity of hV4/VO1. The GLM variance explained in this area was roughly half of that explained within V1. To more fully characterize these regions, we fit the QCM to the median time course from the subject specific registrations of V4 and VO1 as defined by the retinotopic atlas from Wang et al. (2015) (implemented in Neuropythy). The parameters of the QCM fit for V4 and VO1 were generally consistent with those found for V1, although fit quality was worse. Overall, as our spatially uniform stimuli were not highly effective at eliciting reliable responses outside of V1, we refrain from drawing definitive conclusions about responses outside of V1. The average variance explained map within EVC for the GLM is shown in Figure 8 – figure supplement 1.

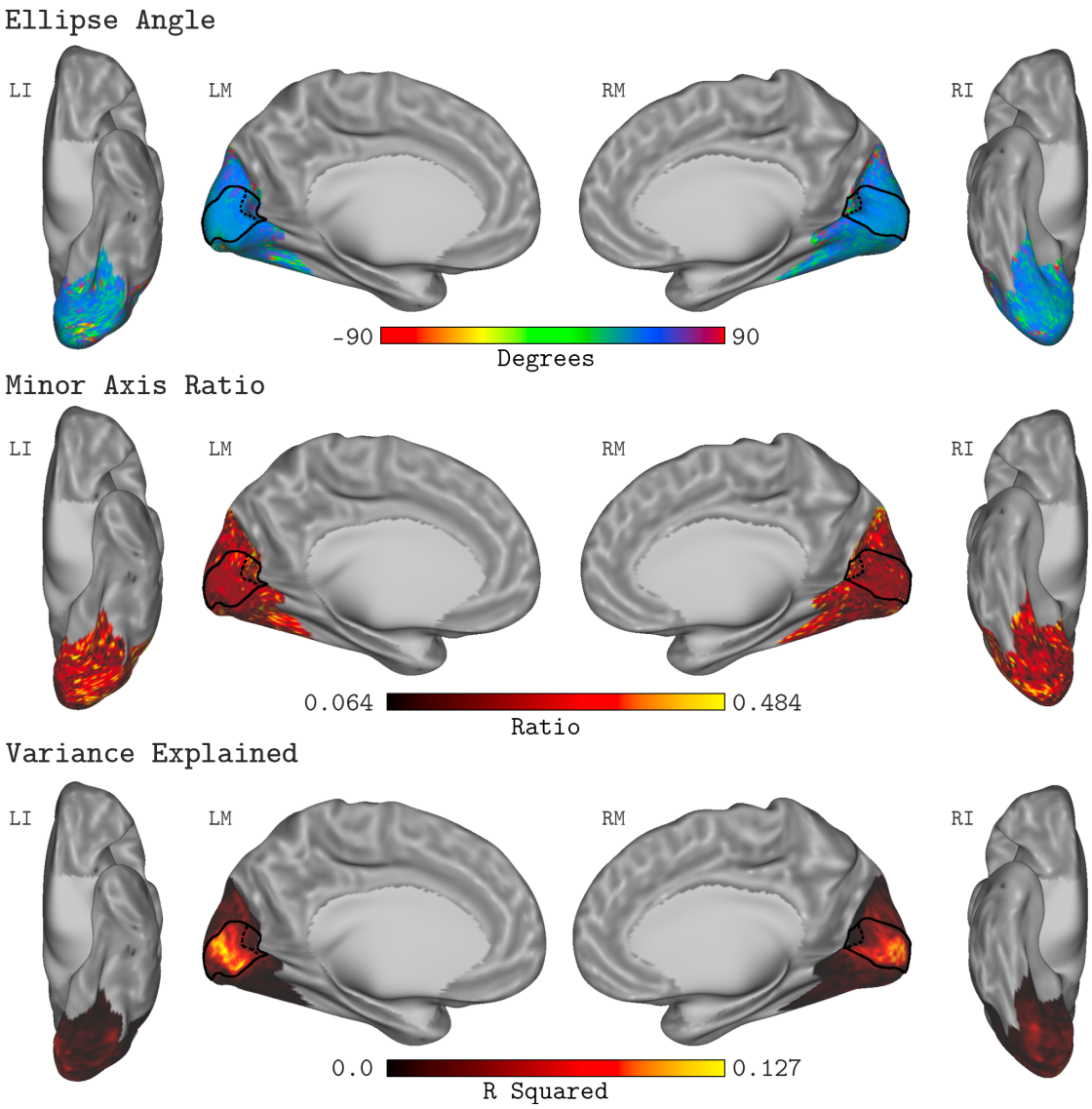

Figure 2-8: QCM Average Parameter Maps.

The QCM parameters, fit at all vertices within the visual cortex mask, averaged across all subjects and measurement sets. The top, middle, and bottom rows show maps of the average ellipse angle, minor axis ratio, and variance explained, respectively. The scale of the corresponding color map is presented below each row. The nomenclature in upper left of each surface view indicates the hemisphere (L: left or R: right) and the view (I: inferior, L: lateral, or M: medial). The medial views show the full extent of the V1 ROI on the cortical surface (denoted by the solid black outline). The 20° eccentricity boundary used to define the V1 ROI used for all analyses is shown by the black dashed line.

No Change in V1 Chromatic Sensitivity with Eccentricity:

We leveraged the QCM to examine how chromatic sensitivity varies with eccentricity within V1. Figure 2-9 plots the V1 QCM parameters as a function of eccentricity, for Subject 2. The left panel shows the minor axis ratio and the right panel shows the ellipse angle. In both plots, individual points represent a single vertex, with the x-axis giving the visual field eccentricity of that vertex obtained from the Benson et al. (2014) template, and the y-axis giving the parameter value. The transparency of each point indicates the R^2 value of the QCM fit for the corresponding vertex. The maximum R^2 value across vertices for Measurement Sets 1 and 2 were 0.25 and 0.24, respectively. The lines in each panel reflect a robust regression fit to the points. We found that there is little change in either parameter with eccentricity. For Subject 2, the best fit lines had slightly negative slopes for the minor axis ratio and slightly positive slopes for the ellipse angle, with good agreement across measurement sets. The overall change in parameter values from 0° to 20°, however, was small compared to the vertical spread of values at each eccentricity. We compared the change in parameter values from 0° to 20° to the variability across measurement sets for all three subjects (Table 2-1 for ellipse angle, and Table 2-2 for minor axis ratio). Across subjects, the majority of sessions showed small differences in parameter values from 0° to 20°, but we note that these did in some cases exceed the measurement set-to-set difference in the parameter values obtained for all of V1.

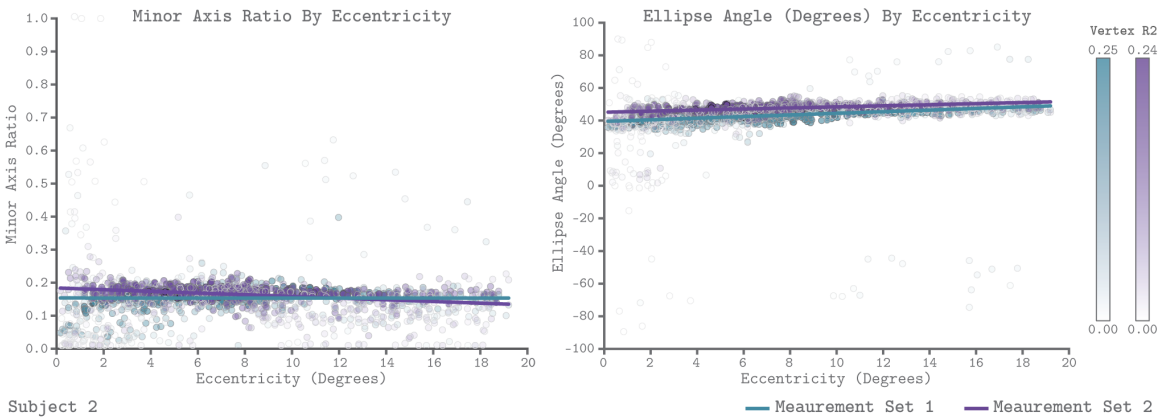

Figure 2-9: QCM parameters as a function of eccentricity for Subject 2.

The left and right panels show scatter plots of the minor axis ratio and ellipse angle plotted against their visual field eccentricity, respectively. Each point in the scatter plot shows a parameter value and corresponding eccentricity from an individual vertex. Green indicates Measurement Set 1 and purple indicates Measurement Set 2. The lines in each panel are robust regression obtained for each measurement set separately. The transparency of each point provides the R^2 value of the QCM at that vertex. The color bars provide the R^2 scale for each measurement set.

The plots shown in Figure 2-9 examine how the QCM parameters vary with eccentricity. To allow comparison with prior studies of how the BOLD response varies with eccentricity within V1 (Vanni, Henriksson, Viikari, & James, 2006; Mullen, Dumoulin, McMahon, de Zubicaray, & Hess, 2007; D'Souza, Auer, Frahm, Strasburger, & Lee, 2016), we also used the QCM to predict how the response would vary for stimuli in the L+M and the L-M directions, and plot these predicted responses as a function of eccentricity (Figure 9 – figure supplement 2). This was done on a vertex-by-vertex basis, using within-vertex QCM parameters. Specifically, we chose the 50% contrast stimulus condition for both the L-M and the L+M direction (contrasts of 0.06 and 0.30 respectively). Using these stimuli, we computed the predicted neuronal response by applying the

QCM forward model (the transformation to equivalent contrast and the Naka-Rushton steps) using the parameter values corresponding to that particular vertex. Examining the data in this way reveals a negligible change in response as a function of eccentricity for both the L+M and L-M directions, for all subjects and measurement sets. We return in the discussion to consider the relation between our results and those found in prior studies.

Minor Axis Ratio:

Subject	Set	Slope	Offset	Δ 0° to 20°	Δ Set to Set
S1	1	0.039	46.2	0.78	2.61
S1	2	0.313	41.4	6.26	
S2	1	0.496	39.5	9.92	3.76
S2	2	0.330	45.1	6.60	
S3	1	0.247	39.3	4.94	5.62
S3	2	0.425	43.3	8.50	

Table 2-1: Robust Regression Line Parameters - Minor Axis Ratio.

Robust regression line parameters summarizing the change in minor axis ratio with eccentricity for all subjects. These parameters are the same as seen for Subject 2 in Figure 2-10. The subject and set columns indicate the subject and measurement set of the robust regression fit. The slope and offset columns show the parameters of the regression line. The Δ 0° to 20° column is the magnitude of the change in the minor axis ration between 0° and 20° eccentricity. The Δ Set to Set column shows the absolute difference in the minor axis ratio fit to the V1 median time course between Measurement Set 1 and 2 (individual parameters are reported in Figure 2-7).

Ellipse Angle:

Subject	Set	Slope	Offset	Δ 0° to 20°	Δ Set to Set
S1	1	-1.19e-3	0.163	0.0238	0.09
S1	2	-4.17e-4	0.24	0.0084	
S2	1	-7.54e-6	0.154	0.0002	0.00
S2	2	-2.51e-3	0.183	0.0504	
S3	1	-3.27e-3	0.114	0.0654	0.03
S3	2	-3.9e-4	0.158	0.0078	

Table 2-2: Robust Regression Line Parameters - Ellipse Angle.

Robust regression line parameters summarizing the change in ellipse angle with eccentricity for all subjects. Columns are formatted the same as Table 2-1.

Discussion:

We develop a quantitative model of the visual cortex response to chromatic stimuli in the LM contrast plane, the quadratic color model (QCM), and examine its ability to fit V1 BOLD fMRI responses to spatially uniform chromatic stimuli. We find that the QCM accounts for the same cross-validated variance as a conventional GLM, with far fewer free parameters (6 as compared to 41). The model generalizes across both chromatic direction and contrast to predict V1

responses to a set of stimuli that were not used to fit the model parameters. The experiment was replicated for each subject using the same stimuli across separate measurement sets. Both the data and the model fits replicate well for each subject and are similar across subjects, giving us confidence in the power of the measurements.

The QCM is a separable model with respect to the effects of chromatic direction and contrast. This allowed us to evaluate the chromatic sensitivity in V1 of our subjects in a manner that is independent of the effects of contrast. We find that V1 is most sensitive to L-M contrast modulations and least sensitive to L+M contrast modulations, when contrast is defined using vector length in the LM contrast plane. This was shown in all subjects and measurement sets by the isoresponse contours of each subject being oriented at approximately 45° and having a minor axis that is roughly 5 times smaller than the major axis. This result is broadly consistent with previous fMRI studies of V1 chromatic contrast sensitivity, although the exact sensitivity ratio varies with the spatial and temporal properties of the stimuli (Engel, Zhang, & Wandell, 1997; Liu & Wandell, 2005; Mullen, Dumoulin, McMahon, de Zubicaray, & Hess, 2007; D'Souza, Auer, Frahm, Strasburger, & Lee, 2016; Mullen, Dumoulin, & Hess, 2010). By considering cortical responses in terms of the parameters of the QCM fit, we are

able to provide a quantitative account of chromatic sensitivity, as opposed to a categorical assignment of voxels as “color” or “luminance” responsive.

The QCM also allows us to examine the equivalent contrast response nonlinearity, although doing so is not the focus of this paper. This non-linearity depends on chromatic direction only through a direction-dependent contrast gain that is captured by the isoresponse contour. This can be observed in Figure 2-7 through the overlap of the non-linearity and the transformed GLM beta weights. Although we used the Naka-Rushton function to fit the nonlinearity, this was a choice of convenience and the precise shape of the non-linearity is not strongly constrained by our data set. This is because our stimuli did not drive the response into the saturating regime (Figure 2-7, Figure 7 – figure supplement 1). A stronger test of the contrast/direction separability embodied by the QCM, as well as stronger constraints on the shape of the non-linearity, would be provided by stimuli that drive the V1 response to saturation.

Neither the QCM nor the GLM explain all of the variance in the data. Since our experimental design did not involve multiple measurements with the same stimulus sequence (stimulus sequences were randomized across runs and measurement sets), we cannot untangle the degree to which the unexplained variance is due to systematic but unmodeled aspects of the response or to measurement noise. In comparing our reported R^2 values to those in other

studies, it is important to bear in mind that R^2 values are expected to be higher in cases where the signal being fit is the average time course over multiple runs with the same stimulus sequence, as compared to when the R^2 values are computed with respect to fits to individual runs, even if there is no difference in the quality of the underlying response model. Another factor that can affect R^2 is un-modeled physiological effects on the BOLD signal due to blinking, breathing, heart beats, etc. We did not collect eye tracking measurements or pulse oximetry, so we cannot model such effects.

In certain cases, attentional task difficulty can modulate BOLD responses (Kay & Yeatman, 2017). We employed only one level of attentional task difficulty and thus do not have data on how varying the attentional task might affect the responses we measured. We do not, however, have any particular reason to think that the chromatic tuning and contrast response functions we measured would have been substantially different in the context of different attentional task difficulty. In this regard, we note that Tregillus et al. (2021) measured contrast response functions for L-M and S-(L+M) color directions within V1 under two different attentional tasks and found no significant effect of task on the two contrast response functions.

Relation to Psychophysics:

A goal of systems neuroscience is to link measurements of neuronal properties to measurements of behavior. To make these links, the measurements made in each domain must be placed into a common space for comparison. The QCM provides a way to represent fMRI measurements in a manner that makes such comparisons straightforward. The contrast-invariant isoresponse contour from the QCM provides us with a stimulus-referred characterization of the BOLD fMRI response. Other methodologies, such as psychophysics or electrophysiology, may be used to obtain similar characterizations, allowing for comparisons across response measures within this common framework. For example, an approach to studying chromatic sensitivity is to characterize the isothreshold contour, which specifies the set of stimulus modulations that are equally detectable. Engel, Zhang, and Wandell (1997) took this approach and found that for low temporal frequencies the psychophysical isothreshold and BOLD fMRI isoresponse contours in the LM contrast plane were well-described as ellipses and had similar shapes. While some work has argued that psychophysical isothreshold may deviate subtly from ellipses (for review see (Stockman & Brainard, 2010), two studies that attempted to reject the elliptical form of such contours did not do so (Poirson, Wandell, Varner, & Brainard, 1990; Knoblauch & Maloney, 1996). Consistent with Engel, Zhang, and Wandell (1997), we found elliptical BOLD isoresponse contours at our 12 Hz temporal frequency with highest sensitivity in the L-M direction. As they note, although

psychophysical isothreshold contours remain well-described by ellipses at higher temporal frequencies, their orientation changes to favor L+M sensitivity over L-M sensitivity. This dissociation in the particulars of the isothreshold and BOLD isoresponse contours makes it unlikely that the mechanisms that contribute to the BOLD response in V1 limit psychophysical detection at the higher temporal frequencies, unless there are important temporal-frequency dependent changes in response variability that are not captured by the BOLD measurements.

Relation to Underlying Mechanisms:

Many theories of color vision postulate that signals from the L-, M- and S-cone photoreceptors are combined to form three post-receptoral mechanisms, roughly characterized as an additive combination of L- and M-cone contrast (L+M), an opponent combination of L- and M-cone contrast (L-M), and an opponent combination of S-cone contrast with L- and M-cone contrasts (S-(L+M)) (Stockman & Brainard, 2010; Shevell & Martin, 2017). Our finding that the major and minor axes of the isoresponse ellipse are well-aligned with the L+M and L-M modulation directions agrees with such theories. More generally, a quadratic isorepsonse contour can be produced by a quadratic mechanism that computes a sum of the squared responses of two underlying linear mechanisms, where the output of each linear mechanism is a weighted sum of L- and M-cone contrasts

(Poirson, Wandell, Varner, & Brainard, 1990). If the two linear mechanisms are L+M and L-M mechanisms with the weights appropriately chosen to represent the relative sensitivities (L-M sensitivity greater than L+M sensitivity), then the isoresponse contour of the resulting quadratic mechanism will be a close match to those we measured

Note, however, that other pairs of underlying mechanisms are also consistent with the same elliptical isoresponse contours (Poirson, Wandell, Varner, & Brainard, 1990), so that our isoresponse contours do not uniquely determine the sensitivity of the underlying linear mechanisms, even within the QCM together with the assumption that there are two such mechanisms.

More generally, one can construct non-quadratic models whose isoresponse contours approximate the ellipse we found using the QCM, and if this approximation is good our data will not reject such models. To illustrate this point, we developed and fit an alternate model, the Linear Channels Model (LCM), a variation on the Brouwer and Heeger channel model (Brouwer & Heeger, 2009; Kim, Hong, Shevell, & Shim, 2020), that accounts for our data about as well as the QCM (see Model Appendix; Figure 4 – figure supplement 1). The best fitting isoresponse contours found with the LCM, which could in principle deviate considerably from an ellipse, none-the-less approximate the ellipse we found using the QCM, but are not perfectly elliptical (Figure 6 – figure

supplement 1). Despite the agreement at the functional level of the isoresponse contours, the properties of the mechanisms underlying the LCM differ from those of the QCM, and these properties also differ across different instantiations of the LCM that account for the data equally well (see Model Appendix).

Because of the similarity in cross-validated R^2 values across the GLM, Naka-Rushton, QCM and LCM models, the reader may wonder whether the data have sufficient power to reject any isoresponse contour shape. To address this, we fit and cross-validated a form of the QCM with the angle constrained to 0 degrees. This resulted in a noticeably lower cross-validated R^2 for this model as compared to all other models we tested (Figure 4 – figure supplement 1, labeled at “QCM locked”) and provides reassurance that the data indeed have power to inform as to the shape of the isoresponse contour. We expect that other isoresponse contour shapes that differ from the best fitting QCM contour to a degree similar to that of the constrained ellipse would also be rejected.

Thus, while measurements of the BOLD response place constraints on the population response properties of the neuronal mechanisms, these properties are not uniquely determined given the BOLD response alone. The ambiguity is further increased if we consider properties of individual neurons, as the aggregate BOLD response will be shaped both by the response properties of such neurons and the numbers of different types of neurons in the overall neural

population. With that caveat, we make some general observations. Our stimuli were large, spatially uniform (effectively 0 c.p.d.) chromatic modulations that were temporally modulated at 12Hz. These stimuli could drive 'color', 'luminance' and 'color-luminance' cells as described by Johnson et al. (2001), depending on the particular chromatic direction. The 0 c.p.d. stimuli would presumably produce strong responses in the 'color' cells for our L-M direction, given that these cells are thought to behave as low-pass filters in the spatial domain and have unoriented receptive fields. It is less clear how strongly 'luminance' and 'color-luminance' cells would respond to our spatially uniform stimuli given that these cells are spatially bandpass. Schluppeck and Engel (2002)plot the spatial frequency response function estimated from the data from Johnson et al. (2001). These functions plot the average firing rate as a function of spatial frequency for the color, color-luminance, and luminance cells. Taking the lowest spatial frequency present in the dataset (0.1 c.p.d.), firing rates for color cells are roughly 5x times higher than the firing rates for luminance and color-luminance cells. This is the same as our average minor axis ratio which indicates V1 is roughly 5 times more sensitive to L-M than to L+M. A caveat here is that the 12 Hz flicker rate of our stimuli might shift responses relative to the analysis of Schluppeck and Engel (2002).

It is also important to note that our data do not distinguish the extent to which the response properties of the BOLD signals we measure in V1 are inherited from the LGN or are shaped by processing within V1. The spatiotemporal properties of our stimuli would robustly drive cells in cell in the LGN that project to V1(Lankheet, Lennie, & Krauskopf, 1998). Even though the signals measured in our experiment are spatially localized to V1, we cannot ascribe the observed response properties to particular neural processing sites. As such, the V1 sensitivities found from fitting the QCM may be inherited from areas prior to V1. In principle, they could also be affected by feedback from other cortical areas. We also undertook an analysis of data from the LGN, but found that these signals were too noisy to reveal reliable stimulus-driven responses in our data.

Finally, it is interesting to observe that quadratic models have been used to characterize the isoresponse properties of individual neurons in macaque V1 (Horwitz & Hass, 2012). Roughly half of the neurons tested in this paper were best fit by quadratic isoresponse surfaces (in the L-, M- and S-cone contrast space) while the other half were well fit by a linear model whose isoresponse surfaces were parallel planes. Of the quadratic isoresponse surfaces, some were ellipsoidal while others were hyperbolic. As noted above, despite this qualitative similarity, connecting the diverse population of individual neural responses to the

aggregated BOLD fMRI response remains a challenge for future work. The QCM fit to our data aids in this endeavor through the constraint its isoresponse contour places on the aggregated neural response.

Change of Chromatic Sensitivity with Retinal Eccentricity:

Many aspects of visual function change with eccentricity (Rosenholtz, 2016), and understanding and quantifying this variation is a key part of a functional characterization of vision. In addition, prior work attempts to relate such functional variation with eccentricity to variation in the underlying neural mechanisms. Relevant to the present work is the idea that variation of chromatic sensitivity with eccentricity can inform as to how signals from separate cone classes are combined by retinal and cortical neural circuitry (Lennie, Haake, & Williams, 1991; Mullen & Kingdom, 1996; Wool et al., 2018; Baseler & Sutter, 1997). In this context, we examined how the parameters of the QCM for individual vertices varied with eccentricity across V1. Overall, we find little change in the isoresponse contours with eccentricity within the central 20° of the visual field (Figure 2-9; Table 2-1 & 2-2; Figure 9 – figure supplement 1), and an analysis of how predicted response to L+M and L-M modulations would change with eccentricity also shows little or no effect (Figure 9 – figure supplement 2). In addition, we do not observe any clear change in the parameters of the contrast-

response function with eccentricity (analysis not shown). Overall, the BOLD response to chromatic modulations, as evaluated in our data using the QCM, is remarkably stable across V1. That the orientation of the elliptical isoresponse contours does not change with eccentricity is consistent with psychophysical studies that show that the relative L- and M-cone inputs to an L-M mechanism are stable across the visual field (Newton & Eskew, 2003; Sakurai & Mullen, 2006)}. The fact that our data do not show a loss in L-M sensitivity relative L+M sensitivity with increasing eccentricity, on the other hand, is not commensurate with psychophysical studies that do show such a loss (Stromeyer, Lee, & Eskew, 1992; Mullen & Kingdom, 2002; Mullen, Sakurai, & Chu, 2005; Hansen, Pracejus, & Gegenfurtner, 2009). As discussed above, BOLD fMRI sensitivity in V1 does not always mirror psychophysical sensitivity. Thus we focus below on comparison between our results and other fMRI studies of how sensitivity in V1 varies with eccentricity.

Several prior studies have used BOLD fMRI to examine how visual cortex responses vary with eccentricity to stimuli modulated in L-M and L+M directions (Vanni, Henriksson, Viikari, & James, 2006; Mullen, Dumoulin, McMahon, de Zubicaray, & Hess, 2007; D'Souza, Auer, Frahm, Strasburger, & Lee, 2016). Both Mullen et al. (2007) and Vanni et al. (2006) report a decrease in the V1 response to L-M modulations with eccentricity, while the response to L+M remains roughly constant. This differs from our result, and the size of the effects

in these papers are large enough that we would expect that if they were present in our data they would be visible in the analysis shown in Figure 9 – figure supplement 2 (see Figure 8 in Mullen et al., 2007 and Figure 8 in Vanni et al., 2006). Both speculate that the mechanism underlying this observation is non-selective (random) connections between L and M cones and retinal ganglion cell receptive fields. If these connections are non-selective, L-M sensitivity would be expected to decrease with eccentricity. This is because the area in which receptive fields pool cone inputs increases with distance from the fovea, progressively reducing the likelihood that random L- and M-cone inputs to the center and surround will produce chromatic opponency (Lennie, Haake, & Williams, 1991; Mullen & Kingdom, 1996; Wool et al., 2018). In contrast, D'Souza et al. (2016) find, for the majority of spatial frequencies studied, no change in L-M response relative to the response to isochromatic luminance modulations. This result is generally in line with our data, although at their lowest spatial frequencies D'Souza and colleagues observe a modest decline in relative L-M sensitivity. Following the same line of reasoning as Mullen et al. (2007) and Vanni et al. (2006) but reaching the opposite conclusion, D'Souza et al. (2016) take their result as supporting the idea that connections between cones and some classes of ganglion cells are selective for cone type and preserve chromatic sensitivity across the retina.

Comparison across our and the prior studies is complicated by variation in the stimuli used. Indeed, a dependency on spatial frequency is indicated by the data of D'Souza et al. (2016). We used spatially-uniform fields, while other studies use stimuli with higher-spatial frequency content. More generally, other factors could also lead to variation across studies, as well as complicate inferring the properties of retinal wiring from how psychophysical thresholds or measurements of cortical response vary with eccentricity.

One such factor is the changes in cone spectral sensitivity with eccentricity, caused primarily by variation in macular pigment and photopigment optical density. Variation in macular pigment and photopigment optical density can produce eccentricity-dependent deviations in the degree of actual cone contrast reaching the photoreceptors. Prior studies do not account for this variation, leading to the possibility that effects of eccentricity on sensitivity are due to receptoral, rather than post-receptoral mechanisms. In our study, we designed spectral modulations that produce the same contrasts in both 2-degree and 15-degree cone fundamentals (see Methods and Tables 2-5, 2-6 and, 2-7). This reduces the change in cone contrast with eccentricity for our stimuli.

Another factor, not emphasized in previous work, is that the size of the effects will depend on where on the underlying contrast response functions the responses to the stimuli in the chromatic directions being compared lie. To

understand this issue, consider the example in which the response for one chromatic direction is well into the saturated regime of the contrast-response function, while the other direction is not. This could lead to artifacts in the measured ratio of the response to the two directions with eccentricity, where any change in response for the saturated direction is hidden by a ceiling effect. Our study minimizes the role of this factor through measurement and modeling of the contrast response functions in each chromatic direction, allowing the QCM to extract a contrast independent shape for the isoresponse contours.

Although changes in sensitivity with eccentricity can be caused by mechanisms at many levels of the visual system, the lack of such variation in our data is parsimoniously explained by retinal output that preserves chromatic sensitivity with eccentricity. This interpretation is challenged by studies that show random (Wool et al., 2018) or close to random (Field et al., 2010) inputs from L- and M-cones to midget ganglion cell centers in the retinal periphery. Not all studies of midget cell chromatic responses or their parvocelluar LGN counterparts agree with non-selective wiring (Reid & Shapley, 1992; Martin, Lee, White, Solomon, & Ruttiger, 2001; Martin, Blessing, Buzas, Szmajda, & Forte, 2011; Lee, Shapley, Hawken, & Sun, 2012). One possible cortical mechanism that could compensate for the reduced L-M signal-to-noise ratio with eccentricity as predicted by random wiring models is supra-threshold compensation for

reduced signals. Mechanisms of this sort have been postulated in the domain of contrast perception (Georgeson & Sullivan, 1975) and anomalous trichromatic vision (Boehm, MacLeod, & Bosten, 2014; Tregillus et al., 2021). Another possibility is a differential change in stimulus integration area across chromatic directions and with eccentricity. However, this latter possibility is not supported by fMRI population receptive field (pRF) measurements for modulations in different chromatic directions in V1 (Welbourne, Morland, & Wade, 2018).

Generalizing the QCM:

In our study, we only measured responses to stimuli confined to the LM contrast plane. A more general account of chromatic contrast sensitivity requires modulating stimuli in all three-dimension of the full L-, M- and S-cone contrast space**.** The QCM may be generalized in a straightforward manner to handle this expanded stimulus set by replacing the elliptical isoresponse contours with ellipsoidal isoresponse surfaces, but we have yet to test this generalization.

Another way in which the QCM may be generalized, even within the LM contrast plane, is to consider modulations at other temporal frequencies. In our experiment, we fixed the temporal modulation of the stimulus at 12 Hz. The QCM could be readily fit to data from modulations at various other temporal frequencies with the goal of observing how the chromatic sensitivity changes.

With this, one could further examine the BOLD response to mixtures of different temporal frequency modulations. This is particularly interesting in that any arbitrary complex temporal modulation can be decomposed into an additive mixture of modulations at different temporal frequencies and phases (Bracewell, 1978). If the response to temporal frequency mixtures can be predicted via a simple rule of combination (such as linearity), establishing the QCM parameters for a well-chosen set of temporal frequencies would enable prediction of the BOLD response to chromatic stimuli modulated with complex temporal sequences.

Just as we had a fixed temporal frequency in our experiment, the stimulus presented also had a fixed spatial frequency (0 c.p.d.). Similar to the temporal domain, complex spatial images can be broken down into a combination of oriented 2-dimensional sine wave patterns at single spatial frequencies and phases. Examining how the QCM fits change with changing spatial frequencies might allow for models of the BOLD response to arbitrary complex spatial stimuli. Consistent with this general goal, recent work has developed quantitative forward models of the BOLD response of early visual cortex to a variety of achromatic modulations with different spatial patterns (Kay, Winawer, Mezer, & Wandell, 2013; Kay, Winawer, Rokem, Mezer, & Wandell, 2013). These models have sequential stages of processing that operate on an input image and transform it

into a model of the BOLD response. How such models should be generalized to handle chromatic modulations is not known. If the QCM holds for other spatial frequencies, such a result would place important constraints on the appropriate generalization for such forward models to incorporate color.

Materials and Methods

Subjects:

Three subjects (age 23, 25, and 26 years; 2 female) took part in the fMRI experiment. All subjects had normal or corrected to normal acuity and normal color vision. The research was approved by the University of Pennsylvania Institutional Review Board. All subjects gave informed written consent and were financially compensated for their participation.

Experimental Overview:

Each subject participated in four sessions of data collection. The first two sessions constituted Measurement Set 1, and the second two sessions Measurement Set 2 (Measurement Set 2 being a replication of Measurement Set 1). In both sessions, subjects underwent 48 minutes of fMRI scanning, with Session 1 also including two anatomical scans (a T1-weighted and a T2-

weighted scan). Subjects were tested for color vision deficiencies in a separate session, using the Ishihara pseudoischromatic plates (Ishihara, 1977). All subjects passed with no errors. The experimental procedures for Measurement Set 1 were preregistered (https://osf.io/wgfzy/), and an addendum describes the replication Measurement Set 2 (https://osf.io/zw6jp/).

Digital Light Synthesis and Silent Substitution

All stimuli were generated using a digital light synthesis device (OneLight Spectra). This device produces desired spectra through the use of a digital micro-mirror device chip that in the configuration we used allows for the mixture of 56 independent primaries with a FWHM of ~16 nm and a refresh rate of 100 Hz.

Stimuli were generated to evoke specific photoreceptor responses through the use of silent substitution (Estévez & Spekreijse, 1982). Silent substitution operates on the principle that there exist sets of light spectra that, when exchanged, selectively modulate the activity of specified cone photoreceptors. Thus, stimulus modulations relative to a background can be generated such that they nominally modulate the activity of only the L-, M-, or S-cones, or combinations of cone classes at specified contrasts. Additional information on how the stimuli were generated is provided in Spitschan et al. (2015).

The stimuli account for differences in the cone fundamentals between the fovea and the periphery. This was done by treating the L, M, and S cones in the 2- and 15-degree CIE physiologically-based cone fundamentals (CIE, 2007) as six classes of photoreceptors. For any desired set of L-, M-, and S-cone contrasts, we designed modulations that attempted to provide the same contrasts on the 2- and 15-degree L-cone fundamentals, on the 2- and 15-degree M-cone fundamentals, and on the 2- and 15-degree S-cone fundamentals. This is possible because our device has 56 primaries, rather than the typical 3 of RGB displays. Our procedure has the effect of creating light spectra that reduce differences in the L-, M- and S-cone contrasts produced across the retina. The cone fundamentals were tailored to the age of each subject, to account for age-related differences in typical lens density (CIE, 2007). See Tables 2-5, 2-6 and, 2-7 for the central and peripheral maximum stimulus contrast values for each subject and measurement set.

Spectroradiometric measurements of the stimuli were made before and after each experimental session. During the measurements made prior to the experiment, a correction procedure was run in which the spectral power distribution of the modulation in each chromatic direction were adjusted to minimize the difference between the measured and desired cone contrasts for the 2- and 15-degree cone fundamentals. These corrections were made to the modulation spectra at the maximum contrast used in each direction. The order in

which spectroradiometric measurements were taken during an experimental session was 1) five pre-correction measurements for each chromatic direction used in the session, 2) the corrections procedure, 3) five post-correction measurements per direction, and 4) five post-experiment measurements per direction. The mean of post-correction and post-experiment cone contrast measurements for the individual subjects and measurement sets are provided in Tables 2-5, 2-6 and, 2-7.

Visual Stimuli:

The stimuli were confined to the LM plane of cone contrast space (Figure 2-10A; see also Figure 2-1A). Cone contrast space has three axes that are defined by the relative change in the quantal catch of the L, M, and S cones when modulating between the light spectra of interest and a specified reference spectrum. We refer to the reference spectrum used to calculate this relative change in cone excitations as the background (nominal chromaticity; x = 0.459, y = 0.478, luminance Y = 426 cd/m^2; chromaticity and luminance computed with respect to the XYZ 10° physiologically-relevant color matching functions, as provided at https://cvrl.org). The background corresponds to the origin of cone contrast space. The LM contrast plane is a subspace of cone contrast space consisting of modulations that affect only L- and M-cone excitations, but which

leave S-cone excitations unchanged relative to the background. A point in cone contrast space specifies how much L- and M-cone contrast is produced by modulating from the background to the specified stimulus. Points lying along the x-axis of Figure 2-10A modulate only L-cone contrast while M-cone contrast remains constant. Points lying along the y-axis modulate only M-cone contrast while keeping L-cone contrast constant. Points in intermediate directions modulate both L- and M-cone contrast, in proportion to the x- and y-axis components.

All stimuli were spatially uniform (0 c.p.d.), full-field temporal modulations with a radius of 30° visual angle. The temporal modulations were bipolar sinusoids around the reference background, with the positive and negative arms designed to increase and decrease targeted cone excitations in a symmetric fashion. All stimuli were modulated at 12 Hz (Figure 2-10B). A single modulation is thus described by pair of vectors in the LM contrast plane that have an angle of 180° between them, corresponding to the positive and negative arms of the modulation (Figure 2-10A). The entries of the vectors are the L- and M-cone contrasts of the end points of each arm. In this paper, we refer to a modulation by the angle made between its positive arm and the positive x-axis (corresponding to 0° in the LM contrast plane), with angle increasing counterclockwise. We refer to each angle tested as a chromatic direction. In total, we tested the eight chromatic directions: -45°, -22.5°, 0°, 22.5°,45°, 67.5°, 90°, and 112.5°. The -45°,

0°, 45°, and 90° directions correspond to L-M, L-cone isolating, L+M, and M-cone isolating directions respectively. For all chromatic directions, the spectra were designed to produce constant S-cone contrast.

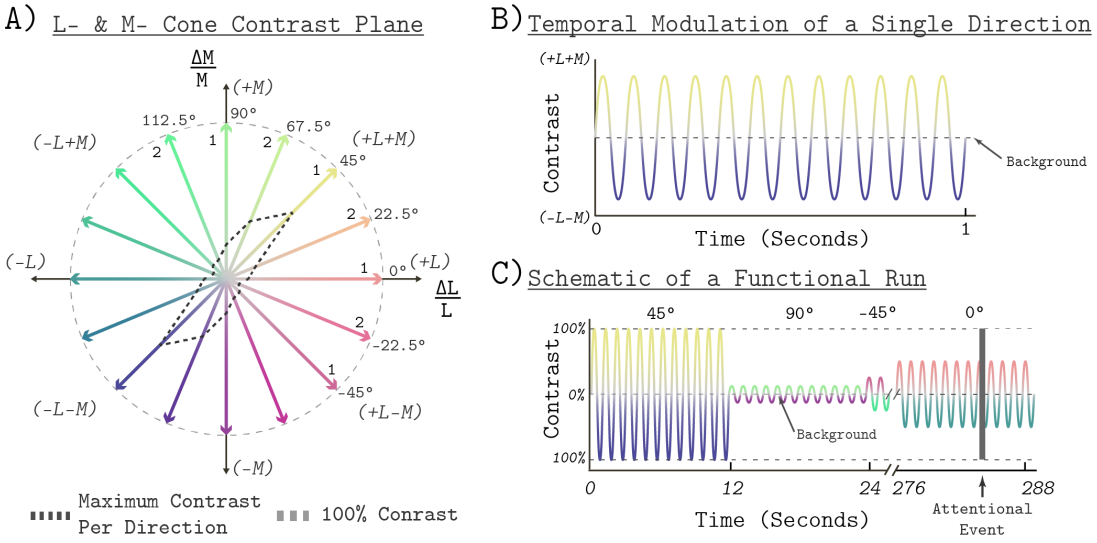

Figure 2-10: Stimulus Space and Temporal Modulations.

A) The LM contrast plane. A two-dimensional composed of axes that represent the change in L- and M-cone activity relative to the background cone activation, in units of cone contrast. Each aligned pair of vectors in this space represents the positive (increased activation) and negative (decreased activation) arms of the bipolar temporal modulations. We refer to each modulation by the angle of the positive arm in the LM contrast plane, with positive ΔL/L being at 0°. The black dashed lines show the maximum contrast used in each direction. The gray dashed circle shows 100% contrast. The "1" or "2" next to each positive arm denotes the session in which a given direction presented. The grouping was the same for Measurement Set 1 and Measurement Set 2. B) The temporal profile of a single bipolar chromatic modulation. This shows how the cone contrast of a stimulus changed over time between the positive and negative arms for a given chromatic direction. The particular direction plotted corresponds to the 45° modulation at 12 Hz temporal frequency. The temporal profile was the same for all chromatic directions. C) Schematic of the block structure of an functional run. Blocks lasted 12 seconds and all blocks were modulated around the same background. The amplitude of the modulation represents the contrast scaling, relative to its maximum contrast, for that block. Each run lasted a total of 288 seconds. The dark gray vertical bar represents an attentional event in which the light stimulus was dimmed for 500 milliseconds.

We express the stimulus contrast of a modulation as the vector length (L2 norm) of the cone contrast representation of its positive arm (Figure 2-10A).

Gamut limitations of the light synthesis engine result in different maximum stimulus contrasts for different chromatic directions (see heavy dashed contour in Figure 2-10A). The maximum contrast used in each direction is provided in Table 2-3. For all directions, we tested five contrast levels. The contrast levels tested for each chromatic direction were selected to be log spaced relative to the maximum contrast used. The relative contrasts were 100, 50, 25, 12.5, and 6.25 percent. We also measured a 0 contrast reference condition in which the background without modulation was presented.

Direction	-45°	-22.5°	0°	22.5°	45°	67.5°	90°	112.5°
L-Contrast	8.49%	7.85%	14%	18.48%	42.43%	15.31%	0%	4.98%
M-Contrast	8.49%	3.25%	0%	7.65%	42.43%	36.96%	22%	12.01%
S-Contrast	0%	0%	0%	0%	0%	0%	0%	0%
Total Contrast	12%	8.5%	14%	20%	60%	40%	22%	13%

Table 2-3: Nominal maximum contrast per direction.

The top row indicates the chromatic direction in the LM plane. The L, M, and S contrast rows show the desired contrast on the L, M, and S cones respectively. The total contrast is the vector length of stimuli made up of the L, M, and S cone contrast components and is the definition of contrast used in this study.

Experimental Design:

We measured whole brain BOLD fMRI responses to stimuli modulated in eight different chromatic directions, each with five contrast levels, using a block design. In total, we tested 40 different combinations of contrast levels and chromatic directions. We split the eight chromatic directions into two separate scanning sessions of four directions each (Figure 2-11A). In Session 1, we

tested -45° (L-M), 0° (L Isolating), 45° (L+M), and 90° (M Isolating). In Session 2, we tested the other four directions (-22.5°, 22.5°, 67.5°, and 112.5°). The order of data collection for the two sessions was randomized across subjects. A session consisted of 10 runs and each run had a duration of 288 seconds. Within a run, each contrast/direction pair was presented within 12 second blocks (Figure 2-11). The order of contrast/direction pairs was psuedorandomized within each run. Along with four presentations of a background-only block, each run consisted of 24 blocks. The background-only blocks contained no temporal contrast modulation, providing a reference condition for data analysis. We chose 12 Hz modulations based upon prior work showing that for stimuli similar to the ones used in this study (L+M and L-M), this frequency elicited a robust response in V1 (Spitschan, Datta, Stern, Brainard, & Aguirre, 2016). Within a block, modulations were ramped on and off using a 500 ms half-cosine. Figure 2-10C provides a schematic of the structure of an functional run.

During each functional run, subjects engaged in an attention task. This task consisted of pressing a button every time the stimulus dimmed (Figure 2-10C). Each attentional event lasted for 500 ms. The probability of an attentional event occurring in a block was 66% in Measurement Set 1 and a 33% in Measurement Set 2. The onset time of an attentional event within a block was random except that the event could not occur during the on and off half-cosine

ramp. The purpose of the attention task was to encourage and monitor subject wakefulness throughout the scan session. All subjects responded to 100% of the attentional events throughout all runs and sessions.

Each subject was studied during an initial pair of scanning sessions that we call Measurement Set 1 (Figure 2-11A), and a subsequent pair of replication scans that we call Measurement Set 2 (Figure 2-11B). Measurement Set 2 tested

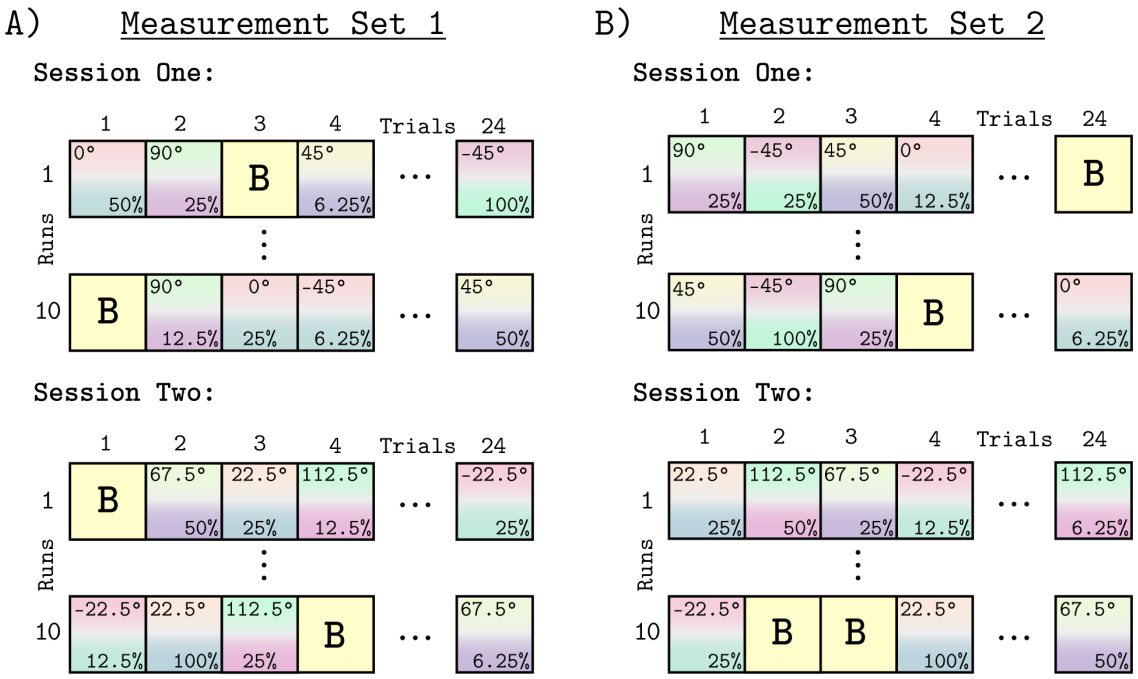

Figure 2-11: Experimental Design.

Panels A and B show the block design used for all runs and sessions. Panel A shows Measurement Set 1 which contained two separate MRI sessions. Each session contained four of the eight chromatic directions. The split of directions across the two sessions was the same for all subjects, but which session each subject started with was randomized. Within a session we collected 10 functional runs, each containing 24 blocks. The 24 blocks consisted of 20 direction/contrast paired stimulus blocks (depicted by the gradient squares with direction noted at top and the contrast at bottom of each square) and 4 background blocks (squares marked “B”). The order of blocks within each run was randomized, with each contrast/direction pair shown once per run. Each run had a duration of 288 second. Panel B shows Measurement Set 2, which was a replication of Measurement Set 1, with session order and order of blocks within run re-randomized. There were 960 blocks across both measurement sets.

stimuli with the same chromatic directions and contrast levels as Measurement Set 1. The grouping of chromatic directions within a session was the same across measurement sets. The two measurement sets used different pseudo-randomized presentation orders. Both measurement sets also randomly assigned which session was acquired first. Across both sessions and measurements sets, we collected a total of 960 blocks per subject. The two measurement sets were analyzed separately.

MRI Data Acquisition:

MRI scans made use of the Human Connectome Project LifeSpan protocol (VD13D) implemented on a 3-Tesla Siemens Prisma with a 64-channel Siemens head coil. A T1-weighted, 3D, magnetization-prepared rapid gradient-echo (MPRAGE) anatomical image was acquired for each subject in axial orientation with 0.8 mm isotropic voxels, repetition time (TR) = 2.4 s, echo time (TE) = 2.22 ms, inversion time (TI) = 1000 ms, field of view (FoV) = 256 mm, flip angle = 8°. BOLD fMRI data were obtained over 72 axial slices with 2 mm isotropic voxels with multi-band = 8, TR = 800 ms, TE = 37 ms, FOV = 208 mm, flip angle = 52°. Head motion was minimized with foam padding.

During MRI scanning, subjects were supine inside the magnet. Visual stimuli were presented through an MRI compatible eyepiece to the right eye of

the subject. Stimuli were delivered from the digital light synthesizer through a randomized optical fiber cable (Fiberoptics Technology Inc.). The randomization of the fiber optic cable helped to minimize any spatial inhomogeneities in the spectrum of the stimulus. The eye piece provided adjustable focus to account for variation in refractive error. As the stimulus was a spatially uniform field, however, the effect of any spatial blur upon the stimulus was minimal.

Subjects used either button of a 2 button MR compatible response device (Current Designs) to respond to attention events during the functional runs.

MRI Data Preprocessing:

Both anatomical and functional data were preprocessed according to the HCP minimal preprocessing pipeline (Glasser et al., 2013) Briefly, the anatomical data were passed through the pre-freesurfer, freesurfer, and post-freesurfer steps of the HCP minimal preprocessing pipeline. This was used to create an MNI registration, a Freesurfer segmentation (Dale, Fischl, & Sereno, 1999; Fischl, Sereno, & Dale, 1999), and a surface mesh. The functional data were preprocessed with both the volume and surface pipelines. The volume pipeline applied gradient distortion correction, motion correction (FLIRT 6 DoF; Jenkinson, 2002), top-up phase encoding distortion correction (Smith et al., 2004), and registered the functional images to the anatomical images. The

surface pipeline mapped the volume data to the CIFTI grayordinate space which includes a left and right 32K cortical surface mesh and subcortical voxels. Finally, the functional data were passed through the ICAFIX pipeline, which uses independent component analysis and noise/not-noise classification to denoise the time course.

After initial preprocessing, we performed a series of subsequent steps before analyzing the time course data. We used a V1 region of interest (ROI) to extract the time series from primary visual cortex (see below for definition of retinotopic maps). The signals from each voxel were mean centered and converted to percent signal change. We then performed nuisance regression using the relative motion estimates and attentional events as regressors. The relative motion regressors (translation of X, Y, and Z and yaw, pitch, and roll) were mean centered and scaled by their respective standard deviations. The attention event regressor was modeled as a series of delta functions located within the TRs in which the events occurred, convolved with a hemodynamic response function. The nuisance regression was performed using the MATLAB linear regression function *mldivide* (MathWorks) with the residual of the model used as the “cleaned” timed series.

Next, we time-point censored the time series of all voxels based on the motion estimates. This was done using a modified version of Power et al. (2014).

We converted the relative yaw, pitch, and roll estimates to millimeters by using the distance that each of these angles subtend on an assumed 50 mm sphere. We then took the L2-norm of the 6 translation and mm rotation estimates as a metric of frame-wise displacement (FD). We censored three contiguous TRs centered on any time point with an FD > 0.5. Time points that exceeded the threshold were excluded from analysis, and a table of the number of censored frames can be found in Table 2-5. Finally, we applied polynomial detrending by fitting a fifth order polynomial to the time course from each voxel and subtracting it from the signal. Analyses performed at the level of V1 were done using the median value across voxels at each time point to represent the V1 signal. Vertex-wise analyses were performed on the preprocessed time course of individual vertices.

Subject 1 – Measurement Set 2: Session 1										
Run Number	1	2	3	4	5	6	7	8	9	10
Number of Censored Frames (n/360)	0	0	8	18	0	26	47	4	0	0
Subject 1 – Measurement Set 2: Session 2										
Run Number	1	2	3	4	5	6	7	8	9	10

Number of Censored Frames (n/360)	0	0	0	0	0	0	0	7	0	0

Table 2-4: Number of Censored fMRI frames per Run.

Values shown are for Subject 2 measurement set 2. The top set of rows show data for session one and the bottom set of the show data for session 2. Each set of rows show the number of censored frames per run out of 360 frames. Subjects and sessions not shown mean that no frames were censored in those runs.

Definition of Retinotopic Maps:

Retinotopic regions of interest (ROI) were defined using the anatomical template neuropythy (Benson, Butt, Brainard, & Aguirre, 2014) which provides eccentricity and polar angle maps for V1, V2, and V3. From this atlas, we defined a V1 ROI using the voxels in area V1 between 0-20° eccentricity and 0-180° polar angle. We set the eccentricity upper bound of the ROI to be 20° to provide a conservative boundary to ensure that we only analyzed stimulated vertices. This accounts for some uncertainty in the exact retinal size of the stimulated area due to, for example, variation in the distance of the eyepiece to the eye of the subject.

To define the retinotopic regions of interest used for hV4/Vo1 analysis, we registered the Wang et al. (2015) retinotopic atlas to CIFTI space. This was achieved using the subject specific atlas as defined by Neuropythy (Benson & Winawer, 2018). This atlas was then registered to MNI space through the use of ANTs (Avants, Epstein, Grossman, & Gee, 2008). With the atlas in MNI space,

we then transformed it to CITFI greyordinate space and used the hV4 and the VO1 ROIs to extract the time series data.

Subject Specific Hemodynamic Response Function:

We derived subject-specific hemodynamic response functions (HRFs) for each subject and measurement set. The HRF was derived using all the functional runs within a measurement set, using the V1 region of interest median data. The time-series data were fit with a non-linear model that simultaneously estimated the beta weights of the GLM to fit stimulus responses, and the parameters of an HRF model. The HRF model was composed of the first three components of the "FLOBS" basis set (Woolrich, Behrens, & Smith, 2004). The best fitting HRF model was then used to fit that subject's data for both the GLM and QCM models.

General Linear Model:

We used an ordinary least squares regression with a stimulus design matrix that described the stimulus order of a run. The regression matrix contained one regressor per stimulus block as well as a single regressor for the baseline, with the length of the regressor equal to the number of timepoints (360 TRs). The regressor for each stimulus block in a run was modeled by a binary vector that

indicated the timepoints when the stimulus was present (ones) or absent (zeros), convolved with the HRF. This resulted in 21 GLM beta weights per run. For all analyses, model fitting was performed using the concatenation of all functional runs within a measurement set. For fitting of the GLM, we concatenated the stimulus design matrices such that like contrast/direction pairs were modeled by the same regressor. The concatenated stimulus design matrix for a measurement set had a total of 41 regressors (20 direction/contrast pairs from Session 1, 20 direction/contrast pairs from Session 2, and a shared baseline regressor) and 7200 timepoints. Additional details of the GLM are provided in the Model Appendix section.

Contrast Response Functions:

To obtain contrast response function for each color direction, the time course data for each run was fit using a general linear model to obtain the effect that each stimulus had on the BOLD fMRI response. Grouping the GLM beta weights by chromatic direction defined a set of 8 contrast response functions (CRFs), one per direction. A CRF describes the relationship, within a particular chromatic direction, between the contrast of the stimulus and the measured response. The CRFs obtained using the GLM beta weights fit to the concatenated time series of Subject 2 can be seen in Figure 2-3. The panels of

Figure 2-3 show the CRFs for the eight different chromatic directions. The CRFs for Subject 1 and 2 can be seen in Figure 2 - figure supplement 1-2.

Error Bars:

The error bars and error regions in all figures are the 68 percent confidence intervals. We used 68% confidence intervals as this approximates +/- 1 SEM for a normal distribution. The percentiles we use to estimate error are the result of a bootstrap analysis. The bootstrap analysis was implemented as random sampling with replacement of the runs within a measurement set. The randomly drawn runs in both sessions were concatenated and fit by all models. We performed 200 bootstrap iterations and identified the 68% percent confidence interval from the bootstrap results.

Leave-Runs-Out Cross-Validation:

To evaluate model performance, we employed a leave-runs-out cross-validation strategy. For each cross-validation iteration, runs from Session 1 and Session 2 were randomly paired within the same measurement set. These pairs of runs were held out and the models were fit to the remaining 18 runs. From these model fits, a time course prediction for the left-out runs were obtained from

both models. We computed the R^2 value between these predictions and the time course of the held-out runs. The average R^2 value across the 10 cross-validation iterations was used to compare models.

Leave-Session-Out Cross-Validation:

To evaluate the generalizability of the QCM, we implemented a leave-session-out cross-validation. As the eight chromatic directions tested were separated into two sessions with the same grouping across all subjects and measurement sets, we could evaluate the ability of the QCM to make predictions for chromatic directions and contrasts not used to fit the model parameters. Within each measurement set, we fit the QCM to Sessions one and two separately and evaluated how well the parameters of the model predicted responses to stimulus directions in the held-out session. These predicted responses were grouped by chromatic direction in order to construct a set of contrast response functions. The error bars in the CRFs are the 68% confidence intervals computed using bootstrapping, where we randomly sampled runs with replacement and compute the leave-session-out cross-validation a total of 200 times.

Surface Parameter Map Generation:

Cortical surface maps were generated to visualize the ellipse angle and minor axis ratio parameters of the QCM on the V1 cortical surface. To generate the surface parameter maps, we fit the QCM, within a single vertex, to the concatenated time course from all runs in a measurement set. We repeat this fit for all vertices within the visual areas template map from neuropythy (Benson, Butt, Brainard, & Aguirre, 2014). To visualize the surface parameter maps in a manner that highlights differences in fits as a function of cortical position, we created a series of scatter plots that relate the minor axis ratio and angle parameters to the eccentricity of their respective vertices. The regression lines in the scatter plots are robust regression lines implemented through the built in MATLAB function *robustfit* which adaptively reweights the data to discount the effects of outliers.

Parameter Fitting:

We fit QCM the model to the concatenated time series for both sessions within a measurement set for each subject. The data were fit using the MATLAB function *fmincon* to find a set of model parameters that minimize the difference between the actual fMRI time course and the QCM prediction of the time course, computed as the root mean squared error.

Preprocessing and Analysis Code:

All code used to perform analyses in this paper may be found in our public GitHub repository: https://github.com/gkaguirrelab/LFContrastAnalysis.

Spectroradiometric Stimulus Validations

The tables below show the stimulus validation measurements for all subjects and sessions. The tables show the mean and standard deviation of stimulus vector angles and lengths computed from 10 validation measurements (5 pre-experiment, 5 post-experiment). Center and periphery denote which set of cone fundamentals were used to calculate cone contrast of the stimuli referring either the 2° or 15° CIE fundamentals, respectively.

Subject 1 – Measurement Set 1								
Nominal Angle	-45°	-22.5°	0°	22.5°	45°	67.5°	90°	112.5°
Center Angle	-41.23 ±3.13	-15.90 ±6.59	2.17 ±1.05	23.43 ±0.23	45.21 ±0.23	69.36 ±1.61	87.98 ±1.26	120.94 ±8.45
Periphery Angle	-42.85 ±3.04	-16.31 ±6.18	1.61 ±0.44	22.75 ±0.22	44.78 ±0.22	68.13 ±1.54	88.72 ±0.18	119.67 ±8.04

Nominal Contrast	12%	8.5%	14%	20%	60%	40%	22%	13%
Center Contrast	12.14 ±0.05	9.02 ±0.75	14.44 ±0.37	21.05 ±0.79	60.92 ±0.09	38.01 ±1.97	21.39 ±0.85	12.56 ±0.38
Periphery Contrast	12.00 ±0.04	8.93 ±0.72	13.98 ±0.35	20.28 ±0.73	58.73 ±0.09	37.81 ±1.89	21.42 ±0.55	12.48 ±0.36
Subject 1 - Measurement Set 2								
Nominal Angle	-45°	-22.5°	0°	22.5°	45°	67.5°	90°	112.5°
Center Angle	-45.09 ±0.55	-22.44 ±0.98	3.49 ±2.27	22.97 ±0.15	45.18 ±0.03	67.75 ±0.24	87.81 ±1.69	112.99 ±1.03
Periphery Angle	-46.16 ±0.55	-22.32 ±0.99	3.24 ±2.77	22.39 ±0.19	44.92 ±0.02	66.85 ±0.21	87.33 ±1.24	68.34 ±0.92
Nominal Contrast	12%	8.5%	14%	20%	60%	40%	22%	13%
Center Contrast	11.75 ±0.01	8.28 ±0.08	13.78 ±0.09	20.35 ±0.22	60.26 ±0.48	37.62 ±0.11	21.82 ±0.08	12.69 ±0.05
Periphery Contrast	11.65 ±0.02	8.29 ±0.08	13.53 ±0.09	19.79 ±0.18	58.47 ±0.48	38.16 ±0.10	21.99 ±0.10	12.81 ±0.06

Table 2-5: Stimulus Validation Measurements for Subject 1.

The top set of rows show data for measurement set one and the bottom set show data for measurement set 2. The dark gray rows show the nominal angle and contrast. Each cell shows the mean and standard deviation of stimulus vector angles and lengths computed from 10 validation measurements (5 pre-experiment, 5 post-experiment). Center and periphery denote which set of cone fundamentals were used to calculate cone contrast of the stimuli referring either the 2° or 15° CIE fundamentals, respectively.

Subject 2 - Measurement Set 1								
Nominal Angle	-45°	-22.5°	0°	22.5°	45°	67.5°	90°	112.5°
Center Angle	-45.73 ±1.06	-19.23 ±2.51	1.71 ±0.98	24.04 ±0.39	45.43 ±0.09	68.36 ±0.53	87.87 ±1.64	114.92 ±1.90
Periphery Angle	-47.03 ±1.02	-18.91 ±2.40	1.63 ±0.77	23.65 ±0.38	44.99 ±0.09	67.18 ±0.52	87.65 ±1.09	114.11 ±1.86
Nominal Contrast	12%	8.5%	14%	20%	60%	40%	22%	13%
Center Contrast	12.04 ±0.11	8.41 ±0.21	14.01 ±0.08	20.45 ±0.52	60.72 ±0.38	39.68 ±0.63	21.82 ±0.23	12.73 ±0.16
Periphery Contrast	11.88 ±0.11	8.36 ±.21	13.58 ±0.07	19.81 ±0.51	58.56 ±0.35	39.41 ±0.59	21.82 ±0.24	12.62 ±0.14
Subject 2 - Measurement Set 2								
Nominal Angle	-45°	-22.5°	0°	22.5°	45°	67.5°	90°	112.5°
Center Angle	X	-25.85 ±3.20	X	22.72 ±0.38	X	67.42 ±0.16	X	112.03 ±1.22
Periphery Angle	X	-26.43 ±3.04	X	22.35 ±0.35	X	66.36 ±0.16	X	110.12 ±1.17
Nominal Contrast	12%	8.5%	14%	20%	60%	40%	22%	13%
Center Contrast	X	8.36 ±0.16	X	19.77 ±0.23	X	39.75 ±0.13	X	12.75 ±0.15
Contrast	X	8.34 ±0.17	X	19.21 ±0.23	X	40.04 ±0.15	X	12.95 ±0.13

Table 2-6: Stimulus Validation Measurements for Subject 2.

The format of this figure is the same as Table 2-5. Cells that contain an "X" mark stimulus directions in which validation measurements were not recorded due to technical difficulty.

Subject 3 - Measurement Set 1								
Nominal Angle	-45°	-22.5°	0°	22.5°	45°	67.5°	90°	112.5°
Center Angle	-48.84 ±5.02	-27.84 ±6.02	5.29 ±4.45	23.61 ±0.77	45.41 ±0.15	67.48 ±0.42	85.96 ±3.11	108.56 ±4.89
Periphery Angle	-50.40 ± 4.90	-28.48 ±5.97	5.09 ±4.72	23.26 ±0.77	45.02 ±0.13	66.33 ±0.43	86.12 ±3.24	107.49 ±4.78
Nominal Contrast	12%	8.5%	14%	20%	60%	40%	22%	13%
Center Contrast	12.25 ±0.32	8.39 ±0.06	13.96 ±0.08	19.78 ±0.20	61.92 ±1.40	40.87 ±1.14	22.91 ±1.30	13.53 ±0.75
Periphery Contrast	12.13 ±0.31	8.30 ±0.08	13.52 ±0.09	19.17 ±0.21	59.76 ±1.36	40.65 ±1.13	22.97 ±1.26	13.47 ±0.71
Subject 3 - Measurement Set 2								
Nominal Angle	-45°	-22.5°	0°	22.5°	45°	67.5°	90°	112.5°
Center Angle	X	-24.51 ±1.57	X	22.92 ±0.07	X	67.65 ±0.19	X	111.23 ±1.11
Periphery Angle	X	-24.17 ±1.53	X	22.65 ±0.06	X	66.57 ±0.19	X	69.95 ±1.07
Nominal Contrast	12%	8.5%	14%	20%	60%	40%	22%	13%
Center Contrast	X	8.24 ±0.07	X	19.93 ±0.09	X	39.77 ±.0.27	X	12.88 ±0.11

Periphery Contrast	X	8.23 ±0.07	X	19.45 ±0.26	X	40.16 ±0.26	X	12.92 ±0.10

Table 2-7: Stimulus Validation Measurements for Subject 3.

The format of this figure is the same as Table 2-5 and 2-6. Cells that contain an "X" mark stimulus directions in which validation measurements were not recorded due to technical difficulty.

Acknowledgments:

This work has been supported by the National Institutes of Health (Grants:RO1 EY10016 and Core GrantP30 EY001583; https://www.nih.gov/) and National Science Foundation Graduate Research Fellowship (DGE-1845298). We would like to thank Joris Vincent, Jack Ryan, Ozenc Taskin, and Nicolas Cottaris for technical assistance.

Competing Interests:

The authors have no competing interests with this work.

CHAPTER 3

Temporal dynamics of color processing measured using a continuous tracking task.

Michael A. Barnett, Benjamin M. Chin, Geoffrey K. Aguirre, Johannes Burge, David H. Brainard.

Abstract:

We characterized the rich temporal dynamics of color processing using a continuous tracking paradigm. Specifically, we estimated temporal impulse response functions associated with tracking chromatic Gabor patches and measured how the lag functions change as a function of chromatic direction and contrast, confined to the LS cone contrast plane. In the same set of subjects, we measured detection thresholds for stimuli matched in their spatial, temporal, and chromatic properties. Further, we develop the color tracking model (CTM) and the color detection model (CDM) and examine their ability to fit the measurements of lag and percent correct, respectively. We use a framework assuming common mechanisms to test if the same set of mechanisms underlie both the color tracking task and the color detection. We find that the fitted elliptical isoresponse contours have the same orientation across the two tasks. What differs across the task is the ratio of the most to least sensitive mechanism

directions. What we find is consistent with chromatic mechanisms being the same across tasks but differed in the relative importance they assign to S-cone signals.

Introduction:

To exhibit behaviors based on colors in the environment, light must be encoded by the three classes of cone photoreceptors (L, M, and S). The encoding of light by the photoreceptors is the initial stage of color vision processing and is well characterized by a set of spectral sensitivity functions, one function per cone class (Brainard & Stockman, 2010). The subsequent stage of color processing compares the output of these cone signals to create three post-receptoral mechanisms. Both psychophysical and physiological evidence suggest that these mechanisms consist of two cone-opponent mechanisms and a luminance mechanism. The cone-opponent mechanisms represent the differences between cone signals (S-(L+M) and L-M) while the luminance mechanism represents an additive combination (L+M) (Krauskopf, Williams, & Heeley, 1982). These mechanism are referred to as the cardinal mechanisms, or directions, and their recombination begins in the retina with correlates observed in the responses of retinal ganglion cells (as well as neurons of the lateral

geniculate nucleus) (DeValois, Abramov, & Jacobs, 1966; Derrington, Krauskopf, & Lennie, 1984; Lennie & Movshon, 2005).

This mechanistic approach to studying color vision, in its current form, can be traced back to the pi-mechanisms of Stiles (Stiles, 1949) and has been widely used in various forms ever since (Stockman & Brainard, 2010). The main objectives of this approach have been to estimate the number of color processing stages, the number of mechanisms within each stage, and the computations performed by these mechanisms. Much debate exists over the claims made on each of these points. The further along the color vision processing pipeline these mechanisms are, the more disagreement exists in empirical findings about their existence and function. Since their proposal by Krauskopf et al. (1986), the higher order color mechanisms have been one of the main areas of research. These mechanisms are posed as being a recombination of the cardinal mechanisms. These mechanisms have been studied using a variety of tasks, primarily from detection and adaptation, with the conflicting results present especially from noise-masking experiments (Eskew, 2009).

One approach to study mechanisms is in a framework that asserts common mediating mechanisms and then tests the validity of the assumption. This approach has been used in various aspects of perception research, notably in the work of Philbeck and Loomis (1996) who use this to examine the behaviors

that are mediated by perceived distance. They explain that if the two measured behaviors vary in a predictable manner whenever the stimulus cues are varied, the variation in each behavior is linked to the variation in the same latent percept (Philbeck, Loomis, & Beall, 1997; Foley, 1977). To apply this logic to color vision mechanisms, if the behavioral measurements vary in a locked relationship when the color direction is varied, then one has good reason to suppose that these behaviors are mediated by the same underlying color vision mechanism. Importantly, it is not expected that any two measured behaviors yield commensurate values, therefore, we relate stimulus to measurement via task-specific nonlinearities. In the present work, we apply this logic using two distinct behavioral tasks, to examine the underlying chromatic mechanisms.

The first behavioral task we employ is the continuous tracking paradigm of Bonnen et al. (2015). This task measures a subject's ability to track, with a computer cursor, a target undergoing a random walk (Brownian motion). This paradigm provides an efficient way of estimating the temporal impulse response function (tIRF) of the visual-motor system that is associated with the tracking behavior. In a time-invariant linear system, the tIRF is a complete description of the input-output relationship of a system in response to a brief presentation of a stimulus (Watson, 1982). An accurate estimation of the tIRF provides a means to predict the response of the system to any stimulus input. Further, the tIRF

provides estimates of temporal properties that we can use to characterize the behavioral response of the subject. Of these parameters, the lag of the tIRF is used as the behavioral measure in the tracking task.

Previous studies have investigated the lags of the post-receptoral pathways using either a two-pulse detection or reaction time paradigm. This revealed that lags to S-(L+M) stimuli were larger than those to for L-M stimuli (Smithson & Mollon, 2004; McKeefry, Parry, & Murray, 2003). Similar results have also been found from electrophysiological recordings in the primary visual cortex of nonhuman primates showing the largest lags to S-cone isolating stimuli (Cottaris & De Valois, 1998).

The other behavioral measure we used to estimate the color vision mechanism is a detection task. Specifically, we used a two-interval force choice (2IFC) paradigm in which subjects discriminate which of two intervals contained a Gabor patch target. From these data, we obtain full psychometric functions for each chromatic direction tested. These functions provide us with the stimulus contrast required to reach the detection threshold. Detection thresholds have been used in numerous studies to probe the sensitivity the chromatic mechanisms (Krauskopf, Williams, & Heeley, 1982; Wandell & Pugh, 1980; Hillis & Brainard, 2007). One example, similar to the present study, is the work of Poirson et al. (1990) in which they use detection threshold data to attempt to best

estimate the weighting and combination rule used by the chromatic mechanisms underlying their specific task. To best estimate the mechanism in our present study, we used stimuli that are matched across tasks, as best as possible, in terms of their spatial, temporal and, chromatic properties. This maximizes the likelihood that any mechanism differences we find are not simply due to a difference in stimulus properties.

In the present study the same set of subjects completed both the color tracking task (CTT), to estimate tracking lag, and the color detection task (CDT) task, to estimate detection thresholds. Using these data, we developed two models, the color tracking model (CTM) and the color detection model (CDM)—each predicts its respective behavioral measure for any arbitrary stimulus in the LS contrast plane, using a small set of parameters. Each model contains two stages. The first stage is an elliptical isoresponse contour that represents the effect of the chromatic direction. The second is a nonlinearity which represent the effect of contrast. Importantly, the isoresponse contours have the same formulation across models and can be compared as a way to examine the underlying chromatic mechanisms. We leverage the behavioral measurements in a common mechanism framework to evaluate whether these distinct behavioral outputs are mediated by common chromatic mechanisms.

Results:

We evaluated the ability of subjects to track moving targets and determine how performance varies as a function of the chromatic content of the target being tracked. Further, we examined the relationship between tracking and the detectability of a stimulus and use this information to test if a common set of mechanisms mediates the pattern of results observed in both tasks. In Experiment 1, subjects completed a continuous tracking task in which they tracked position of moving Gabor targets using a cursor controlled by a computer mouse. The Gabor targets were modulated in 18 chromatic directions each with 6 contrast levels. The Gabor targets were 2° visual angle in diameter and had a spatial frequency of 1 C.P.D. Subjects completed 20 trials per each direction and contrast pair. Each trial had a duration of 11 seconds consisting of an initial 1 second static period followed by 10 seconds of dynamic tracking. Cross-correlation between the velocities of the subject's tracking and the velocities of the of the target yields the temporal impulse response function (see methods). We fit log-gaussian functions to these tIRFs to extract parameters of interest which capture the temporal response (lag, integration time, and amplitude). In the present study, we focus on the relationship between lag and the direction/contrast of the stimuli.

Additionally, we collected detection data in the form of a 2-interval forced choice (2IFC) task. In this second experiment, subjects completed the CDT in which they had to respond with which of two back-to-back intervals contained the Gabor targets. Stimuli in this task were modulated in 12 chromatic directions each with 6 contrast levels. Subjects collected 40 trials per each direction and contrast pair. Each trial had a duration of 1 second consisting of two 400 ms intervals with a 200 ms between-interval gap. For each chromatic direction tested, we obtain a threshold estimate, defined as the stimulus contrast required to achieve 76% correct for that direction (see Methods).

To determine the extent to which tracking performance was accounted for by the visibility of the Gabor targets, we fit a series of mechanistic models and examined which best fit the data. The models we employed contain two mechanisms with a quadratic combination rule to transform the stimulus input into an equivalent contrast. Equivalent contrast is the effective contrast of the output of the mechanisms accounting for differences in the sensitivity of the chromatic stage. This creates a common variable in that it is the input to the task specific non-linearity which determines the task dependent measure. This equivalent contrast step defines the set of relative response patterns that can be generated by the system while the non-linearity controls how these responses scale with contrast. Here we explicitly test if a common set of mechanisms can

produce the relative response pattern necessary to jointly explain the data from both the tracking and detection tasks.

Characterizing the Temporal Impulse Response Functions Associated with Tracking

From each run of the tracking experiment, both a time-course of the subject's cursor positions and a time-course of the target's positions on the monitor was obtained. From this, we can cross-correlate the velocities of both time-courses to recover the tIRF. In order to interpret the cross-correlation as the tIRF, it is important that the target velocities we use not be temporally autocorrelated. Since the target follows Brownian motion, the derivative of its positions produces the necessary white signal. Cross-correlating the concatenation of all the runs, within a subject, provides the mean tIRF. For each of the stimulus conditions, we obtain a mean tIRF which we fit with a log-Gaussian function. Figure 3-1 shows the tIRFs for an example chromatic direction. In this figure, the 90° (S-cone isolating) direction is shown with each panel showing the data for a different contrast level. The thin black line shows the mean cross-correlation function, and the purple line shows the log-Gaussian fit. The log-Gaussian fit provides us with a reliable way to estimate the parameters of interest. We estimate the lag of the tIRF as the time-to-peak which

is the time at which the log-Gaussian reaches its maximum amplitude. This is given by the mode of the function (see Methods). We summarize in more detail the relationship between lag and contrast in the next section.

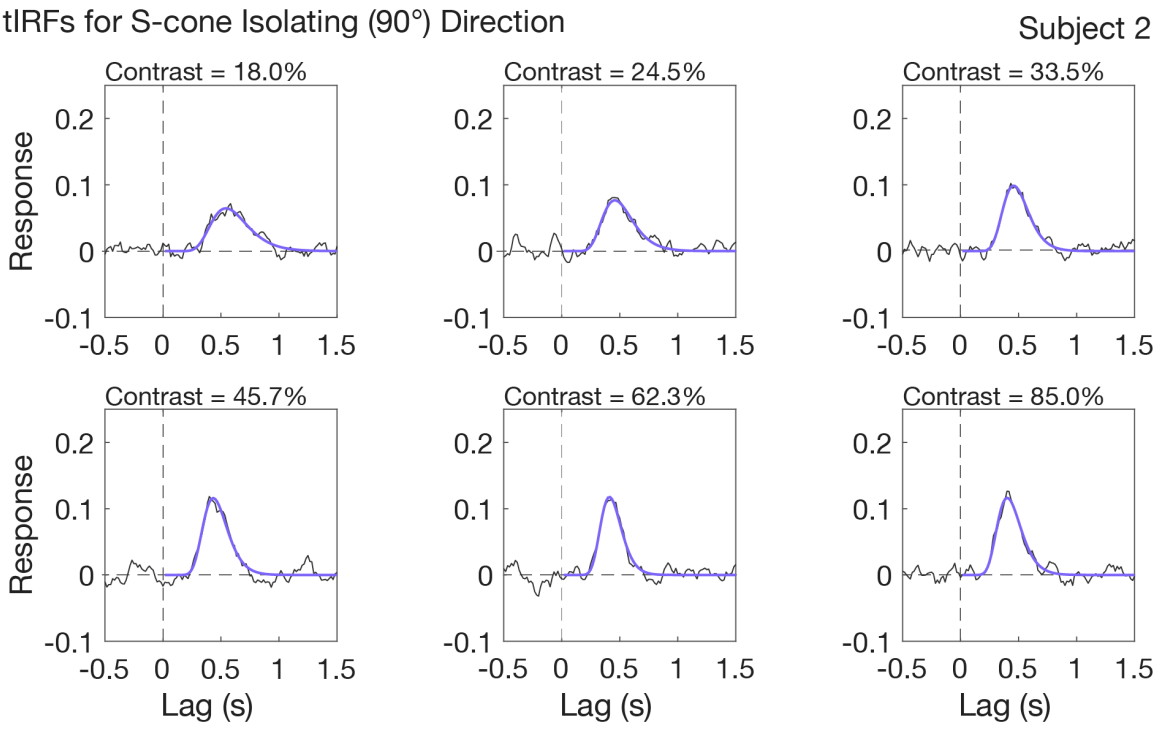

Figure 3-1: Individual Temporal Response Functions.

Each subplot shows the temporal impulse response function corresponding to one of the contrast levels shown for the 90° chromatic direction. The example data is shown for Subject 2. The contrast value corresponding to the functions plotted is displayed at the top of each panel. The thin black line in each panel shows the cross-correlation between the tracking and target velocities. The purple line in each panel shows the log-Gaussian fit to the cross-correlation. We take the log-Gaussian fit to be the tIRF. From the tIRF, we obtain lag as the time-to-peak of the log-Gaussian fit.

Contrast-Lag Functions

We first examined the basic relationship that exists between the contrast of a stimulus and the lag associated with tracking. To examine this relationship, we plot lag as a function of contrast grouped by the chromatic direction of the stimuli. These grouped lags are plotted in Figure 3-2 for Subject 2. Each subpanel shows the lag estimates plotted as closed circles and color coded by their corresponding chromatic direction. Overall, we observe that tracking lags decrease as contrasts of the stimuli increase. This was observed in all subjects and for all chromatic directions.

While lags generally decreased with contrast, the rate at which they decreased, and the minimum lag reached, differed across chromatic directions. This rate of decrease difference can be seen in Figure 3-2 in that the L-cone isolating (0°) stimuli reaches a lag of roughly 325 ms with approximately 20% contrast while it takes nearly 70% contrast to reach the same lag in both the 75° and the -75° directions. This shows that the minimum lag reached across directions was not uniform, when contrast is matched. This can clearly be seen in lag-contrast functions for the L-cone (0°) and S-cone (90°) isolating stimuli. The minimum lag for the highest contrast S-cone stimuli barely reaches the lag for the lowest contrast L-cone stimuli. Interestingly, we observe that lags asymptote, with enough contrast, to a minimum lag and that this is fairly constant if enough

L-cone contrast is mixed into the compound Gabor. If enough L-cone contrast is mixed into the compound Gabor to achieve a deviation of ~10° from the S-isolating direction, then the minimum lag converges. This indicates an unequal contribution of cone stimulation to lag. We quantify the relative contribution of the cones to lag in the section below.

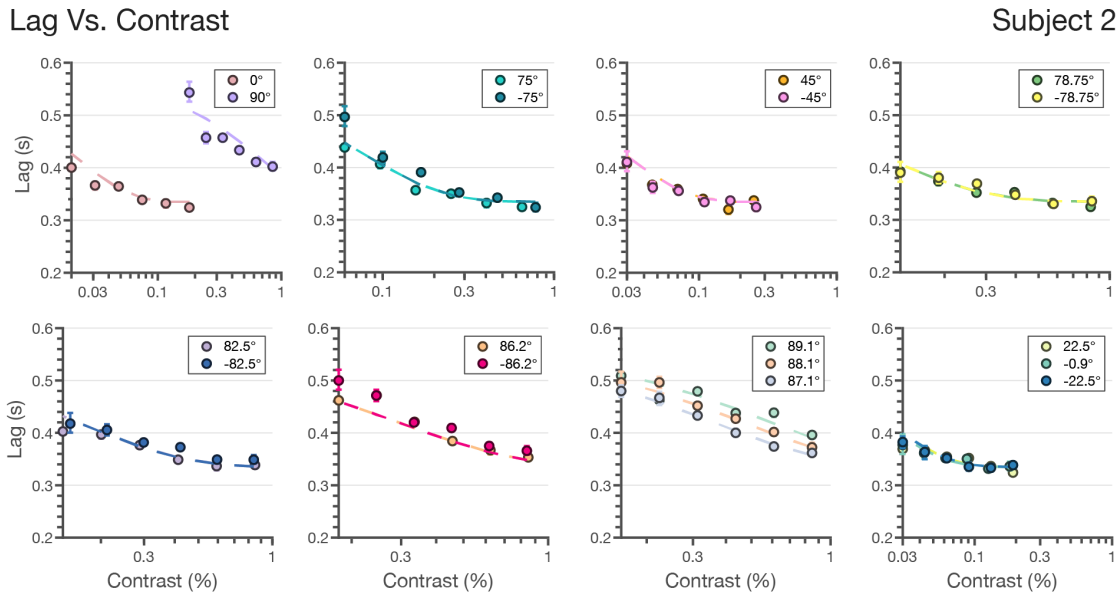

Figure 3-2: Lag Versus Contrast.

Each panel shows tracking lags as a function of the stimulus contrast for each direction used in the experiment. The closed circles in each panel are the lags of the tIRFs and are grouped into their corresponding chromatic direction by their plot colors. The chromatic direction angles are displayed in the legend of each panel. The error bars on each lag estimate are found via a bootstrap procedure and are the 68% confidence intervals. The dashed curves in each panel are the lag predictions of the color tracking model (see the following sections). The plot colors of the model fit lines are matched to the plot colors for the lag measurements.

Isoresponse Contours of the Color Tracking Model:

The CTM provides a way to take in any stimuli, specified in terms of L- and S- cones contrasts, and provide predictions of tracking lags. To achieve this, the model has two stages to convert the stimulus input to lag. First, a quadratic isoresponse contour is defined that allows for the transformation of the stimulus contrast and direction into what we term the 'equivalent contrast'. Equivalent contrast is the effective contrast of the stimulus after it has been weighted by the underlying mechanism sensitivity for the corresponding chromatic direction. This provides a common axis for the lag measurements, collapsing across color direction. Second, a single exponential decay function transforms the equivalent contrast to a prediction of the tracking lag. Here we examine the isoresponse contours.

The isoresponse contour is defined as a set of stimuli that result in the same tracking lags. In the CTM, this contour takes the form of an ellipse in the LS cone contrast plane. The isoresponse contour is specified by two parameters: 1) the ellipse angle (representing the direction of least sensitivity; counterclockwise to the positive abscissa) and 2) the minor axis ratio (the ratio of vector lengths between the most and least sensitive directions). Within this framework, these parameters provide a full account of chromatic sensitivity. Figure 3-3 shows the isoresponse contours for the CTM for all three subjects.

For all subjects, the angle of the isoresponse contours was oriented at approximately 90°. This means that the chromatic mechanisms underlying tracking are least sensitive to stimuli modulated in the S-cone isolating direction. Inspection of the orthogonal direction shows that the underlying mechanisms are most sensitive to stimuli modulated in the L-cone isolating direction. Across all subjects, the average minor axis ratio parameter is 0.03. Taken together, the ellipse parameters state the underlying chromatic mechanisms are ~33x more sensitive to L-cone isolating stimuli than S-cone isolating stimuli in the color tracking task. We found good agreement of the ellipse parameters across subjects. The scale of the ellipses in Figure 3-3 are set via the criterion lag set to 400 ms but the structure of the CTM enforces that the orientation and minor axis ratio of the ellipse be the same across all choices of criterion lag. The parameter values for each subject's isoresponse contour are displayed in their

corresponding panel in Figure 3-3.

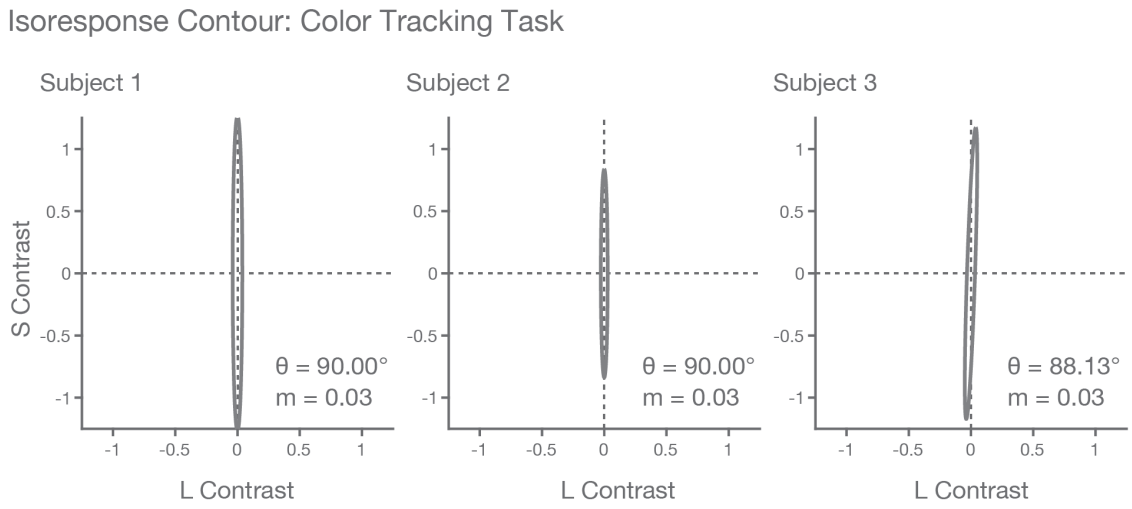

Figure 3-3: Isoresponse Contour for the Color Tracking Model.

The grey ellipse in each panel shows the isoreponse contour associated with the color tracking task for each subject. The isoresponse contour is the set of stimuli that result in the same tracking lags. This contour is constrained to take the form of an ellipse in the LS cone contrast plane. The ellipse is specified by two parameters: 1) the ellipse angle and 2) the minor axis ratio. The ellipse angle represents the direction of least sensitivity defined counterclockwise to the positive abscissa. The minor axis ratio is the ratio of the vector lengths between the most and least sensitive directions. The scale of the ellipses across subjects is set by the criterion lag which was is 400ms in this figure.

Nonlinearity of the Color Tracking Model:

Application of the isoresponse contour to convert stimulus contrast to equivalent contrast creates a scalar equivalent contrast which we can use to predict the lag response. This equates stimuli across different color directions making them a function of this single variable. Therefore, we can transform equivalent contrast into predicted tracking lag via a single static non-linear function. The functional form we employ to convert equivalent contrast to lag is a three-parameter exponential decay function (see Methods).

Figure 3-4 shows the nonlinearity of the CTM for all subjects. Across all subjects, these functions describe how the tracking lag decreases with increasing equivalent contrast. Across the subjects, lags asymptote at a minimum lag of ~340ms. This indicates that even with increasing contrast, there exists a limit on minimum tracking lag imposed by the sensory and motor systems. Table 3-1 has the nonlinearity parameters for all subjects.

	Scale	Amplitude	Minimum Lag
Subject 1	1.94	0.65	0.34
Subject 2	1.50	0.23	0.33
Subject 3	1.88	0.45	0.35

Table 3-1: Parameters of the nonlinearity for the tracking task.

Columns corresponds to individual parameters. Rows correspond to individual subjects.

One assumption built into the CTM is that underlying processing stages are color–contrast separable. The color stage is represented by the isoresponse contours and the contrast stage by the nonlinearity. To demonstrate the validity of this assumption, we used the isoresponse contour to convert each stimulus contrast from the tracking experiment into its equivalent contrast. With this, we replot the lags (as seen in Figure 3-2) on the equivalent contrast axis as the closed circles in Figure 3-4. For Subjects 1 and 2, the single nonlinearity well

captured the relationship between lag and equivalent contrast for all chromatic directions. While the data for subject 3 grossly follows the nonlinearity, it appears this relationship would be better fit by two separate exponential decay functions. In this case the CTM places the nonlinearity in the middle of this bifurcation to maximally capture the variance. The grouping of these directions do not correspond to the grouping of directions in the experimental sessions, ruling out better tracking performance for a particular session. Overall, the general agreement between the tracking lags and nonlinearity indicate that it is appropriate to separate the effects of chromatic direction and contrast.

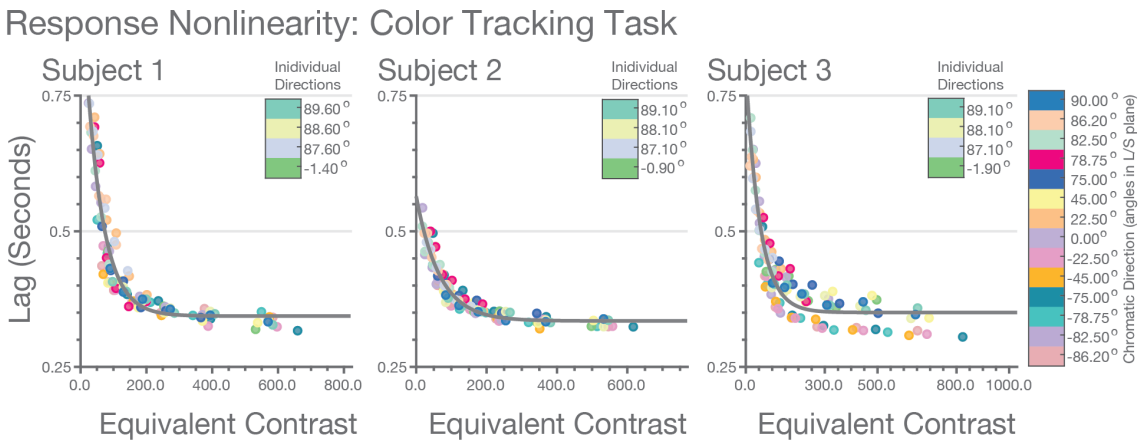

Figure 3-4: Nonlinearity of the Color Tracking Model.

The grey curve in each panel shows the nonlinearity of the color tracking model. The x-axis it the equivalent contrast which is the result of the isoresponse contour. The y-axis respresent the response, which in this figure, is the lag from the tracking task in seconds. The closed circles in each plot are the tracking lags from the tIRF. The stimulus contrasts of the for each lag has been adjusted by the isoresponse contour allowing the lags for all stimuli to be plotted on the equivalent contrast axis. The color map denotes which color correspond to which directions. The inset color map in each panel marks the directions tested which were unique to each subject.

Characterizing Thresholds Associated with the Detection Task:

In the detection experiment, subjects participated in a 2IFC task in which they were asked to report which of 2 intervals contained the Gabor target. The Gabor target varied in its chromatic direction and contrast just as in the previous tracking task. For each direction and contrast, we obtain a percent correct which is the number of times a subject correctly identified the interval containing the target divided by the number of trials for that stimulus condition. Just as with the tracking lag estimates, we examine the relationship between percent correct and contrast by grouping the measurements by their chromatic direction. These grouped percent correct measures are plotted in Figure 3-5 as a series of psychometric functions shown for Subject 2. Each subpanel shows the percent correct plotted as closed circles. For all subjects and chromatic directions, we observed that percent correct increases as the contrasts of the stimuli increase.

In the detection task, we define threshold as the stimulus contrast required for the subject to reach 76% correct. We obtain a threshold for each of the 12 chromatic directions tested in the detection experiment. For Subject 2, the threshold for each direction, as found by individually fitting cumulative Weibull functions for each direction, are displayed in the corresponding panels in Figure 3-5. Examining threshold as a function of chromatic direction reveals that the subjects are much more sensitive to targets modulated in the 0° direction than

the 90° direction. For Subject 2, the contrast required to reach threshold in the L-cone isolating (0°) direction is 0.35% while it takes nearly 4.4% contrast to reach threshold S-cone isolating direction. The testing direction were well sampled in that the range of contrast tested produced percent corrects ranging between ~50% correct (chance) at the lowest contrast to 100% at the highest.

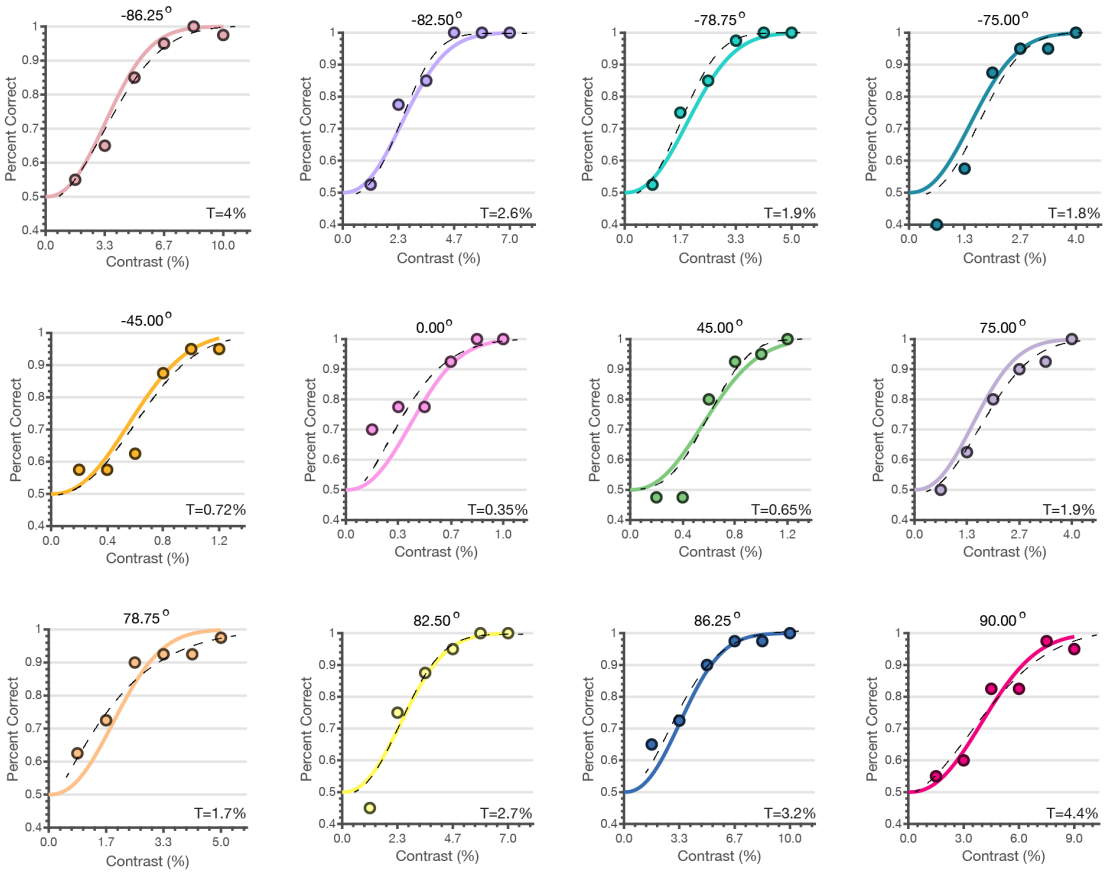

Figure 3-5: Detection Vs. Contrast.

Each panel shows the percent correct in the detection task as a function of the stimulus contrast for each direction used in the experiment. The closed circles in each panel are the percent correct for an individual stimulus condition. The percent correct are grouped into their corresponding chromatic direction plotted in individual panels. The chromatic direction angle is displayed above each panel. The dashed black line in each panel shows the cumulative Weibull function fit separately for each direction. We use these curves to find the threshold in each direction. This is the contrast need to detect the stimulus 76% of the time.

Thresholds are displayed in the bottom right of each panel. The solid curves in each panel are the percent correct predictions of the color detection model which is fit to all the data simultaneously (see the below sections).

Isoresponse Contours of the Color Detection Model:

Just as with the tracking task, we would like a way to take any stimulus contrast in the SL plane and produce a prediction of percent correct for the detection task. To accomplish this, we employ the Color Detection Model (CDM). The CDM is structured the same as the CTM with two stages to convert the stimulus input to percent correct. The first stage uses the same formulation of the quadratic isoresponse contour as defined in the CTM to transform the stimulus contrast into equivalent contrast. The second stage is a task-specific linking function that takes equivalent contrast and produces estimates of the variable of interest, in this case percent correct. The functional form we use for the detection task is a cumulative Weibull offset by the guess rate of 50%. This allows us to convert the equivalent contrast to a prediction of the precent correct which is bound between 50% and 100% correct.

The elliptical isoresponse contours of the CDM for each subject are plotted in the panels of Figure 3-6. These isoresponse contours show that the ellipses are oriented at approximately 90° for all subjects. This shows that the chromatic mechanisms underlying detection are least sensitive to stimuli

modulated in the S-cone isolating direction and most sensitive to stimuli modulated in the L-cone isolating direction. The minor axis ratio ranged between 0.08 and 0.10 across the subjects. Therefore, the ellipse parameters show the underlying chromatic mechanisms for detection are ~11x more sensitive to L-cone isolating stimuli than S-cone isolating stimuli for the detection of the Gabor target. We find good agreement in both the ellipse angle and the minor axis ratio across the subjects. The scale of the ellipses in Figure 3-6 is set via the criterion percent correct set to 76%. The parameter values of subject's isoresponse contour are displayed in their corresponding panel in Figure 3-6.

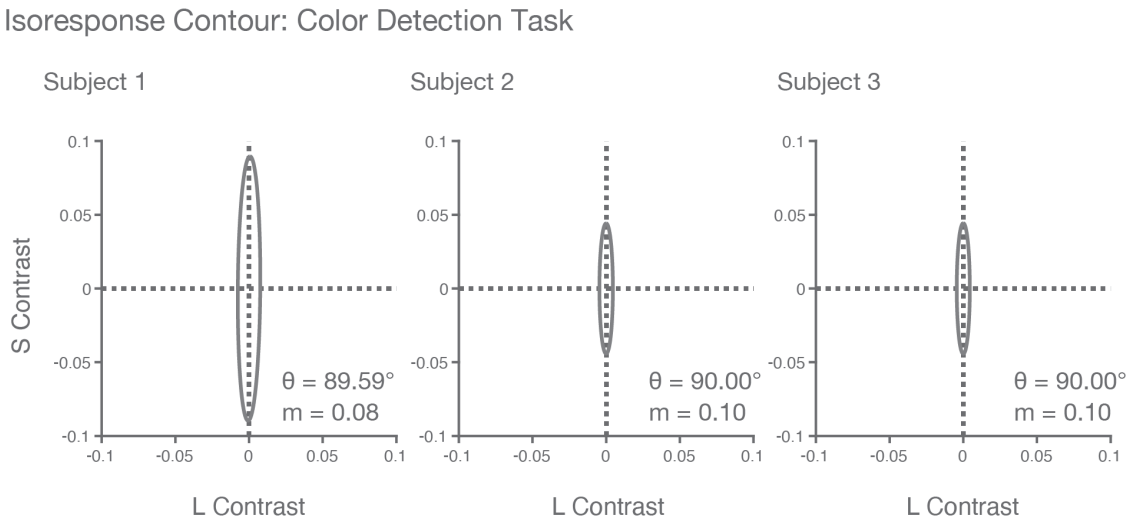

Figure 3-6: Isoresponse Contours for the Color Detection Task.

The grey ellipse in each panel shows the isoreponse contour associated with the color detection task for each subject. These contours define a set of stimuli which produce the same percent correct in the detection task. The isoresponse contour of the color detection model has the same parameterization as the color tracking model. The scale of the ellipses across subjects is set by the criterion percent correct which was set to 76% correct in this figure.

Nonlinearity of the Color Detection Model:

Figure 3-7 shows the nonlinearity of the CDM for each subject plotted as the grey line in each panel. These functions constrain how the percent correct of the detection task grows with increasing strength of the equivalent contrast. Just as with the individual psychometric functions, we can define a threshold for the nonlinearity as the equivalent contrast required to reach 76% (creating an 'equivalent threshold'). Across the subjects, the equivalent threshold ranged between 4.5% to 9% contrast. This captures the overall chromatic mechanism signal strength required for a subject to detect the presence of a target, independent of color direction. Table 3-2 has the nonlinearity parameters for all subjects.

	Lambda	Exponent
Subject 1	0.10	1.98
Subject 2	0.05	2.04
Subject 3	0.05	2.32

Table 3-2: Parameters of the Nonlinearity for the Detection Task.

Columns corresponds to individual parameters. Rows correspond to individual subjects.

The CDM shares the same assumption of separability that is built into the CTM (color–contrast separability). Just as with the CTM, the color stage is

represented by the isoresponse contours and the contrast stage by the nonlinearity. To demonstrate this, we plot the percent as a function of its equivalent contrast (closed circles in Figure 3-4). For all Subjects, the single nonlinearity captures this relationship well for all chromatic directions. For most directions, it appears that the slopes of the psychometric function are fairly constant with a few exceptions in Subject 1. The overall agreement between the adjusted percent correct and the nonlinearity indicate that, like the CTM, the separability assumption is reasonable for the CDM.

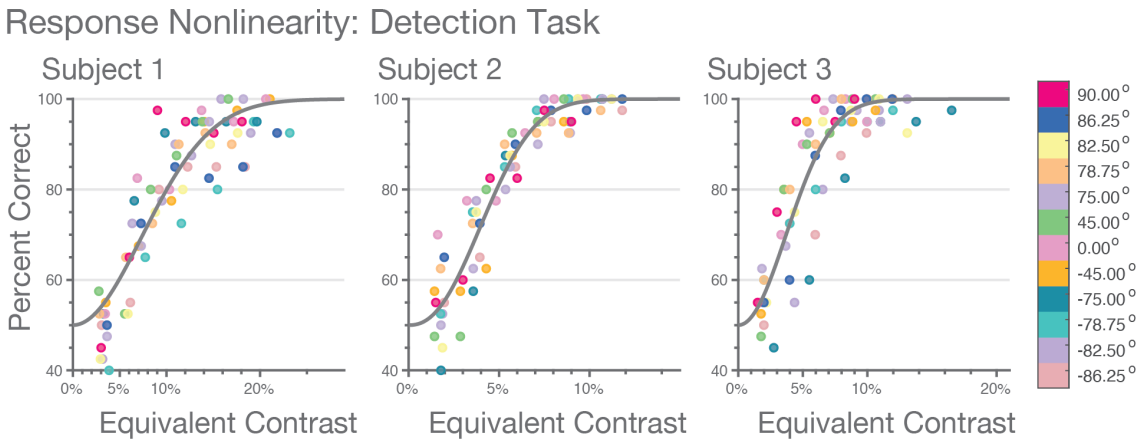

Figure 3-7: Nonlinearity of the Color Detection Model.

The grey curve in each panel shows the nonlinearity of the color detection model for all subjects. The x-axis is equivalent contrast. The y-axis is the response, which in the figure, is the percent correct of the detection task. The closed circles in each plot are the percent correct for each condition tested. The stimulus contrasts for each closed circle has been adjusted by the isoresponse contour allowing the percent correct to be plotted on the equivalent contrast axis. The color map denotes which color correspond to which directions.

Cross-Model Comparison:

To evaluate the extent to which these two behaviors share common mechanisms, we evaluate how well each model fits when it is constrained to have the other model's isoresponse parameters. This is accomplished by first fitting the CTM and the CDM to their respective data sets. This yields the parameters reported in the sections above. The CTM and the CDM have the same general structure and the parameterization of their isoresponse contours is identical. Because of this, we can simply lock the angle and minor axis ratio of the CTM to be the parameter values found in the original CDM fit and vice versa. This yields two models in which we have swapped their chromatic processing stage. With the parameters locked, we refit the parameters of the task nonlinearity. The results of this exercise can be seen in Figure 3-8 for Subject 2. The top row shows the color tracking task and the bottom row shows the color detection task. The columns correspond to different chromatic directions. As in Figure 3-2 and Figure 3-5, the closed circle represents the behavioral measure, and the dashed lines show the output of their respective models when fit to their own data. The lower saturation dashed line in each panel is the result of model fitting with the locked parameters. We observe that the general pattern of the predictions is preserved across the two fitting methods, but the locked method provides a worse account to the data overall.

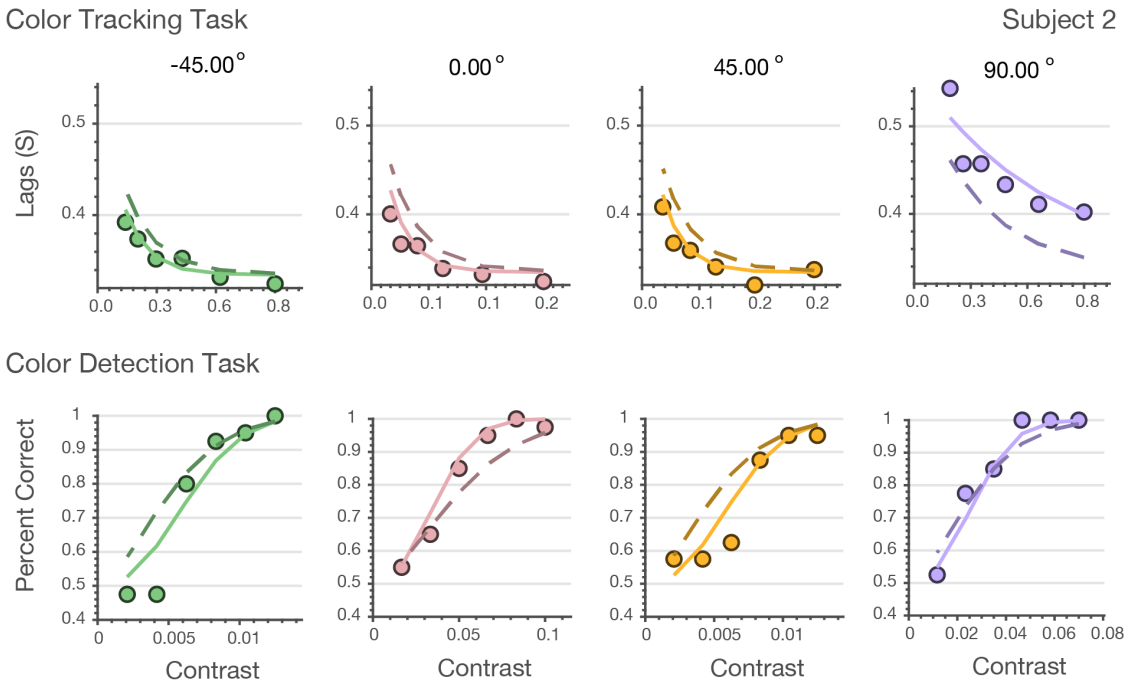

Figure 3-8: Cross-Parameter Model Comparison.

The top row corresponds to the color tracking task and the bottom row is the color detection task. The columns correspond to different chromatic directions. The data shown in the figure are for Subject 2. The format of each panel is the same as in Figures 3-2 and 3-5. The closed circle represents the lags (top), and the percent correct (bottom). The solid line in each panel shows the output of the respective model when it is fits its own data. The dashed line in each panel is the result of the model fits in which the isoresponse contour parameters were swapped and locked in a subsequent refit.

Conclusions:

We set out to examine what factors support tracking behavior and how this behavior varies as a function of both the chromatic direction and contrast. To achieve this, we made measurements of the temporal dynamics of color processing using a continuous tracking paradigm. We measured the processing lags associated with tracking chromatic Gabor patches modulated in 18

directions. The cross-correlation between the target and tracking velocities yielded estimates of the tIRF for each direction. From log-Gaussian fits to these empirical cross-correlation functions, temporal lag was extracted for each stimulus condition. We examined how these lags changed as a function of chromatic direction and contrast. For all subjects and color directions, we found that temporal lag decreases as contrast increases. Lags varied as a function of the chromatic direction with the shortest lags to stimuli modulated in the L-cone isolating direction and the largest lag to S-cone isolating stimuli.

Additionally, we collected 2IFC detection data in the same set of subjects. To obtain thresholds estimates, defined as the contrast required to reach 76% correct, we fit a cumulative Weibull function separately to the detection data from each chromatic direction tested. We observe the same pattern of sensitivities for tracking lags and detection thresholds. Thresholds were smallest for detecting stimuli modulated in the L-cone isolating direction and the largest for S-cone isolating stimuli, when contrast is matched. Given that the relative sensitivities were similar across the two experiments, we were interested in comparing them to determine if the underlying mechanisms are the same.

To quantitatively examine the data from both experiments in a manner that allows for the comparisons of the underlying chromatic mechanisms, we develop models of both tracking lag and threshold detection. These models are the color

tracking model (CTM) and the color detection model (CDM). Both models operate in two stages. The first stage, which is the same in both models, is a quadratic isoresponse contour which allows for the conversion to 'equivalent contrast'. Equivalent contrast represents the output strength of the color mechanism stage of the model creating a single response variable. The second stage of the model uses a task-specific nonlinearity to transform the equivalent contrast to a prediction of behavioral variable of interest. Interpreting the isoresponse contour parameters of the CTM reveal that the underlying chromatic mechanisms are ~33x more sensitive to L-cone isolating stimuli than S-cone isolating stimuli for the color tracking task. The isoresponse contour parameters of the CDM show that the underlying chromatic mechanisms for detection are ~11x more sensitive to L-cone isolating stimuli than S-cone isolating stimuli for the detection of the Gabor target.

What does this tell us about chromatic mechanisms?

Prior work on uncovering the chromatic mechanisms of human color vision have reliably found two sets of mechanisms. The first set of mechanisms, primarily found via color matching experiments, reveal the spectral sensitivities of the L-, M-, and S-cone photoreceptors (Stockman & Sharpe, 1999). These three independent mechanisms are the first stage of color vision and have been well

characterized. A subsequent set of chromatic mechanisms have been revealed which are referred to as the post-receptoral or cardinal mechanisms (Krauskopf, Williams, & Heeley, 1982; Derrington, Krauskopf, & Lennie, 1984). These correspond to two chromatic mechanisms and one luminance mechanism. The two chromatic mechanisms, which represent the differences between cone signals, are the L-M (red-green) and the S-(L+M) (blue-yellow) mechanisms. The luminance mechanism represents an additive combination (L+M). This line of experimentation seeks to answer a set of questions, primarily if there are additional mechanisms to the cardinal ones, and where in the visual system these exist. Psychophysics has been used in a variety of experiments (detection, adaptation, noise masking, etc.) to address the question of how many mechanisms exist beyond the cardinal mechanisms (Eskew, 2009; Gegenfurtner, 2003; Stockman & Brainard, 2010). The result for both estimating the number and location have been highly variable. The differences in the findings come down to differences in the number of mechanisms as well as the computation performed by these mechanisms (linear vs. nonlinear).

The current study allows us to ask if set of mechanisms that underly the color tracking task are the same set of mechanisms that underly the color detection task. We assess this through examining the shapes of their respective isoresponse contours, following the logic set forth by of Philbeck and Loomis (1996). Importantly, we controlled (as well as possible) the spatial, temporal, and

chromatic proprieties of the stimuli across the tracking and detection tasks. This allows us to be more certain that the differences are due to internal factor rather than stimulus driven. Across the two tasks, we find that the orientations of the ellipses are the same (90°). This indicates that the two chromatic mechanisms in the LS plane are oriented in the same direction across tasks. What does differ across the tasks is the minor axis ratio of the ellipses. This shows that the relative sensitives of the two mechanisms are different across the two tasks. The mechanism aligned with the L-cone isolating direction is ~33x and ~11x more sensitive than the one aligned with S-cone isolating direction for the tracking and detection tasks, respectively. Taken together, the contours tell us that the chromatic mechanisms are the same across tasks and what changes is the relative importance of the S-cone signals. The relative sensitivity difference is ~3x higher for the tracking task than the detection task meaning that the tracking task makes less use of the S-cone signals.

The implication that the elliptical isoresponse contours can be used to describe the underlying chromatic mechanism comes with caveats. We would like to be able to treat the principle axes of the ellipse as defining the chromatic mechanisms. Since the elliptical model does not have a unique way to recover these axes, we cannot say for certain that the axes of the ellipse are the visual mechanisms. Despite the angle and minor axis ratio of the CTM and CDM being

the best fitting parameters, no pair of axes can be uniquely interpreted as the mechanisms from the resulting ellipse shape. Chromatic mechanism estimates from the ellipse are unique only up to an orthogonal transformation. Despite this, the agreement of the ellipse orientations across our tasks as well as their agreement with prior psychophysical results point to their interpretation as the mechanism in the LS plane as being the most parsimonious explanation of the data. For further reading on the point see (Poirson, Wandell, Varner, & Brainard, 1990) and (Barnett, Aguirre, & Brainard, 2021).

Previous work examining chromatic sensitivity that took a similar approach found results that aligned with the ones in the present study, particularly the work of Poirson and Wandell (Poirson & Wandell, 1990). They examined detection thresholds obtained under two separate experimental paradigms. These were a color matching task and a color discrimination task. The primary variable that was manipulated was the amount of time subjects had to make a judgement. Subjects had free response time for the matching task and a temporally restricted response period for the detection task. From this data, they fit elliptical isodetection contours and examined how the size and orientation changed across tasks. They found that the ellipses for the color-matching task was ~7x smaller than the discrimination ellipse. This result parallels our findings in that we observe a similar reduction in sensitivity in the task that is more temporally

demanding. Overall, Poirson and Wandell found that the fitted ellipsoids differed in both their minor axis ratios and orientation across tasks. Our results differ in that we only find changes in the minor axis ratio and not in the orientation.

Relation to psychophysics:

Importantly, the formulation of the CTM and CDM allow for predictions of their respective behavioral measures for any input stimulus. This is an advance over previous studies of color vision temporal properties. Previous studies used methods that were laborious and restricted the number of directions tested. These directions were usually restricted to the cardinal directions. Therefore, most previous studies assumed the mechanisms a priori. Within this framework, a well-studied aspect of temporal processing of the chromatic mechanisms specifically examined the latency of the S-cone pathway. A common metric used has been reaction time to estimate the latencies. Smithson and Mollon (2004) measured thresholds and reaction times and claim that when luminance cues are masked, S-cone latency differences from the L/M direction drop to within 20-30ms. Using two-pulse detection method, Shinomori and Werner (2008) found that the lags of their tIRF for increment and decrement S-cone isolating modulations were 50–70 and 100–120 ms, respectively. Mollon and Krauskopf (1973) measured reaction time as a function of background illuminance for 430,

500, and 650nm stimuli and found reaction times of ~300-400 ms with the highest latencies associated with the 430mn stimuli.

To our knowledge, we are presently the only study to implement the continuous tracking paradigm to estimate the lags associated with tracking S-cone isolating stimuli. This paradigm allows for the efficient estimation of the tIRF which made it possible to measure tracking lags along 18 different chromatic directions in the LS plane, each with 6 contrast levels. We find that with sufficient S-cone contrast we can push the tracking lags associated with the S-cone isolating direction within 50 ms of the L-cone isolating direction. Across the previously described studies examining S-cone lags, it is clear that the exact value of this latency is dependent on the task. Therefore, it is important to characterize lags in terms of the relative latencies across the different chromatic directions. The CTM allows for the easy implementation of examining this relative metric.

Chromatic Direction – Contrast Separable Models:

Both the CTM and the CDM are separable models with respect to how they treat the effects of chromatic direction and contrast on the predicted response. This separability allows for the evaluation of the chromatic mechanisms that is independent from the effects of contrast. We find that for

both tasks, the most sensitive direction is to L-isolating contrast modulations and least sensitive to be S-isolating modulations. The separable assumption of the model allows for the sensitivity finding to be valid at any contrast level tested. An explicit test of the validity of the separability assumption can be seen in Figures 3-5 and 3-7. In both plots, the stimulus contrasts of the behavioral measures have been adjusted by the isoresponse contour to expressed as equivalent contrast and are plotted as the closed circles in each panel. The validation of the separability assumption can be seen in the lack of biased deviations in the overlap between these closed circles and their respective nonlinearities. The chromatic direction and contrast separability allows for more confident estimations of the isoresponse contours since their shape does not depend on the specific contrast levels chosen in the experiments.

Generalizing the CTM and the CDM:

A more general account of the present study is one that includes modulating stimuli in all three-dimension of L-, M-, and S-cone contrast space. The current set of results are restricted to the LS contrast plane. Therefore, it is not known if the axes of the elliptical isoresponse contour we found will overlap with two of the three axes of an ellipsoidal isoresponse surface. It is only the case that the current contours are a 2-dimensional cross section of the larger 3-

dimesional surface, specifically the LS plane. Tracking and detection measurements made using stimuli that modulated in the M-cone isolating direction (and combinations and 3 classes of cones) would allow for a fuller account of the mechanisms serving these tasks. The generalization of the CTM and the CDT is straightforward in that this expanded measurement set would be modeled using an ellipsoidal isoresponse surface rather than the elliptical contour. The ellipsoidal isoresponse surface converts stimuli, specified by their L-, M-, and S-cone contrast, into equivalent contrast just as is done in the current first stage of the CTM and CDM. The second stage of these models, the task-specific nonlinearities, would remain unchanged. With this expanded dimensionality of the model, the assumptions of separability would need to be checked for the newly tested directions in order to test this generalization.

The CTM and the CDM may be further generalized, even within the current LS contrast plane, by variations in the mean of the velocity distribution that defines the random walk of the Gabor patches. In the current experiment, we fixed the mean of the velocity distribution to ~4 °/s with 90% of the velocity distribution within ~10°/s. Changing the mean of this distribution will have the effect speeding up or slowing down the average walk speed. The CTM and CDM could be fit to data from patches at various other velocities with the goal of observing how the chromatic mechanisms change. The stimuli in our experiment

are of a fixed spatial configuration, the stimuli were presented at a size of 2° of visual angle and at spatial frequency of 1 C.P.D. Either of these parameters could be varied and the models fit to this new data. Examining how the CTM and CDM fits change with changing size and spatial frequencies might allow for models of tracking that are for any arbitrary complex spatial stimuli.

Finally, more examination of the other tIRF parameters may reveal interesting relationships in the data that have yet to be explored. The log-Gaussian fits provide an additional two parameters that can be explored. The first parameter is the amplitude of the tIRF. The amplitude is the maximal correlation of the cross-correlation between the tracking and target velocities. This parameter is difficult to interpret since multiple factors in tracking behavior affect this value. The other parameter is the width of the log-Gaussian. This value has a more straightforward interpretation as the dependance on the stimulus history. Either of these parameters could take the place of lag and the analyses of this paper could be redone.

Materials and Methods:

Subjects:

Three subjects (age 28, 29 ,33; two male) took part in all psychophysical experiments. All subjects had normal or corrected to normal acuity and normal color vision. All subjects gave informed written consent. The research was approved by the University of Pennsylvania Institutional Review Board. Two of the subjects are authors on the on this paper and one was naïve to the purpose of the study.

Experimental Session Overview:

All subjects participated in both the color tracking task and color detection task experiments. In total, all experiments spanned eight sessions. The first six sessions were for the CTT paradigm, and the remaining sessions were used for the CDT. Each of the CCT sessions lasted approximately 1.5 hours and each CDT session lasted 1 hour. Subjects completed the full set of tracking experiments before completing the detection experiment. All experiments were preregistered: the Color Tracking Task (Exp. 1: https://osf.io/xvsm3/; Exp. 2: https://osf.io/5y2dh/; Exp. 3: https://osf.io/e6dfs/) and the Color Detection Task (Exp. 4: https://osf.io/ekv24/; Exp. 5: https://osf.io/ekv24/).

Stimulus Display and Generation:

The stimuli were designed to create specific responses of the cone photoreceptors using silent substitution (Estévez & Spekreijse, 1982). Silent substitution is based on the principle that sets of light spectra exist that, when exchanged, selectively modulate the activity of cone photoreceptors. Therefore, modulating the stimuli, relative to a background, can selectively modulate the activity of the L-, M-, or S-cones, or combinations of cones for a specified contrast. These calculations require a model of the spectral sensitivities of the cone photoreceptors and spectral power distributions of the monitor primaries. We use the Stockman–Sharpe 2-degree cone fundamentals as the model of the cone sensitivities. To obtain the spectral power distribution of the monitor RGB primaries, we performed a monitor calibration using a PR-650 SpectraScan radiometer. This also allowed us to obtain the gamma function for each primary as well.

All stimuli were generated using a ViewSonic G220fb CRT monitor with three primaries which had a refresh rate of 60 Hz. The horizontal and vertical resolution of the monitor was 1024x768 pixels, respectively, corresponding to a screen size of 405 x 303 mm. Subjects viewed the monitor at distance of 92.5 mm for tracking and 105 mm for detection.

The Visual Stimuli:

The stimuli for all experiments were restricted to the LS plane of cone contrast space. Cone contrast space is a three-dimensional space with each axis showing the change in the quantal catch of the L, M, and S cones relative to a specified reference spectrum. This reference spectrum is referred to as the background light. The background used in all experiments was luminance: Y = 30.75 cd/m2, chromaticity: x = 0.326, y = 0.372. These were calculated using the XYZ 2° color matching functions, https://cvrl.org). We set the origin of the LS cone contrast plane to be this background and confined all modulation to this plane. Modulations made around this background have the effect that they only modify the L- and S-cone excitations, while leaving M-cone excitations unchanged. We refer to the chromatic component of the stimuli used in this experiment as vectors in this plane. Each stimulus has an L-cone and S-cone vector component, and we refer to the stimuli by the angle computed by the ratios of these components. In this space, S-cone isolating stimulus vectors are oriented at 90° and L-cone isolating stimulus vectors are oriented at 0°. We refer to these angles as the chromatic directions. The contrast of a stimulus is defined as the L2-norm of the stimulus vector in the LS plane.

The spatio-temporal parametrization of the stimuli are identical across both experiments. The stimuli used were sine phase Gabor patches. The frequency of the sine wave was set to 1 C.P.D. and the standard deviation of the

Gaussian window was set to 0.6 degrees of visual angle (DVA). This standard deviation corresponds to a FWHM of 1.41° and 90% of the Gaussian envelope being contained in a 2° diameter window. The Gabor patch performed a random walk confined to move horizontally across the monitor. The Gabor target updated its position on each frame according to a Gaussian velocity distribution. This distribution was centered on 0 °/s with a standard deviation of 2.6 °/s and a FWHM of 6.1 °/s. Values drawn from this distribution with a negative sign corresponded to leftward motion and values with a positive sign corresponded to rightward motion. This resulted in an average speed of 2.07 °/s and an average step size of approximately 0.63 mm. What varied across stimuli was the chromatic content of the Gabor with the spatio-temporal parameters fixed for all directions and contrasts. The exact chromatic directions and contrasts used in each experiment are reported their respective sections below.

The Color Tracking Task:

Subjects participated in the continuous tracking task in which they are asked to track the position of a target Gabor patch. On each trial, the Gabor patch spatially jittered its position along a horizontal linear path across the middle of the monitor in accordance with the temporal parameters noted in the prior section. The subjects were instructed to indicate the position of the Gabor patch

by continuously trying to keep the cursor in the middle of the patch. Subjects controlled the position of the cursor though the use of a computer mouse. At the end of each trial, we obtain a time-course of the target positions on the screen and the subjects cursor responses. Each trial lasted 11 seconds with an initial static period of one second. Example traces of the target (grey line) and tracking (black line) position as a function of time can be seen in the upper left panel in Figure 3-9.

The Gabor patches were modulated in 18 different chromatic directions each with 6 contrast levels. Tables 3-3 and 3-4 summarize the directions and contrast used in the Color Tracking Task for all subjects. These directions were split into three sets of experiments each with 6 directions. Within each set, subjects completed 2 sessions each made up of 10 experimental runs. An experimental run consisted of 36 trials corresponding to a single presentation of each of the conditions (6 directions and 6 contrast). Across the runs, we flip the handedness of the sine-phase Gabors such that alternating runs are offset by 180° spatial phase of the Gabor. The order of trials within a run was pseudo-randomized such that each session contained the desired number of repeats. Subjects controlled the pace of the trials and between trials only the background was present. A single session contained 360 trials lasting approximately 1 hour.

In total, across all three experimental sets, 2,160 trials were collected per subject equal to 6 hours of tracking data.

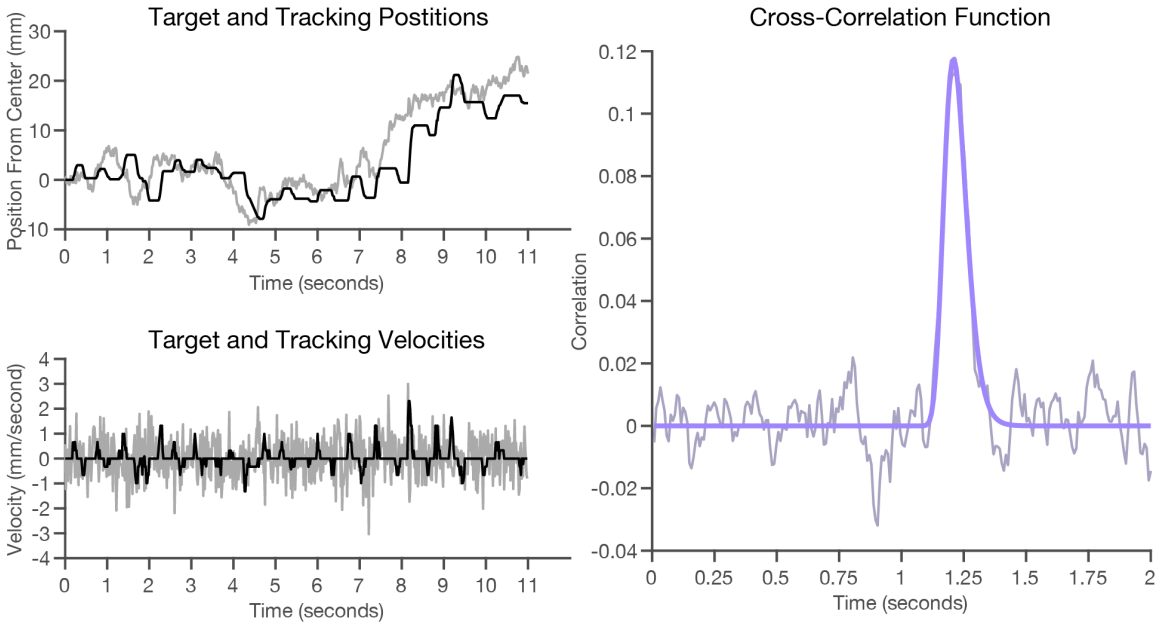

Figure 3-9: Overview of the Color Tracking Task.

The top left panel shows example position (mm) traces for an example run in the experiment. The grey line shows the target's position from center as a function of time. The black line shows the subject's cursor position from center as a function of time. The lower left panel show the velocities for the example data in the panel above. The grey line shows the velocity of the target as a function of time. The black like shows the cursor velocity as a function of time. The right panel shows the resulting tIRF. The light grey line shows the cross-correlation between the two velocities in the lower left panel. This cross-correlation function is the tIRF and the purple line show the log-Gaussian fit. We use the mode of the log-Gaussian to estimate the tracking lag.

	-86.2°	-82.5°	-78.75°	-75°	-45°	-22.5°	0°	22.5°	45°	75°	78.75°	82.5°	86.2°	90°
Max	84%	84%	84%	78%	26%	19%	18%	19%	25%	65%	83%	85%	85%	85%
Min	18%	15%	13%	6%	3%	3%	2%	3%	3%	6%	13%	14%	18%	18%

Table 3-3: The Chromatic Directions and Contrasts – CTM.

The chromatic directions and maximum/minimum contrasts of the tracking task. This table includes the chromatic directions common to all subjects.

Subject 1	**89.6°**	**88.6°**	**87.6°**	**-1.4°**
Max Contrast	85%	85%	85%	18%
Min Contrast	16	16%	16%	3%
Subject 2	**89.1°**	**88.1°**	**87.1°**	**-0.9°**
Max Contrast	85%	85%	85%	18%
Min Contrast	16	16%	16%	3%
Subject 3	**89.1°**	**88.1°**	**87.1°**	**-1.9°**
Max Contrast	85%	85%	85%	18%
Min Contrast	16	16%	16%	3%

Table 3-4: Subject Specific Directions and Contrasts – CTM.

The chromatic directions and maximum/minimum contrasts of the tracking task. This table includes the chromatic directions specific to an individual subject.

The Temporal Impulse Response Function:

From the time-courses of the target and the tracking positions, we can compute the temporal impulse response function associated with the color tracking task for each chromatic direction and contrast condition within an individual subject. In a linear system, the temporal impulse response function is

the response of the system, as a function of time, to a brief presentation of the input. In the context of the color tracking task, the tIRF describes the response of the visual-motor system to the movements of the random walk of the Gabor target. To obtain the tIRF, we perform a cross-correlation between the velocities of the target's random walk and the velocities of the subject's tracking. The velocities of the targets have a white noise power spectra containing no temporal autocorrelations. Example velocity traces for a given run can be seen in the lower left panel of Figure 3-9. In this panel, the target velocity is show as the grey line and the tracking velocity is shown as the black line.

Here, build to the interpretation of the tIRF. If the subject were to perfectly track the Brownian motion of the target, we would end up with two identical white noise velocity traces. The cross correlation of two white noise signals produces a delta function centered on 0 meaning they are perfectly correlated only when the signals are temporally aligned and have no other correlation as a function of delaying one signal relative to the other. Now if the subject perfectly tracked the target motion but had a consistent 2 second delay in their tracking then the resulting cross-correlation function would again be a delta function but centered at 2 second rather than 0. Deviation from the delta function shape is due to factors such as noisy tracking or dependance on the stimulus history to inform of

the target's current position. In the current experiment, we use the tIRFs to inform us of the delay of the visual-motor system associated tracking.

The tIRFs are obtained via the cross-correlation of the concatenation of position and tracking for all runs with a stimulus condition. This provides us with a mean tIRF for each chromatic direction and contrast pair. An example mean tIRF is plotted as the grey line in the right panel of Figure 3-9. This shows the correlation between the two signals as function of delaying one relative to the other for a particular direction and contrast. To reliably estimate lag from the mean tIRF, we fit a log-Gaussian function and take its mode as the lag of the tIRF. This tells us the time at which the log-Gaussian reaches its maximum correlation. An example log-Gaussian fit can be seen as the purple curve in the right panel of Figure 3-9 (as well as the purple curves in Figure 3-1). Overall, we obtain one lag estimate per stimulus condition.

The error bar on the lag estimates plotted in Figure 3-2 are computed as the 68 percent confidence intervals from a bootstrap analysis. The 68% confidence intervals are approximately +/- 1 SEM for a normal distribution. The bootstrap analysis was done via random sampling (with replacement) of the runs that went into the concatenation of the cross-correlation. We performed 200 bootstrap iterations and took the 68% percent confidence interval of the lag estimates for the log-Gaussian fit.

The Color Tracking Model:

The Color Tracking Model (CTM) is a 5-parameter model that provides a prediction of tracking lag for any input stimulus specified in terms of its L- and S-cones contrasts. A detailed formulation of a related model maybe found in the model appendix of Barnett et al. 2021. Converting chromatic direction and contrast into lag is done through two stages. The first stage is the application of a quadratic isoresponse contour. The isoresponse contour effectively weights the input stimulus contrast by the underlying chromatic mechanism sensitivity for the corresponding chromatic direction. This weighting produces a single output variable from the L- and S-cone contrast inputs, collapsing across color direction. We refer to this output variable as 'equivalent contrast' and it represent the strength of the chromatic mechanism output which is now independent of the original chromatic direction. The isoresponse contour represents sets of stimuli that when shown to a subject result in equal tracking lags. In the CTM, the shape of the isoresponse contour is constrained to be an ellipse restricted to the LS cone contrast plane.

Of the 5 parameters in the CTM, 2 of them are used to specify the elliptical isoresponse contour. One of these parameters is the ellipse angle. The ellipse

angle represents the direction of least sensitivity in the LS plane and read counterclockwise to the positive abscissa. Since the parametrization of the model enforces two orthogonal mechanisms, the second mechanism represents the direction of maximal sensitivity. The other parameter is the minor axis ratio. This is the ratio of the minor to major axis vector lengths. In this model, the length of the major axis is locked to unit length and the minor axis is constrained to be less than the major axis. Within this, minor axis vector length can be readily interpreted as this ratio. Together, these parameters provide a complete account of the chromatic stage of the model.

The second stage of the CTM employs a single nonlinearity which transforms the equivalent contrast to a prediction of the tracking lag. Since the isoresponse contour allows us to collapse across chromatic directions to a scalar equivalent contrast, we can use a single nonlinear function to map to tracking lag. The functional form we employ to convert equivalent contrast to lag is a the three-parameter exponential decay function:

$$lag = A * e^{-m*s} + d$$

In this expression, the parameters are *A*, *s*, and *d* which represent the amplitude, scale, and offset, respectively. The scale parameter operates on the equivalent contrast (*m*) and acts as gain on the output of the chromatic stage of

the model. The offset (*d*) is interpreted as the minimum lag, this is the point at which the decay function asymptotes.

The Color Detection Task:

Subjects participated in a color detection task which allowed for estimates of detection threshold to be obtained for each color direction. The detection task used a two-interval forced choice task paradigm in which a Gabor stimulus was presented in one of two sequential intervals. The start of each interval was marked with a brief tone as well as the disappearance of the fixation dot. Each interval had a duration of 400 ms and were separated a 200 ms gap between intervals in which the fixation dot was present. At the end of the trial, the subject indicates via a gamepad button press the interval in which they think the stimulus was presented. Based on this response, the subject receives auditory feedback (high pitch tone for correct, low pitch tone for incorrect).

The Gabor stimuli in the detection task had the same spatio-temporal properties as those used in the tracking task. Therefore, the stimuli, during their presentation, performed the same random walk for 400 ms. The primary way in which the non-chromatic properties of the stimuli differed across tasks was in the stimulus ramping. At the beginning and end of the interval containing the target, the contrast of the Gabor was temporally windowed. This window was a half-

cosine ramp with a duration of 100 ms. The structure of the target interval was as follows: a 100 ms ascending ramp at the beginning, 200 ms of full stimulus contrast, and a 100 ms descending ramp at the end.

For this experiment, we modulated the Gabor stimuli in 12 chromatic directions, these directions being a subset of the 18 directions used in the tracking. These chromatic directions were modulated around the same background across the two tasks. Within each chromatic direction, we tested at 6 evenly spaced contrast levels between the maximum contrast and 0 (excluding 0). The maximum contrasts were determined in pilot experiments for each subject and are intended to effectively sample the rising portion of the psychometric function. The directions tested and their corresponding maximum contrasts are reported in Table 3-5.

Subject	-86.25°	-82.5°	-78.75°	-75°	-45°	0°	45°	75°	78.75°	82.5°	86.25°	90°
1	14%	10%	9%	6%	2.5%	1.75%	2%	7%	7%	10%	18%	18%
2	10%	7%	5%	4%	1.25%	1%	1.25%	4%	5%	7%	10%	9%
3	10%	8%	5.5%	6%	1.5%	1%	1.5%	4%	5.5%	8%	10%	15%

Table 3-5: The Directions and Maximum Contrasts of the Detection Task.

The stimuli were displayed on the same CRT monitor as the previous experiments. One difference is the need for finer control of contrast than was needed for the previous tracking experiments. To achieve the required bit depth, we used a Bits++ device (Cambridge Research Systems) to enable 14-bit control

of the R, G, and B channel inputs to the CRT. In addition, a different host computer was used to control the experiment (Asus RoG laptop and Ubuntu 20.04) for compatibility with the Bits++ device.

Trials were blocked so that 60 trials of a given direction will be shown consecutively. Each block contained 10 presentations of all the contrast levels. The contrasts are pseudorandomized such that a random permutation of all 6 levels were shown before repeating a contrast. To orient the subject to the color direction of the block, there were 3 practice trials shown at the start of each block for the highest contrast level. Subjects completed a total of 40 trials per contrast/direction pair, that is 4 blocks per direction. Half of the blocks for each direction will be left-handed Gabors and the other half will be right-handed Gabors. We have 12 directions each with 6 contrast levels for a total of 240 trials per direction and a total of 2,880 trials.

Threshold Detection:

From the detection data, we estimate a threshold for each of the color directions tested. Threshold is the stimulus contrast needed, per direction, to reliably detect the Gabor target. We estimate this value by fitting a psychometric function to the percent correct as a function of stimulus contrast for each direction. Specifically, we fit a cumulative Weibull function and use it to determine

the contrast needed to reach 76% correct. The cumulative Weibull use is bounded between 50% to 100% by the inclusion of a guess rate scaling. See the equation in the next section for the function used.

The Color Detection Model:

The Color Detection Model (CDM) is a 4-parameter model that provides a prediction of the percent correct in the detection task for any input stimuli specified in terms of its L- and S- cones contrasts. The CDM parallels the CTM in its construction. It also employs two stages in order to convert stimulus contrast to percent correct. The first stage is an elliptical isoresponse contour identical to the one used in the CTM (see The Color Tracking Model section). Since the relationship between equivalent contrast and the variable of interest across the two tasks have different forms, we need to employ task-dependent nonlinearities as the second stage. In the CTM, this relationship was captured with an exponential decay function. For the detection task we use the cumulative Weibull as the nonlinearity that converts the equivalent contrast into percent correct. The functional form we use is:

$$PC = 1 - (1 - 0.5) * e^{-(\frac{m}{\lambda})^k}$$

In this expression, the parameters are λ and k which represent the scale, and shape, respectively. The scale parameter operates on the equivalent contrast (m) and acts as gain on the output of the chromatic stage of the model. The shape parameter (k) controls the slope. The guess rate is locked at 0.5 since this is chance in a 2IFC, therefore the part of the expression '(1-0.5)' bounds the output precent correct between 0.5 and 1.

Parameter Fitting:

We fit both the CTM and CDM to their respective measurements as a function of their stimulus contrasts. These data were fit using the MATLAB function *fmincon* to find a set of model parameters that minimize the root mean squared error between the actual tracking lags or percent correct and the predicted values of the CTM and the CDM, respectively

CHAPTER 4

Discussion

Understanding the Representation of Color in Primary Visual Cortex

The measurements presented in Chapter 2 show that area V1 is most sensitive to modulation made in the L-M direction and least sensitive to L+M, when modulations are restricted to the LM cone contrast plane. Further, these results did not vary as a function of eccentricity. These results are specific to the choice of the spatial and temporal configuration of the stimulus. From the data collected, we developed a quantitative model of these V1 responses. The quadratic color model (QCM) captures the V1 response to any stimulus in the LM plane. This model performed well in a cross-validated sense when compared to more flexible models. The model also generalized to chromatic directions not used to train the model. These results replicated within each subject.

The QCM is a separable model with respect to the effects of chromatic direction and contrast. The effect of chromatic direction is captured by an elliptical isoresponse contour. The effect of contrast is captured by the saturating nonlinearity. This allowed for the evaluation of the chromatic sensitivity of V1 in a manner that is independent of the effects of contrast.

The work in Chapter 2 only measured responses to stimulus modulations restricted to the LM contrast plane. This work provides a starting point and a validation of this separable model framework in fMRI data. One interesting direction would be to get a full account of the L-, M-, and S-cone contrast space. Generalizing the QCM to handle stimuli defined in terms of all three cone classes requires changing the elliptical isoresponse contours to an ellipsoidal isoresponse surfaces. The same sets of validations performed in chapter 2 could then be applied in this 3-dimensional space. Additionally changes to the flicker rate of the stimulus could be made and the resulting shape of the isoresponse contours could be examined as a function of this temporal rate. We know from prior work that the temporal properties of the stimulus affect the pattern of responses in V1(Engel, Zhang, & Wandell, 1997). Similarly, the size of the stimulus could be varied from a full field stimulus to a restricted spot stimulus. This spot stimulus could then be presented in peripheral location and the eccentricity findings could be examined in a new test of peripheral responses.

Another variation on the stimulus that would inform us about the computation of V1 is to add spatial structure. The stimuli in Chapter 2 were spatially uniform. Measuring how the elliptical isoresponse contours change due to variations in the spatial structure could inform us of separate sets of mechanisms. These could correspond to the functionality of the ‘color’,

'luminance' and 'color-luminance' cells as described by Johnson et al., (2001) in which the high-spatial frequency would drive the 'color' cells less. Importantly, adding spatial structure would add the benefit of being able to fit the QCM outside of V1. In our data, we were unable to fit the QCM reliably outside V1 and this is most likely due to the full field spatially uniform stimuli which is not commonly used in fMRI. Driving more cortical area with our stimulus would allow us to assess how the color representation changes as a function of the visual area. It also informative to know how and where the model stops capturing the cortical response to the stimulus. This would imply that the responses of certain cortical areas cannot be modeled by a separable 2-stage model with a single color and contrast stage. Separable channel models that do not consider chromatic spatial interactions do not completely describe the color information in the scene. Knowing which areas behave in a manner consistent with the QCM and which need additional computations added will provide important insight into the cortical processing of color.

Moreover, generalizing the QCM to any arbitrary spatial stimuli would provide a solid foundation for examining the representation of color. Previous quantitative forward models of the BOLD response have made progress in the domain of achromatic modulations with arbitrary spatial patterns (Kay et al., 2013a; Kay et al., 2013b). These operate on an input image and transform it into

a model of the BOLD response via multiple sequential stages. To add color to these models the color-spatial interactions must be handled but the exact form of these interactions is not known. If the QCM can account for other spatial stimuli, this would constrain the generalizations for such forward models to incorporate color.

Understanding the Interaction Between Color and Tracking

Measurements of the temporal dynamics of color processing were made using a continuous tracking paradigm. From this, we estimated the tIRF for each direction tested using a log-Gaussian fit to the empirical cross-correlation functions. We examined how these lags changed as a function of chromatic direction and contrast. Detection data were also collected in the same set of subjects. We observe the same pattern of relative sensitivities in the detection task as for the tracking task. Thresholds were smallest for detecting and tracking stimuli modulated in the L-cone isolating direction and the largest for S-cone isolating stimuli, when contrast is matched.

Similar to the QCM, we developed models of both tracking lag and threshold detection. Both models have the same two stage structure. The first stage, which is the same in all models, is the quadratic isoresponse contour which allows for the conversion to ‘equivalent contrast’, representing the output

strength of the color mechanisms. The second stage of the model is a task-specific nonlinearity which transforms the equivalent contrast to a prediction of either lag or percent correct. Interpreting the isoresponse contours of the CTM and CDM reveals that the mechanisms aligned with the L-cone isolating direction are ~33x and ~11x more sensitive than to the S-cone isolating direction for tracking and detection, respectively. Assuming common mechanisms across tasks, the contours tell us that the chromatic mechanisms are the same across tasks and what changes is the relative importance of the S-cone signals. The relative sensitivity difference is ~3x lower for the tracking task than the detection task meaning that the tracking task makes less use of the S-cone signals.

Just as with the QCM, the tracking task can be expanded to include stimulus modulations in all three-dimension of L-, M-, and S-cone contrast space. It is not known from the experiments in Chapter 3 what shape relative sensitivities will take outside the LS plane, when the M-cone axis is added. In the exact same way as the QCM, expanding the CTM and the CDM is simply changing to an ellipsoidal isoresponse surface rather than the elliptical contour. Tracking and detection measurements made using stimuli that are modulated in the L-, M-, and S-cone isolating directions (and their combinations) provide a fuller account of the mechanisms serving these tasks.

Another generalization is to change the mean of the gaussian velocity distribution that defines the random walk of the Gabor patches. This would change how fast the target was moving on the screen. In Chapter 3, we fixed the mean of the velocity distribution to ~4 °/s. The addition of sampling in the velocity space would allow for the examination of speed-color interactions. From this we could see how the relative sensitivities of the mechanisms change as a function of mean velocity. Additionally, we can also vary the size and spatial frequency of the stimuli to examine similar interactions. Any additional stimulus variable tested would go towards building models of tracking for any arbitrary spatiotemporal stimuli.

Another way in which we can better examine the underlying mechanisms is to add additional tasks. We have used tracking and detection tasks but tasks such as reaction time, two pulse detection and, discrimination could be added to the common mechanism framework. In all cases, we would use the ellipsoidal isoresponse surfaces to convert stimuli, specified by their L-, M-, and S-cone contrast, into equivalent contrast providing a single representation of the output strength of the chromatic mechanisms. The second stage for any additional task will need to be task-specific nonlinearities. With this expanded gamut of tasks, we will have a clearer picture of which behaviors are mediated by these common mechanisms.

Examination of the other aspects of the tIRF can reveal further interesting relationships in the data. The log-Gaussian fits, which we take as the tIRF, provide both the amplitude and width of the tIRF. The amplitude is the maximum correlation and width is the full width half maximum of the cross-correlation function. In a linear system, the width has an interpretation as the dependance on the stimulus history. Either of these parameters could be examined for their relationship with chromatic direction and contrast. In its current form, the QCM is one way of evaluating a single parameter. Another way in which we could analyze the data is to create a model that predicts the tracking given a temporal order of the stimulus chromatic directions and velocities. This model would make an explicit estimation of the tIRF instead of using the nonlinearity (exponential decay function). A sensible start would be to optimize the parameters of the log-Gaussian and use this as the kernel of the convolution to convert stimulus positions into subject tracking. This type of model would still need to model the effect of color on tracking. To handle this, the elliptical isoresponse contour could transform the cone contrast of the stimuli to equivalent contrasts. An additional stage may be required to account for how cursor movements scale with equivalent.

APPENDIX A: Supplemental Tables and Figures

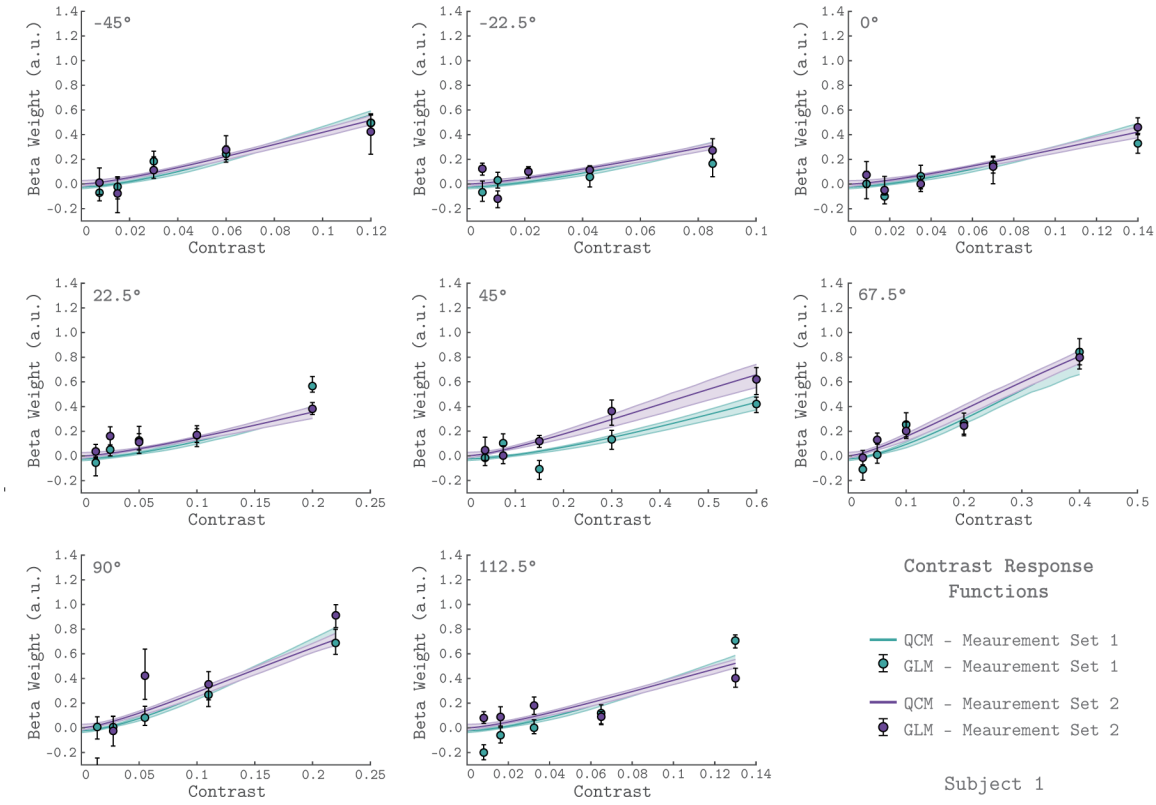

Figure 2 – figure supplement 1: Subject 1 V1 contrast response functions

V1 contrast response functions for the eight measured chromatic directions from Subject 1. The format of the figure is the same as Figure 2-2 in the main text. The x-axis is contrast; the y-axis is the beta weight of the GLM. The chromatic direction of each stimulus is indicated in the upper left of each panel. The curves in each panel represent the contrast response function obtained using the QCM. The error bars indicate 68% confidence intervals obtained using bootstrapping. Measurement sets 1 and 2 are shown in green and purple. The x-axis range differs across panels as the maximum contrast used varies with color direction.

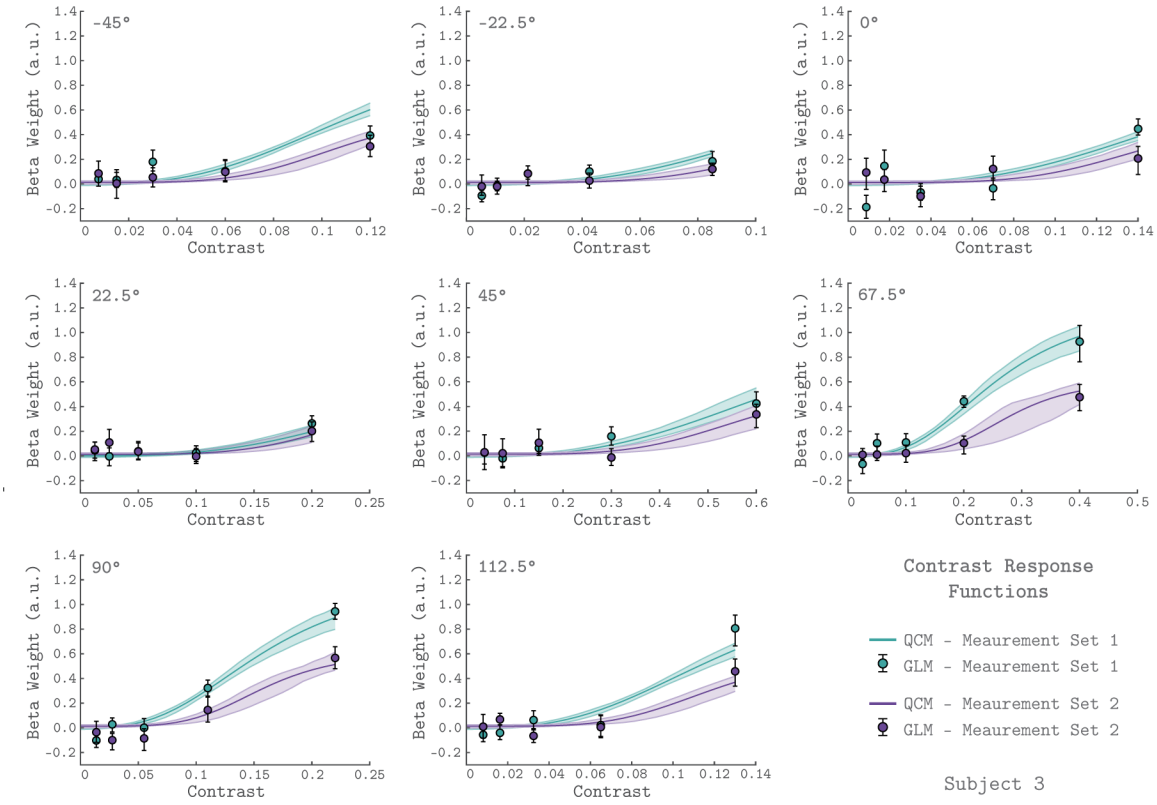

Figure 2 – figure supplement 2: Subject 3 V1 contrast response functions

V1 contrast response functions for the eight measured chromatic directions from Subject 3. The format of the figure is the same as Figure 2 in the main text and Figure 2 – figure supplement 1.

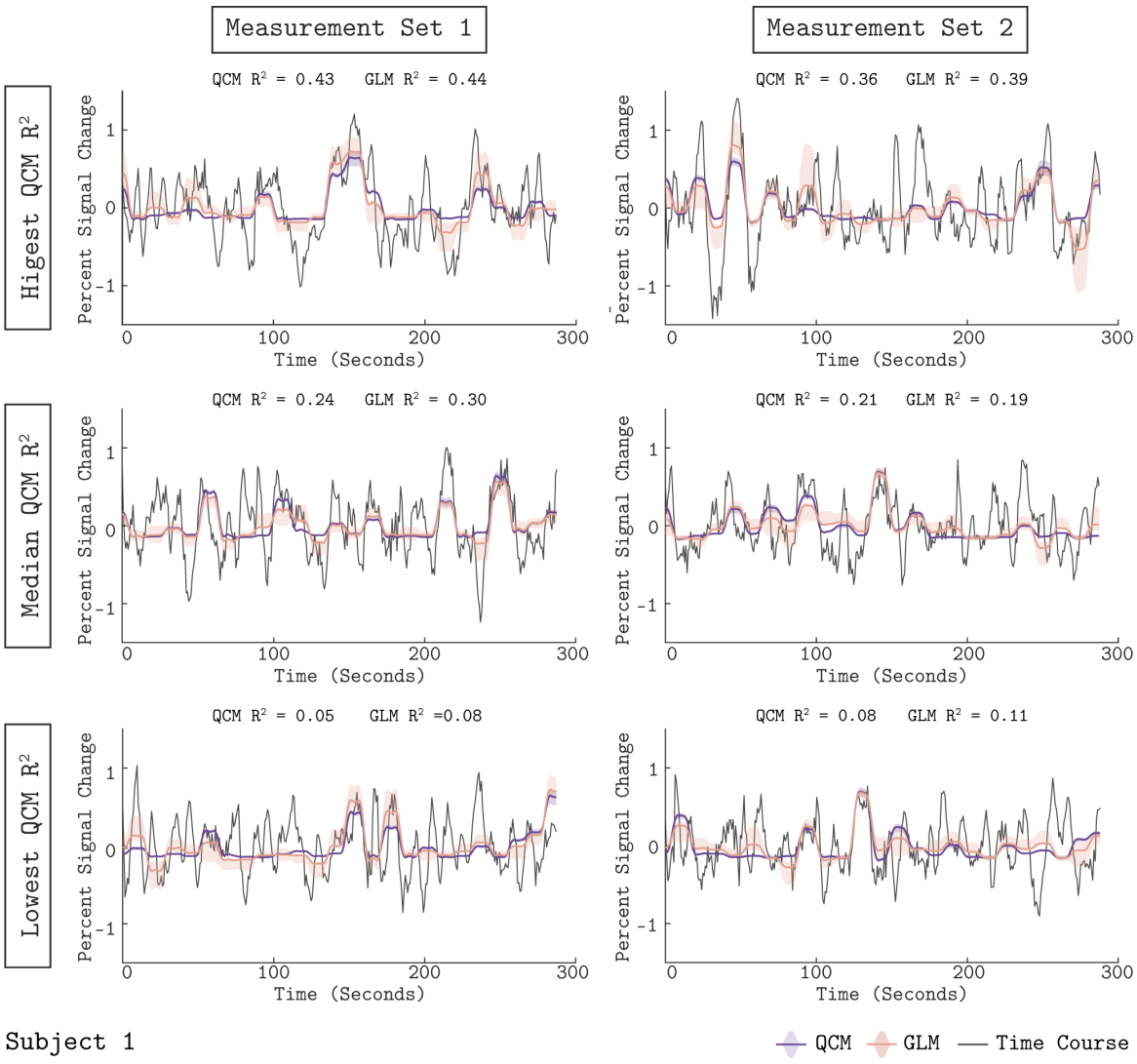

Figure 3 – figure supplement 1: Subject 1 Model time course predictions.

Model predictions of the V1 BOLD time course from Subject 1. The format of the Figure is the same as Figure 3 in the main text. The measured BOLD time course (black line) is shown along with the model outputs from the QCM (thick purple line) and GLM (thin orange line) for 6 acquisitions. The left column shows data and predictions from measurement set 1 and the right column for measurement set 2. The three acquisitions presented for each measurement set were chosen to correspond to the highest, median, and lowest QCM R^2 values within the respective measurement set. The R^2 values for the QCM and the GLM are displayed at the top of each panel. The shaded regions represent the 68% confidence intervals obtained via the bootstrap analysis.

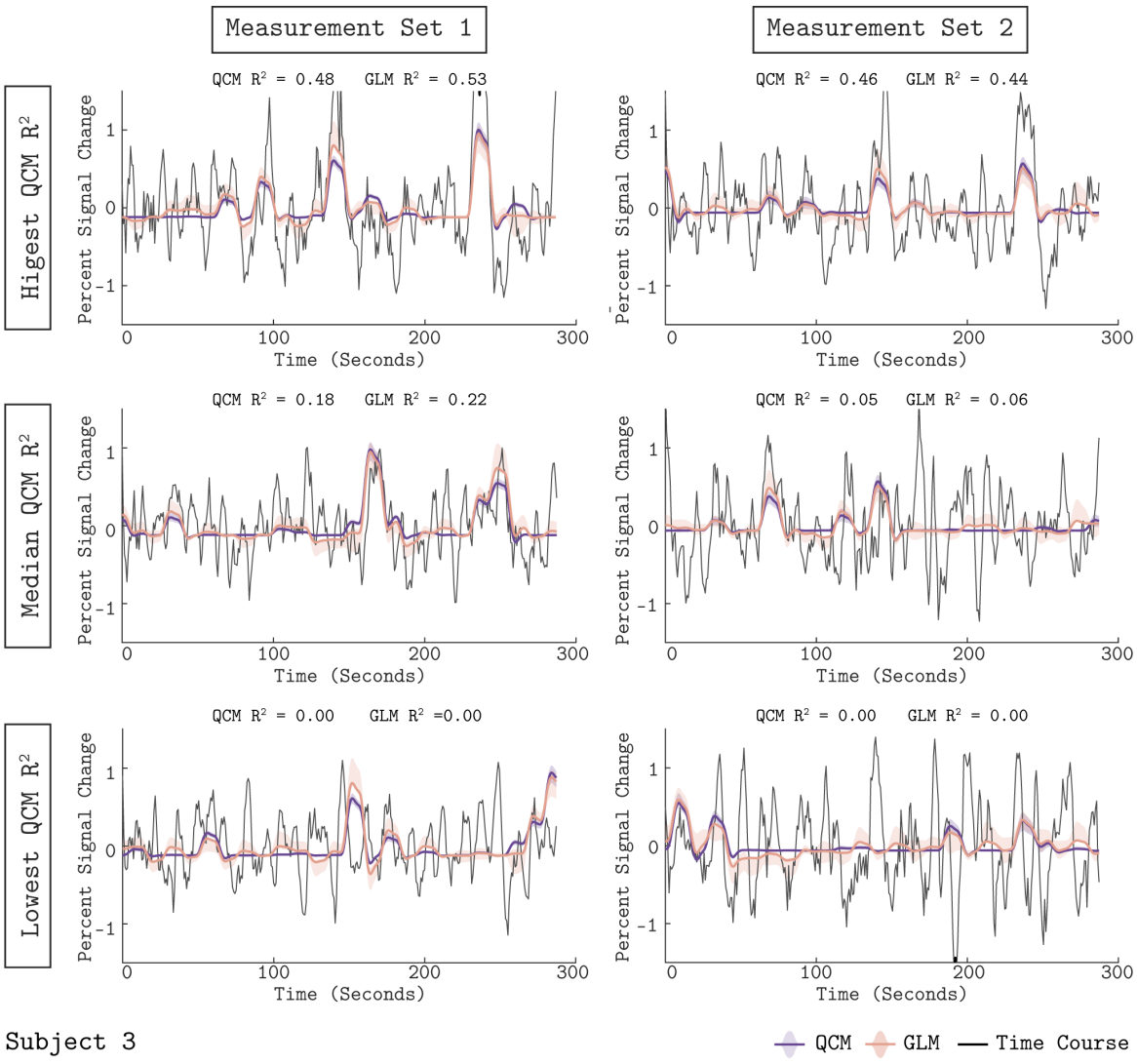

Figure 3 – figure supplement 2: Subject 1 Model time course predictions

Model predictions of the V1 BOLD time course from Subject 3. The format of the figure is the same as Figure 3 in the main text and Figure 3 - figure supplement 1 The measured BOLD time course (black line) is shown along with the model outputs from the QCM (thick purple line) and GLM (thin orange line) for 6 acquisitions.

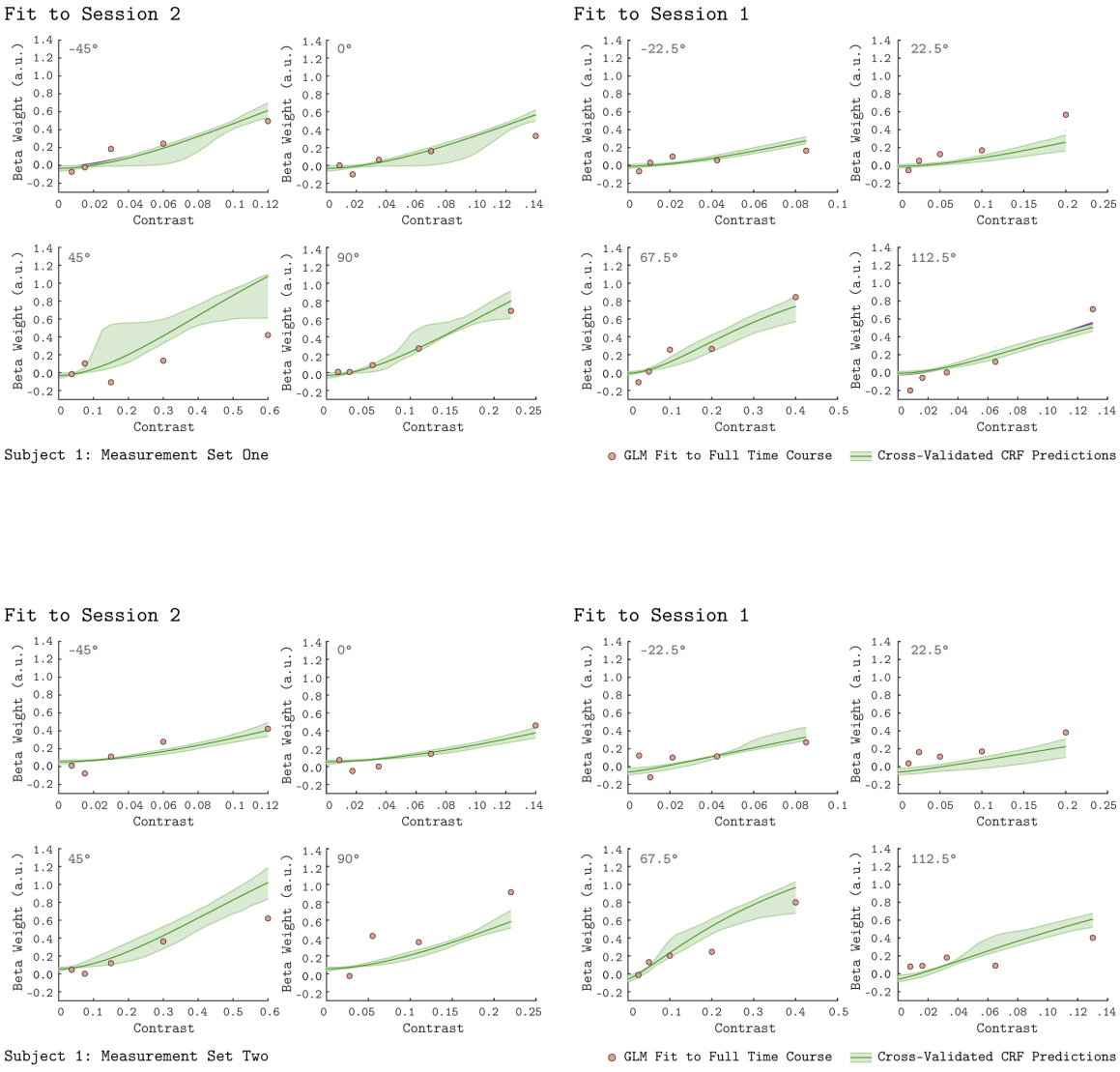

Figure 5 – figure supplement 1: Subject 1 Leave-Sessions-Out Cross Validation

Leave-Sessions-Out Cross Validation for Subject 1. The format of the Figure is the same as Figure 2-5 in the main text. The contrast response functions in each panel (green lines) are the result of a leave-sessions-out cross-validation to test the generalizability of the QCM. In both the top and bottom eight panels, the QCM was fit to data from four of the eight tested chromatic directions, either from session 1 or session 2. The fits were used to predict the CRFs for the held-out chromatic directions. The orange points in each panel are the GLM fits to the full data set. The data shown here are for Subject 1 with the top eight panels from measurement set 1 and the bottom eight panels from measurement set 2. The shaded green error regions represent the 68% confidence intervals for the QCM predictions obtained via the bootstrap analysis.

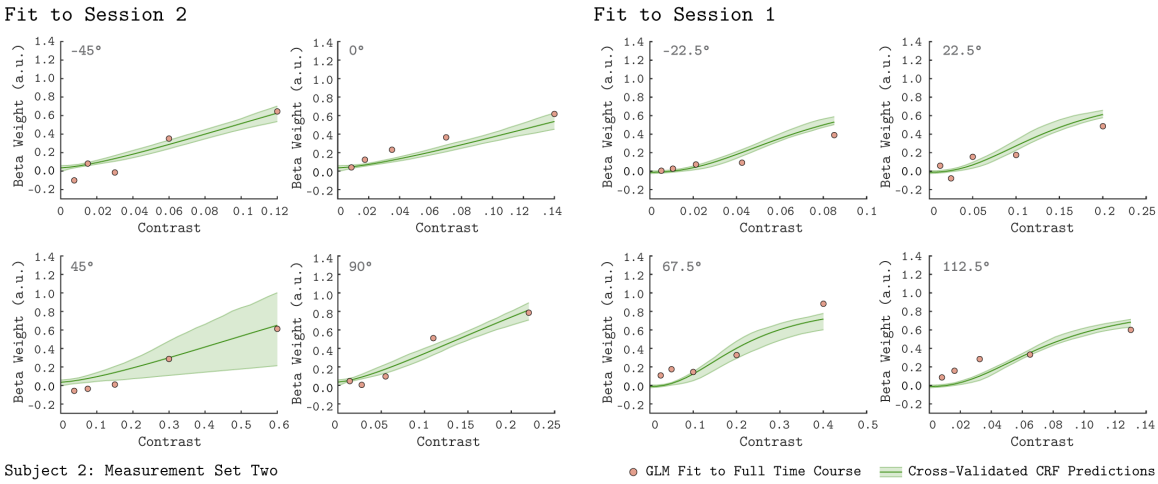

Figure 5 – figure supplement 2: Subject 2 Leave-Sessions-Out Cross Validation

Leave-Sessions-Out Cross Validation for Subject 2. The format of the figure is the same as Figure 2-5 in the main text and Figure 5 - figure supplement 1. The contrast response functions in each panel (green lines) are the result of a leave-sessions-out cross-validation to test the generalizability of the QCM. The orange points in each panel are the GLM fits to the full data set. The data shown here are for Subject 2 measurement set 2; Measurement set 1 can be seen in Figure 2-5 of the main text. The shaded green error regions represent the 68% confidence intervals for the QCM predictions obtained via the bootstrap analysis.

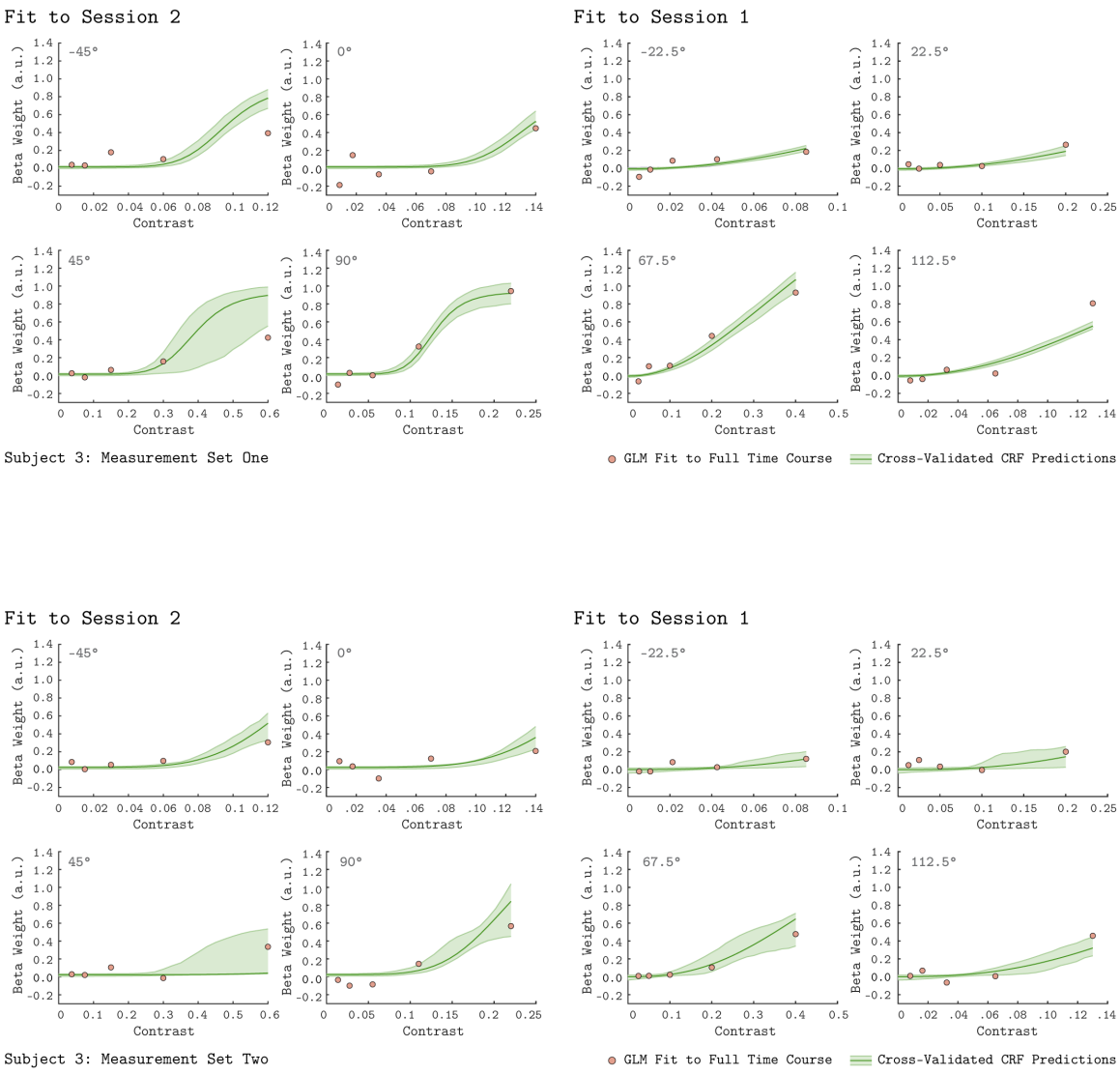

Figure 5 – figure supplement 3: Subject 3 Leave-Sessions-Out Cross Validation

Leave-Sessions-Out Cross Validation for Subject 3. The format of the figure is the same as Figure 2-5 in the main text and Figure 5 - figure supplement 1-2. The green lines are the leave-session-out CRF, and the orange points are the GLM fits to the full data set. The data shown here are for Subject 3 with the top eight panels from measurement set 1 and the bottom eight panels from measurement set 2. The shaded green error regions represent the 68% confidence intervals for the QCM predictions obtained via the bootstrap analysis.

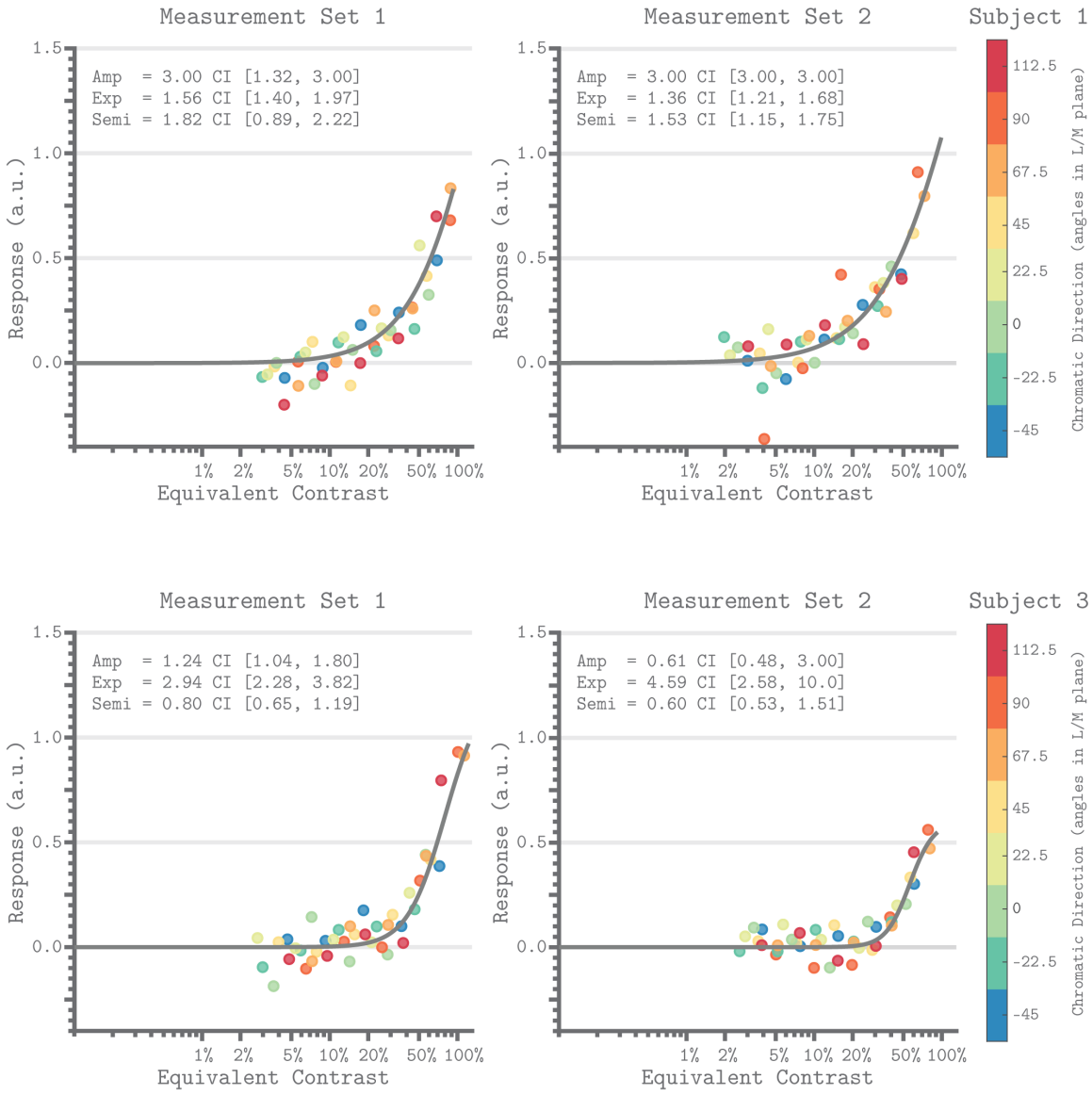

Figure 7 – figure supplement 1: Equivalent Contrast Non-Linearities

Equivalent Contrast Non-Linearities of the QCM for V1. The format is the same as Figure 2-7 in the main text. The x-axis of each panel marks the equivalent contrast and the y-axis is the response. The gray curve in each panel is the Naka-Rushton function obtained using the QCM fit. The upper two panel are from Subject 1 and the bottom 2 panels are from Subject 3. The left panels are for Measurement Set 1 and the right panels are for Measurement Set 2. The parameters of the Naka-Rushton function are reported in upper left of each panel along with the 68% confidence intervals obtained via the bootstrap analysis. The points in each panel are the GLM beta weights of the respective measurement set mapped via the QCM isoresponse contours onto the equivalent contrast axis (see Methods). The color of each point denotes the chromatic direction of the stimuli, as shown in the color bar.

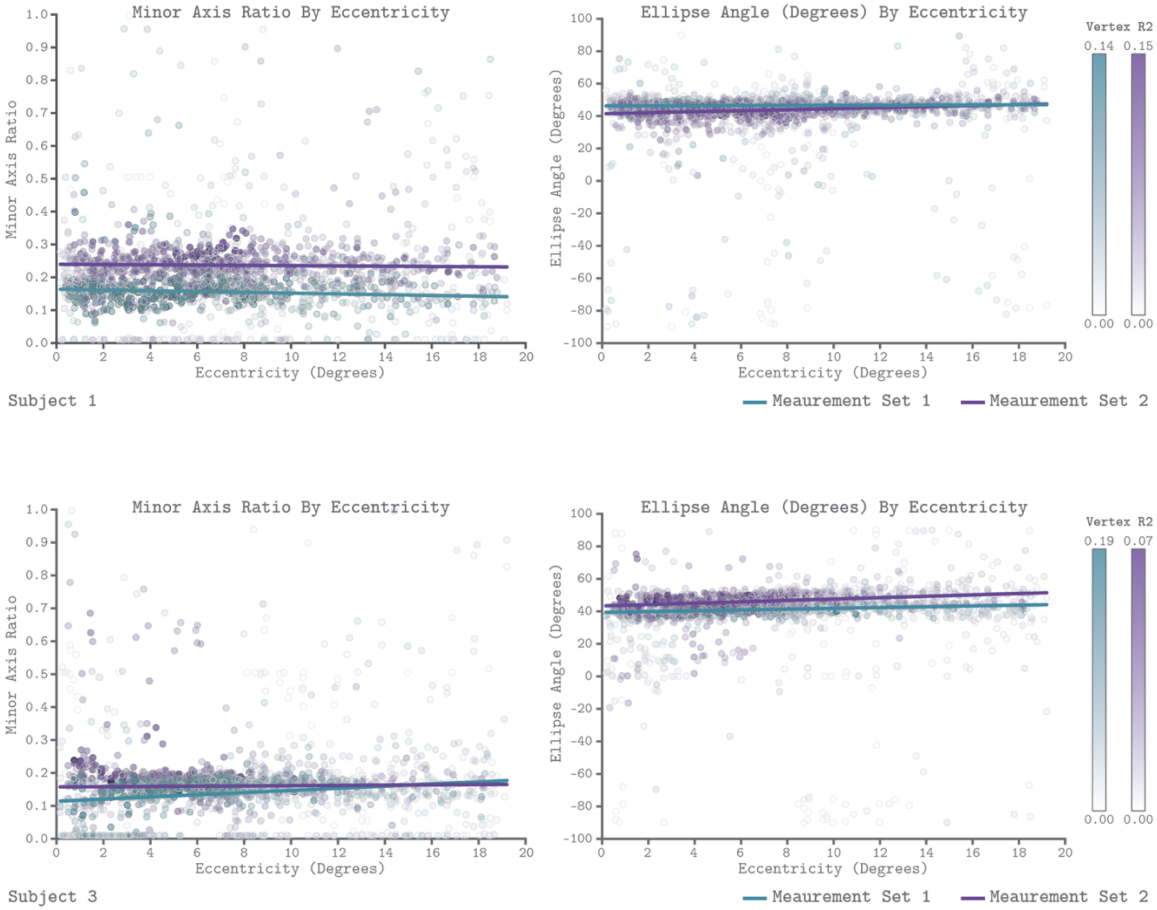

Figure 9 – figure supplement 1: QCM Parameters as a Function of Eccentricity

The format is the same as Figure 2-9 in the main text. The top row shows parameter fits from subject 1 and the bottom row shows fits from Subject 3. The left and right panels show scatter plots of the minor axis ratio and ellipse angle plotted against their visual field eccentricity, respectively. Each point in the scatter plot shows a parameter value and corresponding eccentricity from an individual vertex. Teal indicates measurement set one and purple indicates measurement set two. The lines in each panel are robust regression obtained for each measurement set separately. The transparency of each point provides the R^2 value of the QCM at that vertex. The color bars provide the R^2 scale for each measurement set.

Direction	-45°	-22.5°	0°	22.5°	45°	67.5°	90°	112.5°
L-Contrast	8.49%	7.85%	14%	18.48%	42.43%	15.31%	0%	4.98%
M-Contrast	8.49%	3.25%	0%	7.65%	42.43%	36.96%	22%	12.01%
S-Contrast	0%	0%	0%	0%	0%	0%	0%	0%
Total Contrast	12%	8.5%	14%	20%	60%	40%	22%	13%

Table Supplement 1: Maximum contrast per direction

Table of the nominal maximum contrast per direction. The top row indicates the chromatic direction in the LM plane. The L, M, and S contrast rows show the desired contrast on the L, M, and S cones respectively. The total contrast is the vector length of stimuli made up of the L, M, and S cone contrast components and is the definition of contrast used in this study,

Subject 1 – Measurement Set 1								
Nominal Angle	-45°	-22.5°	0°	22.5°	45°	67.5°	90°	112.5°
Center Angle	-41.23 ±3.13	-15.90 ±6.59	2.17 ±1.05	23.43 ±0.23	45.21 ±0.23	69.36 ±1.61	87.98 ±1.26	120.94 ±8.45
Periphery Angle	-42.85 ±3.04	-16.31 ±6.18	1.61 ±0.44	22.75 ±0.22	44.78 ±0.22	68.13 ±1.54	88.72 ±0.18	119.67 ±8.04
Nominal Contrast	12%	8.5%	14%	20%	60%	40%	22%	13%
Center Contrast	12.14 ±0.05	9.02 ±0.75	14.44 ±0.37	21.05 ±0.79	60.92 ±0.09	38.01 ±1.97	21.39 ±0.85	12.56 ±0.38
Periphery Contrast	12.00 ±0.04	8.93 ±0.72	13.98 ±0.35	20.28 ±0.73	58.73 ±0.09	37.81 ±1.89	21.42 ±0.55	12.48 ±0.36
Subject 1 - Measurement Set 2								
Nominal Angle	-45°	-22.5°	0°	22.5°	45°	67.5°	90°	112.5°
Center Angle	-45.09 ±0.55	-22.44 ±0.98	3.49 ±2.27	22.97 ±0.15	45.18 ±0.03	67.75 ±0.24	87.81 ±1.69	112.99 ±1.03
Periphery Angle	-46.16 ±0.55	-22.32 ±0.99	3.24 ±2.77	22.39 ±0.19	44.92 ±0.02	66.85 ±0.21	87.33 ±1.24	68.34 ±0.92
Nominal Contrast	12%	8.5%	14%	20%	60%	40%	22%	13%
Center Contrast	11.75 ±0.01	8.28 ±0.08	13.78 ±0.09	20.35 ±0.22	60.26 ±0.48	37.62 ±0.11	21.82 ±0.08	12.69 ±0.05
Periphery Contrast	11.65 ±0.02	8.29 ±0.08	13.53 ±0.09	19.79 ±0.18	58.47 ±0.48	38.16 ±0.10	21.99 ±0.10	12.81 ±0.06

Table Supplement 2: Stimulus Validation Measurements for Subject 1

The top set of rows show data for measurement set one and the bottom set show data for measurement set 2. The dark gray rows show the nominal angle and contrast. Each cell shows the mean and standard deviation of stimulus vector angles and lengths computed from 10 validation measurements (5 pre-experiment, 5 post-experiment). Center and periphery denote which set of cone fundamentals were used to calculate cone contrast of the stimuli referring either the 2° or 15° CIE fundamentals, respectively.

Subject 2 - Measurement Set 1								
Nominal Angle	-45°	-22.5°	0°	22.5°	45°	67.5°	90°	112.5°
Center Angle	-45.73 ±1.06	-19.23 ±2.51	1.71 ±0.98	24.04 ±0.39	45.43 ±0.09	68.36 ±0.53	87.87 ±1.64	114.92 ±1.90
Periphery Angle	-47.03 ±1.02	-18.91 ±2.40	1.63 ±0.77	23.65 ±0.38	44.99 ±0.09	67.18 ±0.52	87.65 ±1.09	114.11 ±1.86
Nominal Contrast	12%	8.5%	14%	20%	60%	40%	22%	13%
Center Contrast	12.04 ±0.11	8.41 ±0.21	14.01 ±0.08	20.45 ±0.52	60.72 ±0.38	39.68 ±0.63	21.82 ±0.23	12.73 ±0.16
Periphery Contrast	11.88 ±0.11	8.36 ±.21	13.58 ±0.07	19.81 ±0.51	58.56 ±0.35	39.41 ±0.59	21.82 ±0.24	12.62 ±0.14
Subject 2 - Measurement Set 2								
Nominal Angle	-45°	-22.5°	0°	22.5°	45°	67.5°	90°	112.5°
Center Angle	X	-25.85 ±3.20	X	22.72 ±0.38	X	67.42 ±0.16	X	112.03 ±1.22
Periphery Angle	X	-26.43 ±3.04	X	22.35 ±0.35	X	66.36 ±0.16	X	110.12 ±1.17
Nominal Contrast	12%	8.5%	14%	20%	60%	40%	22%	13%
Center Contrast	X	8.36 ±0.16	X	19.77 ±0.23	X	39.75 ±0.13	X	12.75 ±0.15
Periphery Contrast	X	8.34 ±0.17	X	19.21 ±0.23	X	40.04 ±0.15	X	12.95 ±0.13

Table Supplement 3: Stimulus Validation Measurements for Subject 2

The format of this figure is the same as table supplement 2. Cells that contain an “X” mark stimulus directions in which validation measurements were not recorded due to technical difficulty.

Subject 3 - Measurement Set 1								
Nominal Angle	-45°	-22.5°	0°	22.5°	45°	67.5°	90°	112.5°
Center Angle	-48.84 ±5.02	-27.84 ±6.02	5.29 ±4.45	23.61 ±0.77	45.41 ±0.15	67.48 ±0.42	85.96 ±3.11	108.56 ±4.89
Periphery Angle	-50.40 ± 4.90	-28.48 ±5.97	5.09 ±4.72	23.26 ±0.77	45.02 ±0.13	66.33 ±0.43	86.12 ±3.24	107.49 ±4.78
Nominal Contrast	12%	8.5%	14%	20%	60%	40%	22%	13%
Center Contrast	12.25 ±0.32	8.39 ±0.06	13.96 ±0.08	19.78 ±0.20	61.92 ±1.40	40.87 ±1.14	22.91 ±1.30	13.53 ±0.75
Periphery Contrast	12.13 ±0.31	8.30 ±0.08	13.52 ±0.09	19.17 ±0.21	59.76 ±1.36	40.65 ±1.13	22.97 ±1.26	13.47 ±0.71
Subject 3 - Measurement Set 2								
Nominal Angle	-45°	-22.5°	0°	22.5°	45°	67.5°	90°	112.5°
Center Angle	X	-24.51 ±1.57	X	22.92 ±0.07	X	67.65 ±0.19	X	111.23 ±1.11
Periphery Angle	X	-24.17 ±1.53	X	22.65 ±0.06	X	66.57 ±0.19	X	69.95 ±1.07
Nominal Contrast	12%	8.5%	14%	20%	60%	40%	22%	13%
Center Contrast	X	8.24 ±0.07	X	19.93 ±0.09	X	39.77 ±.0.27	X	12.88 ±0.11
Periphery Contrast	X	8.23 ±0.07	X	19.45 ±0.26	X	40.16 ±0.26	X	12.92 ±0.10

Table Supplement 4: Stimulus Validation Measurements for Subject 3

The format of this figure is the same as table supplement 2 and 3. Cells that contain an “X” mark stimulus directions in which validation measurements were not recorded due to technical difficulty.

Subject 1 – Measurement Set 2: Session 1										
Run Number	1	2	3	4	5	6	7	8	9	10
Number of Censored Frames (n/360)	0	0	8	18	0	26	47	4	0	0
Subject 1 – Measurement Set 2: Session 2										
Run Number	1	2	3	4	5	6	7	8	9	10
Number of Censored Frames (n/360)	0	0	0	0	0	0	0	7	0	0

Table Supplement 5: Number of Censored fMRI frames per Run

Values shown are for Subject 2 measurement set 2. The top set of rows show data for session one and the bottom set of the show data for session 2. Each set of rows show the number of censored frames per run out of 360 frames. Subjects and sessions not shown mean that no frames were censored in those runs.

Appendix B: Model Appendix

General Linear Model

The model used to provide a benchmark for the quadratic color model (QCM) is the general linear model (GLM). The GLM has the form:

$$Y = X\beta + \epsilon$$

This states that the measurement (Y) is equal to the model matrix (X) times the weights (β) plus the residual error (ϵ). For our GLM, Y is a column vector of the concatenated time series from all the fMRI runs within a measurement set (20 runs):

$$Y = \begin{bmatrix} y_1 \\ \vdots \\ y_i \\ \vdots \\ y_t \end{bmatrix}$$

The subscript i indicates a particular time point, with the subscript t being the total number of time points in a measurement set. Here a time point corresponds to one TR of the BOLD response, and t = 7200 (20 runs with 360 TRs). Our model comparison was for the aggregated V1 response, and we took each element y_i of Y to be the median BOLD fMRI response for the corresponding TR, with the median taken across the voxels in the V1 ROI.

The model matrix X contains the predictor variables for the linear model. Each column of X is a regressor corresponding to a single stimulus (a single chromatic direction/contrast pair or the baseline (0 contrast) uniform field). The regressors are created by convolving a binary indicator vector with the hemodynamic response function (HRF) that accounts for the sluggish BOLD response to a stimulus event. The binary indicator vectors contain 1 when the stimulus was present and 0 otherwise. The convolution then produces a predictor of the measured BOLD fMRI response for that stimulus condition. In our study, X has 41 columns corresponding to the pairing of the eight chromatic directions and five contrasts levels plus the baseline

$$X = \begin{bmatrix} x_{1,1} & \dots & x_{1,41} \\ \vdots & & \vdots \\ x_{i,1} & \dots & x_{i,41} \\ \vdots & & \vdots \\ x_{t,1} & \dots & x_{t,41} \end{bmatrix}$$

The general linear model predicts Y as a weighted linear combination of the regressors in the columns of X. The weight applied to each regressor is given by the elements of β:

$$\beta = \begin{bmatrix} \beta_1 \\ \beta_2 \\ \vdots \\ \beta_{41} \end{bmatrix}$$

Using β and X, we can generate a predicted time course $\hat{Y}$. We take each β_i to be a proxy for the aggregate V1 BOLD fMRI response for the corresponding stimulus condition. This interpretation is associated with our particular choice of scaling the indicator variables in the regressors before convolution with the HRF (that is the choice of 1 for the TRs during which the stimulus was present). We determined β using linear regression as implemented in the MATLAB mldivide operation, $\beta = X \backslash Y$ (see https://www.mathworks.com/help/matlab/ref/mldivide.html). The GLM prediction of the BOLD fMRI response at each time point y_i is therefore:

$$\hat{y_i} = x_{(i,1)}\beta_1 + x_{(i,2)}\beta_2 + \ldots + x_{(i,41)}\beta_{41}$$

.

Quadratic Color Model

The quadratic color model allows for the prediction of the BOLD fMRI response to any stimulus that lies in the LM contrast plane. This includes predictions for stimuli not in the measurement set used to fit the model. The QCM makes its predictions through three steps. The first step calculates the "equivalent contrast" of the stimulus which can be thought of as the effective contrast of the stimulus in V1 accounting for the differences in sensitivity across chromatic di-

rections. Equivalent contrast is the vector length of the stimuli after this linear transformation. The next step is a response non-linearity applied to the equivalent contrast to predict the underlying neural response. Finally, a convolution of this underlying response with the HRF results in predictions of the BOLD fMRI response. Here, we provide explanations and equations for the model.

We start by considering a stimulus modulation whose predicted BOLD fMRI response we wish to know. A stimulus modulation is denoted by the column vector c whose two entries are the L and the M cone contrast of the stimulus (l and m respectively):

$$c = \begin{bmatrix} l \\ m \end{bmatrix}$$

The figure below outlines how we transform such a stimulus to a response prior to convolution with the HRF. Panel A shows a 3-dimensional contrast-response space with the (x,y) plane representing the LM contrast plane and the z axis giving the response r corresponding to each point in the LM contrast plane. In this representation, all possible stimuli and responses form an inverted bell shape surface, as illustrated below. At constant values of r (constant height on the z axis), cross sections through this surface shows the elliptical isoresponse contours of the QCM. Each elliptical isoresponse contour describes the set of LM contrast combinations that elicit the same response r. The teal and red dots shown in the LM plane represent example stimulus modulations, chosen in two color directions at contrasts corresponding to the five (dark blue, blue, aqua, green, yellow) isoresponse contours illustrated.

To obtain the equivalent contrast corresponding to stimulus c, we first apply a linear transformation M to c to obtain a transformed representation of the stimulus, $e = Mc$. The vector e is a two-dimensional column vector whose entries we refer to as e_1 and e_2. We call the transformed representation of the stimulus the equivalent contrast space, and as we show below we choose the linear transformation M such that in this space the isoresponse contours are circles. Panel B of the figure shows the same information as in Panel A represented in the equivalent contrast space. Here the (x,y) plane gives the values of e_1 and e_2, and the isoresponse contours plotted with respect to the equivalent contrast plane are circular. Note that in the equivalent contrast plane, the distances between the plotted teal points are the same as the distances between the

corresponding plotted red points. This is a consequence of the fact that the transformation M is chosen to make the isoresponse contours circular.

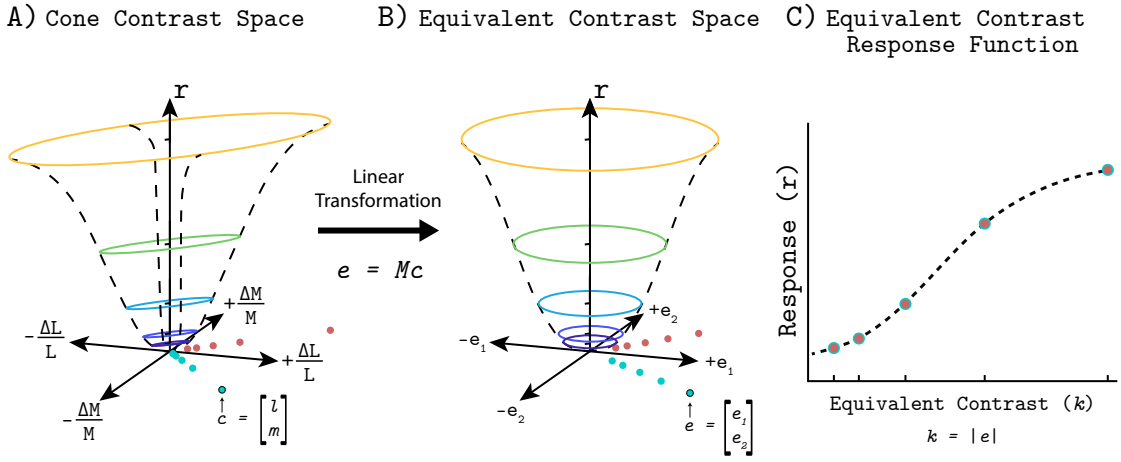

Figure 1: Illustration of Cone to Equivalent Contrast Transformation. Panel A) A 3-dimensional cone contrast-response space with the (x,y) plane representing the LM contrast plane and the z axis giving the corresponding response r to each point in the (x,y) plane. The teal and red dots shown in the LM plane represent example stimulus modulations, chosen in two color directions at contrasts corresponding to the five isoresponse contours illustrated in dark blue, blue, aqua, green, yellow. Panel B) A 3-dimensional equivalent contrast-response space with the (x,y) plane representing equivalent contrast (e_1 and e_2) and the z axis giving the corresponding response r to each point in the (x,y) plane. The teal and red dots shown correspond to same color dots in Panel A after we apply a linear transformation M to c (the L- and M-cone contrast representation of the stimuli) to obtain a transformed representation of the stimulus, $e = Mc$. Note after the application of M, the elliptical contours in Panel A are circular and the distances between the plotted teal points are the same as the distances between the corresponding plotted red points. Panel C) The equivalent contrast response function. The x-axis denotes the equivalent contrast and the y-axis marks the response. The teal and red closed circles shown in Panel C correspond to both the teal and red points shown in Panels A and B.

We define the equivalent contrast k of a stimulus as the vector length of the transformed stimulus e, $k = |e|$.

The next step of the model is a non-linearity that maps between equivalent contrast (k) and BOLD fMRI response (dashed black line). This is possible since all stimuli in equivalent contrast space with the same equivalent contrast predict the same underlying response, regardless of the chromatic direction of the stimuli. Therefore, we can focus solely on the relationship between equivalent contrast and the associated response. This is illustrated by Panel C. We call the static non-linearity the “equivalent contrast-response function”. The teal and red closed circles shown in Panel C correspond to both the teal and red points shown in Panels A and B, and

these overlap since they lie on the same set of isoresponse contours.

The linear transformation M needed to compute the equivalent contrast representation of c is derived by starting with the equation for an ellipse centered at the origin, in which a positive-definite quadratic function of the cone contrasts is equal to a constant for all points on the ellipse. This equation is given below (left hand side) and re-expressed in matrix-vector form (right hand side).

$$k^2 = Al^2 + Blm + Cm^2 = \begin{bmatrix} l & m \end{bmatrix} \begin{bmatrix} A & B/2 \\ B/2 & C \end{bmatrix} \begin{bmatrix} l \\ m \end{bmatrix}$$

Changing the value of the constant k^2 changes the scale of the ellipse without changing its shape, and as we will see below k is the equivalent contrast corresponding to each constant-shape elliptical isoresponse contour. We rewrite the matrix representation of the elliptical locus as:

$$k^2 = c^T Q c$$

This yields

$$k = \sqrt{c^T Q c}$$

Because the coefficients A, B, and C are constrained so that Q is a symmetric positive definite matrix, Q can be factored through its eigenvalue decomposition and rewritten as

$$Q = V \Lambda V^T$$

where V is an orthonormal (rotation) matrix and Λ is a diagonal matrix with positive entries. Since Λ is a diagonal matrix we can further decompose as

$$Q = V S S^T V^T$$

where S is diagonal with entries equal to the square root of the corresponding entries of Λ.

The matrix V expresses a rotation in the cone contrast plane and may be parameterized by

the rotation angle p_1:

$$V(p_1) = \begin{bmatrix} cos(p_1) & -sin(p_1) \\ sin(p_1) & cos(p_1) \end{bmatrix}$$

The matrix S is diagonal and when applied to a vector simply scales the entries of that vector. Although S normally has two degrees of freedom in the general case, we lock the scale of the major axis to 1. Therefore we are only concerned with the scaling of the minor axis (p_2). Thus we can define

$$S(p_2) = \begin{bmatrix} 1 & 0 \\ 0 & 1/p_2 \end{bmatrix}, 0 > p_2 \leq 1$$

In this formulation, p_1 and p_2 parameterize the shape of an elliptical isoresponse contour and k parameterizes its scale. The parameter p_1 is what we call the angle of the major axis in the main text, while p_2 is the minor axis ratio.

We set $M = S^T V^T$ and rewrite Q as:

$$Q = M^T M$$

The matrix M then transforms the cone contrast vector c to the equivalent contrast vector through $e = Mc$. Recall that equivalent contrast is the vector length of e. Therefore, the equivalent contrast of the points on the ellipse corresponding to k is given by

$$||e|| = k$$

To see this, note that

$$||e||^2 = e^T e = c^T M^T M c = c^T Q c = k^2$$

Thus, given Q, we can compute the equivalent contrast for any stimulus c and apply the equivalent contrast-response function to predict the its response. The specific non-linearity we use for the contrast-response function is a Naka-Rushton function. This function is a four parameter

saturating non-linearity that is defined by the following:

$$r(k) = a\frac{k^n}{k^n + s^n} + h$$

The neural response (r) is a function of the equivalent contrast(k). The parameters of the Naka-Rushton function are the amplitude(a), exponent(n), semi-saturation(s), and the offset(h). These parameters control the gain, the slope, the position along the x axis, and the y-axis offset of the non-linearity, respectively. The shape of the non-linearity controls how the underlying response changes with equivalent contrast.

Finally, we need to convert the neural response to a prediction of the BOLD fMRI response($\hat{Y}$). To do this, we convolve the underlying response with the hemodynamic response function (HRF).

$$\hat{Y} = r \circledast HRF$$

Predictions of the BOLD fMRI response via the QCM are thus made using 6 parameters: angle (p_1), minor axis ratio (p_2), amplitude ($p_3 = a$), exponent ($p_4 = n$), semi-saturation ($p_5 = s$), and offset ($p_6 = h$). We can define a parameter vector P for the QCM as:

$$P = \begin{bmatrix} p_1 \\ \vdots \\ p_6 \end{bmatrix}$$

We fit P to the data by using a non-linear parameter search routine fmincon (Matlab, see https://www.mathworks.com/help/optim/ug/fmincon.html) to find the parameter vector that that minimizes the difference between the measured BOLD fMRI time course Y and the prediction $\hat{Y}$ obtained using the QCM. This takes the form of:

$$P^* = \arg\min_P \sqrt{\frac{\sum_{i=1}^{t}(\hat{y}_i - y_i)^2}{t}}$$

where the objective function we are minimizing is the root mean squared error. Once the values of P are found for an individual subject, we can use them to predict the BOLD fMRI response to any c within the LM cone contrast plane.

Linear Channels Model

The linear channels model (LCM) is based on the work of Brouwer and Heeger (2009). They develop a model that decodes the hue angle of a stimulus a subject was viewing from BOLD fMRI measurements. The stimuli in their study were modulations in the isoluminant plane of the CIELAB color space, and were parameterized by hue angle within this plane. Their model is based on linear channels tuned to the this angular representation, and it did not explicitly consider the effect of stimulus contrast. This was sufficient for their analysis, as they studied only a single contrast for each angle. To develop a version of the LCM that may be applied to our stimuli, we need both to adopt the concepts to apply to stimuli in the LM contrast plane and to add a model component that handles contrast.

The angles used in our implementation of the LCM are angles in the LM contrast plane, with 0 corresponding to the positive abscissa, rather than angles in the CIELAB isoluminant plane. These angles are computed from the L- and M-cone contrasts of our stimulus modulations, as the arctangent of the ratio of M- to L-cone contrast:

$$\theta = tan^{-1}(\frac{m}{l})$$

where θ is then the angle corresponding to one one of our stimulus modulations.

Given the angular stimulus representation, each linear channel is characterized by its sensitivity to stimulation from each possible stimulus angle - basically a tuning function over angle. More specifically, the tuning functions are implemented as half-rectified cosines raised to an exponent. What differs across each channel is the phase of the tuning function (the peak sensitivity). Thus the sensitivity of the i^{th} channel may be written as:

$$f_i(\theta) = \begin{cases} \cos^n(\theta - \phi_i) & cos(\theta - \phi_i) \geq 0 \\ 0 & cos(\theta - \phi_i) < 0 \end{cases}$$

where i indicates the channel, n is the exponent which controls the narrowness of the channel tuning functions, and ϕ_i is the peak sensitivity of the i^{th} channel. In calculations, the angle θ is discretized, and both stimuli and mechanism tuning can be represented in matrix-vector form, as we describe below.

The first step of the model is to compute the channel responses. This is done with a vector representation of the stimulus. Each entry of the stimulus row vector represents one angle, and for the stimulus modulations we used, only one entry is non-zero for any given modulation. In our computations, we discretized angle in 1 degree steps (the resolution of the representation of θ). The magnitude of the non-zero entry represents the contrast of the modulation. Similarly, the sensitivity of a channel may be represented by a column vector over the same angular discretization, with each entry of the vector being the sensitivity of the channel at the corresponding angle. The dot product of a stimulus vector with a channel vector yields the response of the channel to the stimulus.

The set of channels can be represented by the columns of a matrix C (nAngles x nChannels) and the set of stimuli represented by a matrix S (nStimuli x nAngles). Therefore, the hypothetical channel outputs, H (nStimuli x nChannels), can be calculated as:

$$H = SC$$

The overall LCM response to a given stimulus is given as a weighted sum of the individual channel responses (H), with the weights, w (nChannels x nVoxels) acting as parameters of the model. If we consider responses across a set of voxels, as was done by Brouwer and Heeger (2009), the response b (nStimuli x nVoxels) for a set of stimuli is given by:

$$b = Hw$$

In our analysis, we fit the LCM to the median time course of V1 and therefore we set $nVoxels = 1$.

In context of the LCM, isoresponse contours are made up by the set of stimuli that satisfy the following:

$$Hw = SCw = k$$

where k is a constant target response.

In their work, Brouwer and Heeger (2009) used six channels and an exponent of 2. The channels had peak sensitivities at 0, 60, 120, 180, 240 and 300 degrees. Since our stimu-

lus modulations were symmetric around around a background, we enforce that channels offset by 180 degrees used the same weights in the linear combination. This results in three symmetric channels with pairs located at 0 and 180, 60 and 240, 120 and 300 degrees.

One key difference between our experiment and the the original Brouwer and Heeger (2009) work is that we varied the stimulus contrast in each chromatic direction. To extend the LCM to handle contrast, we treated the overall LCM response as an equivalent contrast and passed this through a common Naka-Rushton function. This approach mirrors how we handled contrast in the the QCM. To model the BOLD fMRI response, we convolve the output of the Naka-Rushton with the HRF. We fit the LCM to our data using a method analogous to the one used to fit the QCM. More specifically, we found the three linear channel weights and the Naka-Rushton function parameters that yielded the best fit to the BOLD response time course. These parameters were found simultaneously through the use of MATLAB's fmincon optimization routine. We also fit a variant of the LCM analogous to a model used by Kim et al. (2020) with sharper (cos^6) channel tuning and using eight rather than six underlying mechanisms.

Both versions of the LCM yield isoresponse contours similar in shape to those obtained with the QCM (Figure 6 figure supplement 1), with cross-validated R^2 values essentially the same as those obtained using the QCM (Figure 4 figure supplement 1). Notably, that the version of the LCM with more channels yielded an isoresponse contour that more closely approximated the isoresponse contour of the QCM than did the version of the LCM with fewer channels.

A key difference between the LCM and the QCM is in how the functional properties of the model relate to the L- and M-cone contrasts that characterize the early visual system responses to the stimuli. As discussed in the main text, the QCM can be implemented as the sum of the squared responses of two mechanisms, each of which responds as weighted sum of L- and M-cone contrast. Thus underlying the QCM is a quadratic (squaring) non-linearity. In the LCM, on the other hand, the underlying linear channels are tuned for angle in the LM contrast plane. Since angle is obtained as the arctangent of the ratio of M- and L-cone contrasts, the LCM is based on a different form of non-linearity than the QCM, which would entail different neural computations. To put it another way, the apparently simple linear form of the LCM when expressed in terms of stimulus angle is less simple when referred back to the L- and M-cone contrast representation. This same basic point applies to LCMs formulated with respect to hue angle in the CIELAB

isoluminant plane, as in Brouwer and Heeger (2009) and Kim et al. (2020). Measurements of the response to mixtures of modulations might be used in the future to differentiate between the non-linearities embodied by the LCM and the QCM.

REFERENCES

Avants, B. B., Epstein, C. L., Grossman, M., & Gee, J. C. (2008). Symmetric diffeomorphic image registration with cross-correlation: evaluating automated labeling of elderly and neurodegenerative brain. *Med Image Anal, 12(1)*, 26-41.

Barnett, M. A., Aguirre, G. K., & Brainard, D. (2021). A quadratic model captures the human V1 response to variations in chromatic direction and contrast. *eLife, 10*, e65590.

Bartels, A., & Zeki, S. (2000). The architecture of the colour centre in the human visual brain: new results and a review. *European Journal of Neuroscience, 12(1)*, 172-190.

Baseler, H., & Sutter, E. (1997). M and P components of the VEP and their visual field distribution. *Vision research, 37(6)*, 675-690.

Baylor, D. A., Nunn, B. J., & Schnapf, J. L. (1987). Spectral sensitivity of cones of the monkey *Macaca fascicularis*. *Journal of Physiology, 390*, 145-160.

Beauchamp, M. S., Haxby, J. V., Jennings, J. E., & DeYoe, E. A. (1999). An fMRI version of the Farnsworth-Munsell 100-hue test reveals multiple color-selective areas in human ventral occipitotemporal cortex. *Cerebral Cortex, 9(3)*, 257-263.

Benson, N. C., Butt, O. H., Brainard, D. H., & Aguirre, G. K. (2014). Correction of distortion in flattened representations of the cortical surface allows prediction of V1-V3 functional organization from anatomy. *PLoS Comput Biol, 10(3)*, e1003538.

Benson, N. C., & Winawer, J. (2018). Bayesian analysis of retinotopic maps. *Elife, 7*

Boehm, A. E., MacLeod, D. I., & Bosten, J. M. (2014). Compensation for red-green contrast loss in anomalous trichromats. *J Vis, 14(13)*, 19.

Bonnen, K., Burge, J., Yates, J., Pillow, J., & Cormack, L. K. (2015). Continuous psychophysics: Target-tracking to measure visual sensitivity. *Journal of Vision, 15(3)*, 14-14.

Bracewell, R. N. (1978). *The Fourier Transform and its Applications*: McGraw-Hill.

Brainard, D. H. (1996). Cone contrast and opponent modulation color spaces. In P. K. Kaiser & R. M. Boynton (Eds.), *Human Color Vision* (2 ed., pp. 563-579). Washington, D.C.: Optical Society of America.

Brainard, D. H., Pelli, D. G., & Robson, T. (2002). Display characterization. In J. P. Hornak (Ed.), *Encylopedia of Imaging Science and Technology* (pp. 172-188). New York: Wiley.

Brainard, D. H., & Stockman, A. (2010). Colorimetry. In M. Bass, C. DeCusatis, J. Enoch, V. Lakshminarayanan, G. Li, C. Macdonald, V. Mahajan & E. van Stryland (Eds.), *The Optical Society of America Handbook of Optics, 3rd edition, Volume III: Vision and Vision Optics* (pp. 10.11-10.56). New York: McGraw Hill.

Brouwer, G. J., & Heeger, D. J. (2009). Decoding and reconstructing color from responses in human visual cortex. *J Neurosci, 29(44)*, 13992-14003.

CIE. (2007). *Fundamental chromaticity diagram with physiological axes – Parts 1 and 2. Technical Report 170-1*. Vienna: Central Bureau of the Commission Internationale de l' Éclairage.

Cottaris, N. P., & De Valois, R. L. (1998). Temporal dynamics of chromatic tuning in macaque primary visual cortex. *Nature, 395(6705)*, 896-900.

Cottaris, N. P., Jiang, H., Ding, X., Wandell, B. A., & Brainard, D. H. (2019). A computational observer model of spatial contrast sensitivity: Effects of wavefront-based optics, cone mosaic structure, and inference engine. *Journal of Vision, 19(4)*, 8.

D'Souza, D. V., Auer, T., Frahm, J., Strasburger, H., & Lee, B. B. (2016). Dependence of chromatic responses in V1 on visual field eccentricity and spatial frequency: an fMRI study. *J Opt Soc Am A Opt Image Sci Vis, 33(3)*, A53-64.

Dale, A. M., Fischl, B., & Sereno, M. I. (1999). Cortical surface-based analysis. I. Segmentation and surface reconstruction. *Neuroimage, 9(2)*, 179-194.

Derrington, A. M., Krauskopf, J., & Lennie, P. (1984). Chromatic mechanisms in lateral geniculate nucleus of macaque. *Journal of Physiology, 357*, 241-265.

DeValois, R. L., Abramov, I., & Jacobs, G. H. (1966). Analysis of response patterns of LGN cells. *Journal of the Optical Society of America, 56*, 966-977.

Engel, S., Zhang, X. M., & Wandell, B. (1997). Colour tuning in human visual cortex measured with functional magnetic resonance imaging. *Nature, 388(6637)*, 68-71.

Eskew, R. T., Jr. (2009). Higher order color mechanisms: A critical review. *Vision Research, 49(22)*, 2686-2704.

Estévez, O., & Spekreijse, H. (1982). The "silent substitution" method in visual research. *Vision Research, 22*, 681-691.

Field, G. D., Gauthier, J. L., Sher, A., Greschner, M., Machado, T. A., Jepson, L. H., Shlens, J., Gunning, D. E., Mathieson, K., Dabrowski, W., Paninski, L., Litke, A. M., & Chichilnisky, E. J. (2010). Functional connectivity in the retina at the resolution of photoreceptors. *Nature, 467(7316)*, 673-677.

Fischl, B., Sereno, M. I., & Dale, A. M. (1999). Cortical surface-based analysis. II: Inflation, flattening, and a surface-based coordinate system. *Neuroimage, 9(2)*, 195-207.

Foley, J. M. (1977). Effect of distance information and range on two indices of visually perceived distance.

Gegenfurtner, K. (2001). Color in the cortex revisited. *Nature Neuroscience, 4(4)*, 339-340.

Gegenfurtner, K. (2003). Cortical mechanisms of colour vision. *Nature Neuroscience, 4(7)*, 563-572.

Geisler, W. S. (1989). Sequential ideal-observer analysis of visual discriminations. *Psychological Review, 96(2)*, 267-314.

Georgeson, M. A., & Sullivan, G. D. (1975). Contrast constancy: Deblurring in human vision by spatial frequency channels. *Journal of Physiology (London), 253*, 627-656.

Glasser, M. F., Sotiropoulos, S. N., Wilson, J. A., Coalson, T. S., Fischl, B., Andersson, J. L., Xu, J., Jbabdi, S., Webster, M., Polimeni, J. R., Van Essen, D. C., Jenkinson, M., & Consortium, W. U.-M. H. (2013). The minimal preprocessing pipelines for the Human Connectome Project. *Neuroimage, 80*, 105-124.

Goddard, E., Mannion, D. J., McDonald, J. S., Solomon, S. G., & Clifford, C. W. (2011). Color responsiveness argues against a dorsal component of human V4. *J Vis, 11(4)*

Guild, J. (1931). The colorimetric properties of the spectrum. *Philosophical Transactions of the Royal Society of London. Series A, 230*, 149-187.

Hadjikhani, N., Liu, A. K., Dale, A. M., Cavanagh, P., & Tootell, R. B. H. (1998). Retinotopy and color sensitivity in human visual cortical area V8. *Nature Neuroscience, 1(3)*, 235-241.

Hansen, T., & Gegenfurtner, K. R. (2013). Higher order color mechanisms: Evidence from noise-masking experiments in cone contrast space. *Journal of Vision, 13(1)*, 26.21-21.

Hansen, T., Pracejus, L., & Gegenfurtner, K. R. (2009). Color perception in the intermediate periphery of the visual field. *Journal of Vision, 9(4)*, 26.21-26.12.

Hering, E. (1878). *Zur Lehre vom Lichtsinne. Sechs Mittheilungen an die Kaiserliche Akademie der Wissenschaften in Wien*. Wien: Carl Gerold's Sohn.

Hillis, J. M., & Brainard, D. H. (2007). Distinct mechanisms mediate visual detection and identification. *Current Biology, 17(19)*, 1714-1719.

Horwitz, G. D. (2020). Signals Related to Color in the Early Visual Cortex. *Annu Rev Vis Sci, 6*, 287-311.

Horwitz, G. D., & Hass, C. A. (2012). Nonlinear analysis of macaque V1 color tuning reveals cardinal directions for cortical color processing. *Nat Neurosci, 15(6)*, 913-919.

Hunt, R. W. G. (2004). *The Reproduction of Colour* (6 ed.). Chichester, England: John Wiley & Sons.

Hurvich, L. M., & Jameson, D. (1957). An opponent-process theory of color vision. *Psychological Review, 64(6)*, 384-404.

Ishihara, S. (1977). *Tests for Colour-Blindness*. Tokyo: Kanehara Shuppen Company, Ltd.

Jenkinson, M. (2002). Improved Optimization for the Robust and Accurate Linear Registration and Motion Correction of Brain Images. *NeuroImage, 17(2)*:825, 825-841.

Johnson, E. N., Hawken, M. J., & Shapley, R. (2001). The spatial transformation of color in the primary visual cortex of the macaque monkey. *Nature neuroscience, 4(4)*, 409-416.

Johnson, E. N., Hawken, M. J., & Shapley, R. (2004). Cone inputs in macaque primary visual cortex. *Journal of Neurophysiology, 91(6)*, 2501-2514.

Judd, D. B. (1945). Standard Response Functions for Protanopic and Deuteranopic Vision. *Journal of the Optical Society of America, 35(3)*, 199-221.

Judd, D. B. (1966). Fundamental studies of color vision from 1860 to 1960. *Proceedings of the National Academy of Sciences of the United States of America, 55(6)*, 1313-1330.

Kaiser, P. K., & Boynton, R. M. (1996). *Human Color Vision, Second Edition*. Washington, DC: Optical Society of America.

Kay, K. N., Winawer, J., Mezer, A., & Wandell, B. A. (2013). Compressive spatial summation in human visual cortex. *J Neurophysiol, 110(2)*, 481-494.

Kay, K. N., Winawer, J., Rokem, A., Mezer, A., & Wandell, B. A. (2013). A two-stage cascade model of BOLD responses in human visual cortex. *PLoS Comput Biol, 9(5)*, e1003079.

Kay, K. N., & Yeatman, J. D. (2017). Bottom-up and top-down computations in word-and face-selective cortex. *Elife, 6*, e22341.

Kim, I., Hong, S. W., Shevell, S. K., & Shim, W. M. (2020). Neural representations of perceptual color experience in the human ventral visual pathway. *Proc Natl Acad Sci U S A, 117(23)*, 13145-13150.

Knoblauch, K., & Maloney, L. T. (1996). Testing the indeterminacy of linear color mechanisms from color discrimination data. *Vision Research, 36(2)*, 295-306.

König, A., & Dieterici, C. (1886). Die Grundempfindungen und ihre Intensitäts-Vertheilung im Spectrum. *Sitzungsberichte Akademie der Wissenschaften in Berlin, 1886*, 805-829.

Krauskopf, J., Williams, D. R., & Heeley, D. W. (1982). Cardinal directions of color space. *Vision Research, 22(9)*, 1123-1131.

Krauskopf, J., Williams, D. R., Mandler, M. B., & Brown, A. M. (1986). Higher order color mechanisms. *Vision Research, 26(1)*, 23-32.

Lafer-Sousa, R., Conway, B. R., & Kanwisher, N. G. (2016). Color-biased regions of the ventral visual pathway lie between face- and place-selective regions in humans, as in macaques. *Journal of Neuroscience, 36(5)*, 1682-1697.

Lankheet, M. J., Lennie, P., & Krauskopf, J. (1998). Distinctive characteristics of subclasses of red-green P-cells in LGN of macaque. *Vis Neurosci, 15(1)*, 37-46.

Lee, B. B., Shapley, R. M., Hawken, M. J., & Sun, H. (2012). Spatial distributions of cone inputs to cells of the parvocellular pathway investigated with cone-isolating gratings. *Journal of the Optical Society of America A, 29(2)*, A223-A232.

Lennie, P., Haake, P. W., & Williams, D. R. (1991). The design of chromatically opponent receptive fields. In M. S. Landy & J. A. Movshon (Eds.), *Computational models of visual processing* (pp. 71-82). Cambridge, Mass.: MIT Press.

Lennie, P., & Movshon, J. A. (2005). Coding of color and form in the geniculostriate visual pathway. *Journal of the Optical Society of America A, 10(10)*, 2013-2033.

Liu, J., & Wandell, B. A. (2005). Specializations for chromatic and temporal signals in human visual cortex. *J Neurosci, 25(13)*, 3459-3468.

Livingstone, M., & Hubel, D. H. (1984). Anatomy and physiology of a color system in the primate visual cortex. *Journal of Neuorscience, 4(1)*, 309-356.

Martin, P. R., Blessing, E. M., Buzas, P., Szmajda, B. A., & Forte, J. D. (2011). Transmission of colour and acuity signals by parvocellular cells in marmoset monkeys. *The Journal of Physiology, 589(Pt 11)*, 2795-2812.

Martin, P. R., Lee, B. B., White, A. J., Solomon, S. G., & Ruttiger, L. (2001). Chromatic sensitivity of ganglion cells in the peripheral primate retina. *Nature, 410(6831)*, 933-936.

McKeefry, D. J., Parry, N. R. A., & Murray, I. J. (2003). Simple reaction times in color space: The influence of chromaticity, contrast, and cone opponency. *Investigative Ophthalmology & Visual Science, 44(5)*, 2267-2276.

Mollon, J. D., & Krauskopf, J. (1973). Reaction time as a measure of the temporal response properties of individual colour mechanisms. *Vision Research, 13*, 27-40.

Mullen, K., Dumoulin, S., & Hess, R. (2010). Color processing in the human LGN and cortex measured with fMRI. *Journal of Vision, 7(15)*:4, 4-4.

Mullen, K. T., Dumoulin, S. O., McMahon, K. L., de Zubicaray, G. I., & Hess, R. F. (2007). Selectivity of human retinotopic visual cortex to S-cone-opponent, L/M-cone-opponent and achromatic stimulation. *Eur J Neurosci, 25(2)*, 491-502.

Mullen, K. T., & Kingdom, F. A. A. (1996). Losses in peripheral colour sensitivity predicted from "hit and miss" post-receptoral cone connections. *Vision Research, 36(13)*, 1995-2000.

Mullen, K. T., & Kingdom, F. A. A. (2002). Differential distributions of red-green and blue-yellow cone opponency across the visual field. *Visual Neuroscience, 19(1)*, 109-118.

Mullen, K. T., Sakurai, M., & Chu, W. (2005). Does L/M cone opponency disappear in human periphery? *Perception, 34*, 951-959.

Mullen, K. T., Thompson, B., & Hess, R. F. (2010). Responses of the human visual cortex and LGN to achromatic and chromatic temporal modulations: an fMRI study. *J Vis, 10(13)*, 13.

Newton, J. R., & Eskew, R. T., Jr. (2003). Chromatic detection and discrimination in the periphery: A postreceptoral loss of color sensitivity. *Visual Neuroscience, 20(5)*, 511-521.

Philbeck, J. W., & Loomis, J. M. (1996). A comparison of two indicators of perceived egocentric distance under full-cue and reduced-cue conditions. *Journal of Experimental Psychology: Human Perception and Performance, 23*, 72-85.

Philbeck, J. W., Loomis, J. M., & Beall, A. C. (1997). Visually perceived location is an invariant in the control of action. *Perception and Psychophysics, 59*, 601-612.

Poirson, A. B., & Wandell, B. A. (1990). Task-dependent color discrimination. *Journal Of The Optical Society Of America A, 7(4)*, 776-782.

Poirson, A. B., Wandell, B. A., Varner, D. C., & Brainard, D. H. (1990). Surface characterizations of color thresholds. *Journal of the Optical Society of America A, 7(4)*, 783-789.

Power, J. D., Mitra, A., Laumann, T. O., Snyder, A. Z., Schlaggar, B. L., & Petersen, S. E. (2014). Methods to detect, characterize, and remove motion artifact in resting state fMRI. *Neuroimage, 84*, 320-341.

Reid, R. C., & Shapley, R. M. (1992). Spatial structure of cone inputs to the receptive fields in primate lateral geniculate nucleus. *Nature, 356(6371)*, 716-718.

Rosenholtz, R. (2016). Capabilities and Limitations of Peripheral Vision. *Annu Rev Vis Sci, 2*, 437-457.

Sakurai, M., & Mullen, K. T. (2006). Cone weights for the two cone-opponent systems in peripheral vision and asymmetries of cone contrast sensitivity. *Vision Research, 46(26)*, 4346-4354.

Schluppeck, D., & Engel, S. A. (2002). Color opponent neurons in V1: A review and model reonciling results from imaging and single-unit recording. *Journal of Vision, 2*, 480-492.

Shapley, R., & Hawken, M. J. (2011). Color in the Cortex: single- and double-opponent cells. *Vision Research, 51(7)*, 701-717.

Shevell, S. K., & Martin, P. R. (2017). Color opponency: tutorial. *J Opt Soc Am A Opt Image Sci Vis, 34(7)*, 1099-1108.

Shinomori, K., & Werner, J. S. (2008). The impulse response of S-cone pathways in detection of increments and decrements *Visual Neuroscience, 25(3)*, 341-347.

Smith, S. M., Jenkinson, M., Woolrich, M. W., Beckmann, C. F., Behrens, T. E., Johansen-Berg, H., Bannister, P. R., De Luca, M., Drobnjak, I., Flitney, D. E., Niazy, R. K., Saunders, J., Vickers, J., Zhang, Y., De Stefano, N., Brady, J. M., & Matthews, P. M. (2004). Advances in functional and structural MR image analysis and implementation as FSL. *Neuroimage, 23 Suppl 1*, S208-219.

Smithson, H. E., & Mollon, J. D. (2004). Is the S-opponent chromatic sub-system sluggish? *Vision Research, 44(25)*, 2919-2929.

Solomon, S. G., & Lennie, P. (2005). Chromatic gain controls in visual cortical neurons. *J Neurosci, 25(19)*, 4779-4792.

Solomon, S. G., & Lennie, P. (2007). The machinery of colour vision. *Nature Reviews Neuroscience, 8(4)*, 276-286.

Spitschan, M., Aguirre, G. K., & Brainard, D. H. (2015). Selective stimulation of penumbral cones reveals perception in the shadow of retinal blood vessels. *PLoS One, 10(4)*, e0124328.

Spitschan, M., Datta, R., Stern, A. M., Brainard, D. H., & Aguirre, G. K. (2016). Human visual cortex responses to rapid cone and melanopsin-directed flicker. *J Neurosci, 36(5)*, 1471-1482.

Stiles, W. S. (1949). Increment thresholds and the mechanisms of colour vision. *Documenta Ophthalmologica, 3*, 138-163.

Stiles, W. S. (1955). Interim report to the Commission Internationale de l'Éclairage Zurich, 1955, on the National Physical Laboratory's investigation of colour-matching (1955) with an appendix by W. S. Stiles & J. M. Burch. *Optica Acta, 2*, 168-181.

Stiles, W. S., & Burch, J. M. (1959). NPL colour-matching investigation: Final report (1958). *Optica Acta, 6*, 1-26.

Stockman, A., & Brainard, D. H. (2010). Color vision mechanisms. In M. Bass, C. DeCusatis, J. Enoch, V. Lakshminarayanan, G. Li, C. Macdonald, V. Mahajan & E. van Stryland (Eds.), *The Optical Society of America Handbook of Optics, 3rd edition, Volume III: Vision and Vision Optics* (pp. 11.11-11.104). New York: McGraw Hill.

Stockman, A., & Sharpe, L. T. (1999). Cone spectral sensitivities and color matching. In K. Gegenfurtner & L. T. Sharpe (Eds.), *Color vision: From Genes to Perception* (pp. 53-87). Cambridge: Cambridge University Press.

Stromeyer, C. F., III, Lee, J., & Eskew, R. T., Jr. (1992). Peripheral chromatic sensitivity for flashes: a post-receptoral red-green asymmetry. *Vision Research, 32(10)*, 1865-1873.

Svaetichin, G., & MacNichol, E. F. (1958). Retinal mechanisms for chromatic and achromatic vision. *Annals New York Academy of Science, 74*, 385-404.

Tailby, C., Solomon, S. G., Dhruv, N. T., & Lennie, P. (2008). Habituation reveals fundamental chromatic mechanisms in striate cortex of macaque. *Journal of Neuroscience, 28(5)*, 1131-1139.

Tregillus, K. E. M., Isherwood, Z. J., Vanston, J. E., Engel, S. A., MacLeod, D. I. A., Kuriki, I., & Webster, M. A. (2021). Color Compensation in Anomalous Trichromats Assessed with fMRI. *Curr Biol, 31(5)*, 936-942 e934.

Vanni, S., Henriksson, L., Viikari, M., & James, A. C. (2006). Retinotopic distribution of chromatic responses in human primary visual cortex. *Eur J Neurosci, 24(6)*, 1821-1831.

Wandell, B. A., Dumoulin, S. O., & Brewer, A. A. (2006). Computational Neuroimaging; Color Signals in the Visual Pathways. *Neuro-opthalmol. Jpn., 23*, 324-343.

Wandell, B. A., & Pugh, E. N., Jr. (1980). Detection of long-duration incremental flashes by a chromatically coded pathway. *Vision Research, 20(7)*, 625-635.

Wandell, B. A., & Silverstein, L. D. (2003). Digital color reproduction. In S. K. Shevell (Ed.), *The Science of Color* (2 ed., pp. 281-316). Oxford: Optical Society of America; Elsevier Ltd.

Wang, L., Mruczek, R. E., Arcaro, M. J., & Kastner, S. (2015). Probabilistic maps of visual topography in human cortex. *Cerebral cortex, 25(10)*, 3911-3931.

Watson, A. B. (1982). Derivation of the impulse response: comments on the method of Roufs and Blommaert. *Vision Research, 22(10)*, 1335-1337.

Welbourne, L. E., Morland, A. B., & Wade, A. R. (2018). Population receptive field (pRF) measurements of chromatic responses in human visual cortex using fMRI. *Neuroimage, 167*, 84-94.

Weller, J. P., & Horwitz, G. D. (2018). Measurements of neuronal color tuning: Procedures, pitfalls, and alternatives. *Vision Res, 151*, 53-60.

Wool, L. E., Crook, J. D., Troy, J. B., Packer, O. S., Zaidi, Q., & Dacey, D. M. (2018). Nonselective wiring accounts for red-green opponency in midget ganglion cells of the primate retina. *Journal of Neuorscience, 38(6)*, 1520-1540.

Woolrich, M. W., Behrens, T. E., & Smith, S. M. (2004). Constrained linear basis sets for HRF modelling using Variational Bayes. *Neuroimage, 21(4)*, 1748-1761.

Wright, W. D. (1928). A re-determination of the trichromatic coefficients of the spectral colours. *Transactions of the Optical Society, 30*, 141-164.

Young, T. (1802). The Bakerian Lecture: On the theory of light and colours. *Philosophical Transactions of the Royal Society of London, 92*, 12-48.

Zeki, S., & Marini, L. (1998). Three cortical stages of colour processing in the human brain. *Brain, 121*, 1669-1685.